BORON SEGREGATION IN IRON AND STAINLESS STEEL

A Study of the Effects of Trace Amounts of Boron on the Grain Boundary and Surface Energies of Iron and AISI 316 Austenitic Steel.

D A Mortimer

A thesis submitted to the University of Warwick in support of an application for admission to the degree of Doctor of Philosophy.

December 1973

ABSTRACT

Segregation to crystalline interfaces has been considered in terms of its effect on the thermodynamic interfacial energies. The experimental evidence for segregation was reviewed and its effects on interfacial energies and mechanical properties discussed with particular reference to boron in iron and steels. The effects of boron concentration on the surface and grain boundary energies of iron and AISI 316 stainless steel were measured. Grain boundary to surface energy ratios were measured from the dihedral angles at the grooves (and ridges) formed during vacuum annealing where these boundaries intersect the surface. The effect of boron on the absolute grain boundary and surface energies was obtained by the assumption that twin boundary energy is independent of boron concentration. Measurements were made on 316 steels containing 0.001 and ~0.006 wt% boron at 950° to 1250°C, and on iron alloys containing up to 0.020 wt% boron at 950° and 1050°C. Reductions of up to 30% in the surface energies and 40% in the grain boundary energies were found on increasing the boron concentration to 0.004-0.008 wt%. The results were interpreted in terms of segregation of boron to the surfaces and grain boundaries and compared with literature data for other systems including nickel-boron alloys. The relevance of interfacial energy measurements to the effects of boron on mechanical properties was considered.

ACKNOWLEDGEMENTS

I would like to express my gratitude to:

Dr H Mykura, my supervisor at Warwick University, for his constant interest, encouragement and advice.

Dr M G Nicholas, my supervisor at Harwell, for his invaluable advice and guidance throughout this project.

Drs W A Runciman and R G Sowden for their continued support of this work.

Drs D R Harries and J E Antill for several helpful discussions.

Dr J C Rivière for the Auger spectroscopic analyses and Mr J Furnival for the boron autoradiography.

Numerous other colleagues for technical aid and useful discussions.

Mrs D M Matthews for her help with the preparation and typing of this thesis.

My husband Mike, whose constant support and assistance has made the writing of this thesis possible.

The UKAEA for supporting the work and allowing its publication in this thesis.

CONTENTS

ILLUSTRATIONS

TABLES

CHAPTER 1 INTRODUCTION

It has been known for many years that the presence of impurities in metals and alloys affects their mechanical properties, often deleteriously. As production and analysis techniques have improved it has become apparent that in many cases only trace amounts of impurity of the order of a few tens of parts per million are necessary to cause quite profound changes. For example, 10-20 ppm Bi is sufficient to cause embrittlement in copper (Voce and Hallowes [1947]). A large body of evidence has gradually been built up to show that effects caused by trace impurities are often associated with segregation of the impurity atoms to produce much higher local concentrations. The evidence for segregation has been the subject of several reviews, eg Inman and Tipler [1963], Westbrook [1964] and Gleiter and Chalmers [1972]. Segregation can take place at free surfaces, grain boundaries and other interfaces or regions of structural discontinuity, such as precipitate particle/matrix interfaces and dislocations. McLean [1957] has discussed the driving forces for segregation in terms of the distortion produced in the lattice by the solute atoms.

Thermodynamical considerations of the energies of such interfaces predicts that segregation of impurities should be associated with a reduction in free energy. Trace amounts of impurity have been found to have very markedeffects on the interfacial energies in a large number of metallic systems. It is found (see eg Hondros and McLean [1968]) that the elements most likely to segregate to interfaces are those which have a low solubility in the bulk metal as these atoms also

produce relatively large distortions of the solvent lattice. Boron has a low solubility in iron, nickel, austenitic steels and nickel alloys and so is expected to segregate to the available interfaces in these materials, thus changing their structure and hence their energy, cohesion and other properties.

AISI 316* steel is an austenitic stainless steel whose creep-rupture properties are improved by additions of up to 0.01 wt% boron. It is also a candidate material for cladding the fuel elements in the first Civil Fast Reactor which is soon to be built. The materials in the reactor have to withstand very unusual and demanding conditions. It is therefore important to understand as much about the materials to be used as possible. In thermal reactors such as are in use by the Central Electricity Generating Board today, boron is an undesirable impurity as it produces helium atoms under irradiation by slow neutrons and these can agglomerate to produce small bubbles of gas inside the material which are detrimental to its mechanical properties. In a fast reactor, this problem is much lesssevere, firstly because boron has a much lower cross section for the capture of fast neutrons than for slow ones and secondly because helium is produced anyway in much larger quantities by bombardment of the metal atoms which are the major constituents of the clad. It may therefore be permissible, indeed desirable, to have boron in the cladding material in order to increase its ductility and creep rupture life.

---

*American Iron and Steel Institute specification number for an austenitic, non-hardenable, non-magnetic steel containing by weight 16-18% Cr, 10-14% Ni, 2-3% Mo and maximum concentrations of 0.08% C, 2.00% Mn, 0.045% P, 0.030% S and 1.00% Si.

The actions of boron in austenitic steels are complicated and depend on the composition of the steel, its thermal history, the temperature of interest, the metallurgical structure of the steel at that temperature - in particular the presence or otherwise of second phase particles, etc. The present work is intended to cover just one aspect of the effects of boron, namely its effect on the grain boundary and surface energies at temperatures where the 316 steel is single phase. The chemistry of this steel is complex, thus making interpretation of the results difficult. In order to assist the interpretation, therefore, a study of the effects of boron additions on the interfacial energies of pure iron in the austenitic phase was also undertaken.

The techniques used for these measurements are the standard techniques of measuring relative interfacial energies from the profiles formed during vacuum annealing at the intersection of twin and grain boundaries with the surface. A novel feature of the present measurements was the application of a Talystep instrument to measure the twin boundary/surface intersection profiles. The experimental details are described fully in Chapter 3 while the thermodynamic background and the available data on segregation of trace elements and their effects on interfacial energies and mechanical properties are discussed in Chapter 2. The measurements made on 316 steel and on a series of dilute iron-boron alloys are presented separately in Chapters 4 and 5, and some ancillary measurements are given in Chapter 6. Finally, in Chapter 7 the measurements on the two sets of materials are compared with each other and with similar measurements by Hodgson [1972] on nickel-boron alloys, and the combined results

discussed in relation to creep-rupture properties.

CHAPTER 2 BACKGROUND INFORMATION

In the first part of this Chapter the thermodynamic theory of interfaces will be presented. From this it will be shown that small amounts of a solute element can segregate to interfaces and that this segregation is associated with a change in the free energy of the interface. Secondly, some of the available experimental techniques for measuring interfacial energies will be discussed. In section 2.3 the experimental evidence for theoccurrence of interfacial segregation will be considered and some effects of segregation on interfacial energies and mechanical properties will be indicated. Finally some of the effects of boron on properties of iron and steels will be presented.

2.1 Thermodynamics of Interfaces

The surface free energy of a condensed material is the energy required to produce unit area of that surface in an isothermal and reversible manner. The free energy of the surface atoms arises from the fact that they are joined to the solid lattice by fewer atomic bonds than are the atoms in the bulk of the solid. An interface between two dissimilar phases in a system or between two differently oriented crystals of the same material can similarly be characterised thermodynamically by a free energy, which is a reflection of the different density and arrangement of atoms in the interfacial region. This free energy is a function of temperature, structure (ie orientation with respect to solid phases) and composition. The first treatment of interfaces in systems of several components was that of Gibbs [eg 1928] which, although mathematically rigorous, is rather difficult to

visualise in real physical terms because of his introduction of an arbitrary mathematical surface. We shall therefore follow the example of other workers and consider here the more realistic model and treatment given by Guggenheim [1940 and 1967] in which the interface is considered as a separate phase of finite thickness.

The model is illustrated schematically for a planar interface in Fig 2.1 in which α and β are two homogeneous bulk phases and σ is the interfacial or surface phase, separated from the bulk phases by the parallel planes AA' and BB' a distance τ apart. These two planes are positioned so that at AA' the properties are exactly those of phase α and at BB' they are identical with those of phase β. All the properties of phase σ are assumed to be uniform in directions parallel to AA' and BB' but must obviously change in directions normal to these planes.

The basic definition of surface tension, γ, arises from consideration of a two dimensional surface behaving as a stretched membrane. Then the work, dW, required to stretch the surface isothermally and reversibly by an amount dA is given by

$$dW = \gamma dA. \qquad \ldots (2.1)$$

For an isotropic two dimensional surface the surface tension (in dyne cm^{-1}) is equal to the surface free energy (in erg cm^{-2} or mJ m^{-2}). For the three dimensional interface, σ, of the model in Fig 2.1, however, an increase in the interfacial area must also involve a volume change, dV, so that

$$dW = \gamma dA - PdV \qquad \ldots (2.2)$$

where P is the uniform pressure across a plane parallel to AA'.

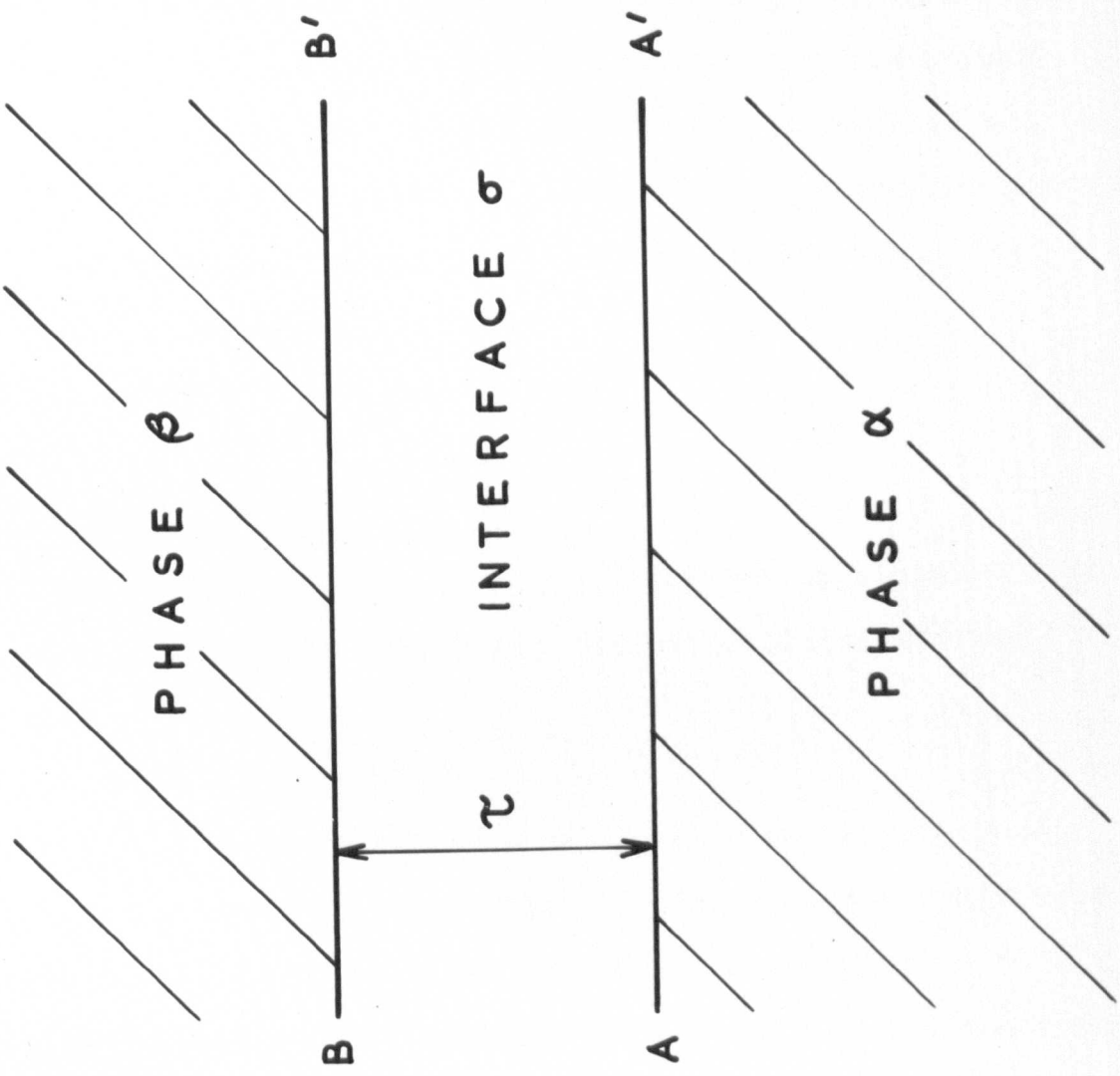

Figure 2.1. Guggenheim's model of an interface between two phases.

The dependence of the free energy of the interface phase σ on temperature and composition will be the same as for that of a bulk phase but equation (2.2) describes the dependence on geometry. Hence the Helmholtz free energy variation, dH^{σ}, is given by

$$dH^{\sigma} = -S^{\sigma}dT - PdV^{\sigma} + \sum_i \mu_i dn_i^{\sigma} + \gamma dA \qquad \ldots (2.3)$$

where the superscript σ indicates that the properties refer to the interface phase, S^{σ} is the entropy, T the absolute temperature and μ_i and dn_i^{σ} are the chemical potential and number of moles of component i present in the interface phase in a multicomponent system. Similarly for the Gibbs free energy, G^{σ}, Guggenheim obtained

$$dG^{\sigma} = -S^{\sigma}dT + V^{\sigma}dP - Ad\gamma + \sum_i \mu_i dn_i^{\sigma} \qquad \ldots (2.4)$$

and

$$G^{\sigma} = \sum_i n_i^{\sigma} \mu_i . \qquad \ldots (2.5)$$

By differentiating equation (2.5), subtracting equation (2.4) and dividing by A we obtain for the variation of surface tension

$$d\gamma = -S_A^{\sigma}dT + \tau dP - \sum_i \Gamma_i d\mu_i \qquad \ldots (2.6)$$

where $S_A^{\sigma} = S^{\sigma}/A$ is the entropy per unit area of interface and $\Gamma_i = n_i^{\sigma}/A$ denotes the amount of component i in unit area of the interface phase. The variables in equation (2.6) are not independent so that in order to make use of the equation certain simplifying assumptions must be introduced for particular cases.

2.1.1 Single Component Systems

The simplest system to consider is one containing only one chemical species when equation (2.6) becomes

$$d\gamma = -S_A^{\sigma}dT - \Gamma d\mu + \tau dP. \qquad \ldots (2.7)$$

Further simplifications can be introduced when it is remembered that the chemical potential must be equal in all phases which are in equilibrium with each other, and secondly, that for condensed phases the terms in PV can be neglected to a first approximation. For an interface between a condensed phase α and a gas β the density of the interfacial phase σ will still be such as to make the second assumption reasonable. We can thus substitute the equation for $d\mu$ from the bulk phase,

$$d\mu = -SdT + VdP \qquad \ldots (2.8)$$

into equation (2.7) and neglect the terms τdP and VdP to obtain a relation for the temperature dependence of the surface tension

$$\frac{d\gamma}{dT} = -(S_A^\sigma - \Gamma S) = -\Delta S. \qquad \ldots (2.9)$$

ΔS is called the interfacial entropy and represents the entropy of unit area of interface minus the entropy of the same number of moles in the bulk phase.

The Gibbs function per unit area of this interface is given by

$$G^\sigma = \Gamma\mu = U^\sigma - TS_A^\sigma - \gamma \qquad \ldots (2.10)$$

where U^σ is the total thermodynamic energy of unit area and we have again ignored the term τdP. Substituting equation (2.10) and the analogous equation for the bulk phase ($G = \mu = U - TS$) into equation (2.9) gives

$$\gamma - T\frac{d\gamma}{dT} = U^\sigma - \Gamma U = \Delta U. \qquad \ldots (2.11)$$

Here ΔU can be called the total interfacial energy and is equal to the total energy of unit area of interface less the energy of the same number of moles of the bulk phase. From equations (2.9) and (2.11) it is seen that γ can be expressed as

$$\gamma = \Delta U - T\Delta S \qquad \ldots (2.12)$$

and thus it behaves as a Gibbs free energy of the interface.

2.1.2 Multicomponent Systems

Guggenheim [1940] gave an analysis of equation (2.6) in terms of independent variables for a system of r components. As this is rather complex, however, and experimental data are only available for two component systems the present discussion will be restricted to binary systems. In this case there are two independent variables: temperature and bulk solute concentration, x. In the following, component 1 will be the solvent and component 2 the solute so that x is the bulk concentration of component 2. Continuing to neglect PV type terms, equation (2.6) becomes for a binary system

$$-d\gamma = S_A^\sigma dT + \Gamma_1 d\mu_1 + \Gamma_2 d\mu_2. \qquad \ldots (2.13)$$

But for a bulk two component system Guggenheim [1967, p 208] shows that

$$d\mu_i = -S_i dT + \left(\frac{\partial \mu_i}{\partial x}\right) dx, \quad i = 1,2 \qquad \ldots (2.14)$$

where S_i is the partial molar entropy of component i.

Hence

$$-d\gamma = (S_A^\sigma - \Gamma_1 S_1 - \Gamma_2 S_2) dT + \left(\Gamma_1 \frac{\partial \mu_1}{\partial x} + \Gamma_2 \frac{\partial \mu_2}{\partial x}\right) dx. \qquad \ldots (2.15)$$

Applying the Gibbs-Duhem relation for a two component system: $(1 - x)\frac{\partial \mu_1}{\partial x} + x\frac{\partial \mu_2}{\partial x} = 0$ at constant temperature and pressure; to equation (2.15) gives for the temperature dependence of interfacial free energy

$$-\frac{d\gamma}{dT} = (S_A^\sigma - \Gamma_1 S_1 - \Gamma_2 S_2) + \left(\Gamma_2 - \frac{x\Gamma_1}{1 - x}\right) \frac{\partial \mu_2}{\partial x} \cdot \frac{\partial x}{\partial T}. \qquad \ldots (2.16)$$

The first term on the right hand side of equation (2.16) is the excess entropy of the interfacial phase compared to the entropy of the same quantity of material in the bulk phases. It can be considered as the direct effect of temperature on interfacial energy and is positive. This means that in the

absence of segregation effects the interfacial energy would decrease with increasing temperature as in a one component system. The second term describes the indirect effect of temperature on interfacial energy due to its effects on adsorption at the interface. This term is negative (because $\partial\mu_2/\partial T$ is negative) and for a strongly adsorbing solute may be dominant, causing the interfacial energy to increase with increasing temperature. At constant temperature equation (2.16) becomes

$$-\left(\frac{\partial\gamma}{\partial x}\right)_T = \left(\Gamma_2 - \frac{x\Gamma_1}{1-x}\right)\frac{\partial\mu_2}{\partial x} \qquad \ldots (2.17)$$

which is the Gibbs adsorption equation and relates changes in interfacial composition to changes in the interfacial energy. For very dilute solutions ($x \ll 1$) we can make use of the relation

$$d\mu = RTd(\ln a) = \frac{RT}{x}\,dx \qquad \ldots (2.18)$$

where a is the chemical activity of component x, to simplify equation (2.17), which becomes

$$\frac{d\gamma}{dx} = -\frac{RT}{x}\Gamma_2. \qquad \ldots (2.19)$$

Γ_2 then represents the solute excess at the interface and can be determined experimentally from measurements of the variation of interfacial energy with solute concentration for very dilute solutions at constant temperature. In general, the Gibbs adsorption equation ((2.17) or (2.19)) indicates that the more a segregating solute lowers the energy of an interface, the more strongly it will segregate to that interface.

2.2 Measurement of Interfacial Energies

Numerous methods have been used for the measurement of interfacial free energies of various types and several reviews of these have appeared in the literature (eg Hondros [1970], Robertson [1970], Inman and Tipler [1963]).

The following discussion will be restricted to the two types of interface of most interest in the present work, namely solid surface/vapour and grain boundary (solid/solid) interfaces. Some of the techniques employed give absolute interfacial energy values and others produce relative values for pairs of interfaces which can be used to derive absolute values of one of the energies if the other is known.

2.2.1 Absolute Interfacial Energy Measurements

The most extensively used method for measuring solid surface energies is Udin's [1952] 'Zero creep' experiment. This is based on the observation that at a temperature close to its melting point, a freely suspended thin wire or foil can contract under the action of surface tension forces, reducing its surface area and hence its surface free energy. If a load is put on the end of the wire it may either contract or extend according to the balance between the applied load and the surface tension forces. The surface tension can be derived by determining the load at which the length change is zero. For a wire of radius r which has all its grain boundaries aligned perpendicular to its axis the load w at zero extension is given by

$$w = \pi r(\gamma_{sv} - \gamma_{gb}.r/d)$$

where d is the average grain length, γ_{sv} is the surface free energy of the material in equilibrium with its own vapour and γ_{gb} is the grain boundary free energy.

In practice, strain/time relations are determined for a range of loads so that some of the wires shrink and some extend, and the load for zero creep is obtained grom a graph of strain rate vs stress. The grain boundary energy can then

be determined from measurements of the grain boundary groove dihedral angles (see next section). Various experimental difficulties have been encountered with this technique, in particular from contamination of the surface by impurities diffusing from the bulk or in the atmosphere, and anomalous shape changes in the wires. Nevertheless with care it can give accurate values for the average surface free energy over all orientations and has been used on a range of metals (Hondros [1970]). Its biggest restriction is that it can only be used at temperatures very close to the melting point (>0.7 T_m) because the creep mechanism depends on atomic diffusion and thus equilibrium is approached in a reasonable time only at these high temperatures.

At the opposite end of the temperature scale ie at liquid nitrogen temperatures, controlled cleavage of a partially cracked crystal has been used to derive surface energy values, in this case for one specific orientation - that of the cleavage plane. Assuming that the experimental conditions correspond to a reversible process the free energy of the newly formed surface is given by

$$dW = dU + \gamma_s dA$$

where dW is the work done, dU the elastic strain energy, γ_s is the surface energy and dA the area of surface produced. The biggest difficulty with this technique is to either eliminate or calculate any plastic flow occurring in the crystal during fracture which would also contribute to the work dW. When comparing the results of this type of experiment to those obtained from other methods several points should be borne in mind. Firstly, not only is the temperature very

different but the interface whose energy is determined is that between the solid and a liquid coolant, not between the solid and its own vapour. Secondly, for a system of more than one component, in which segregation to the surface may take place, the surface energy measured from cleavage experiments may not be the equilibrium surface energy because the lack of mobility of solute atoms at low temperatures may not allow the equilibrium segregation to take place during the relatively short time of the cleavage experiment.

Several more indirect methods have been used to derive surface and grain boundary energies. For example, the kinetics of relaxation of single or multiple scratches can yield a value of surface energy if the diffusion mechanism and the relevant diffusion coefficients are known or can be determined. However, the precision of this technique when used on platinum was estimated by Blakely and Mykura [1962] to be $\pm$ 30%. Precise calorimetry has been used by Astrom [1956] to obtain a value for the grain boundary enthalpy by measuring the heat evolved during grain growth. The grain boundary free energy could then be calculated by assuming a value for the grain boundary entropy. Another method of measuring grain boundary energy was used by Mullins [1956] who applied a magnetic field to a notched bicrystal of bismuth. Because the magnetic susceptibility was different in the two crystals and the grain boundary was held at its ends by the notches it bowed out and its energy could be calculated. Such specialised methods are obviously only applicable to a very restricted number of materials.

2.2.2 Relative Interfacial Energies

Where several interfaces meet an equilibrium configuration is set up which depends on the minimisation of interfacial free energy. Smith [1948] showed that the case of three isotropic interfaces intersecting in a line as shown in Fig 2.2 could be represented by a simple triangle of forces so that

$$\frac{\gamma_1}{\sin \theta_1} = \frac{\gamma_2}{\sin \theta_2} = \frac{\gamma_3}{\sin \theta_3}. \qquad \ldots (2.20)$$

This equation is valid for fluid interfaces. However, when one or more of the phases present is a crystalline solid the possibility of anisotropy in the interfacial energy arises. This is because the different densities of atoms on crystal surfaces of various orientations give rise to different binding energies of the atoms at these interfaces. In other words the interfacial energy is dependent on the orientation of the surface relative to the crystal lattice of the solid. Herring [1951] showed by a virtual work argument that in this case equation (2.20) should be replaced by

$$\sum_{i=1}^{3} [\gamma_i \underset{\sim}{t}_i + (\frac{\partial \gamma}{\partial \alpha})_i \underset{\sim}{n}_i] = 0 \qquad \ldots (2.21)$$

where α_i denotes the orientation of the ith interface, $\underset{\sim}{t}_i$ is the unit vector in the plane of the ith interface normal to the line of intersection of the interfaces, $\underset{\sim}{l}$ is the unit vector along the line of intersection and $\underset{\sim}{n}_i = \underset{\sim}{l} \wedge \underset{\sim}{t}_i$.

Thus anisotropy of an interfacial energy gives rise to a force of magnitude $(\frac{\partial \gamma}{\partial \alpha})$ at right angles to the line of the interface tending to rotate it to an orientation of lower energy. These forces are generally referred to as 'torque terms'. Except for a few cases, such as a surface whose orientation is close to but not equal to a low index plane, or a grain boundary whose misorientation is close to that

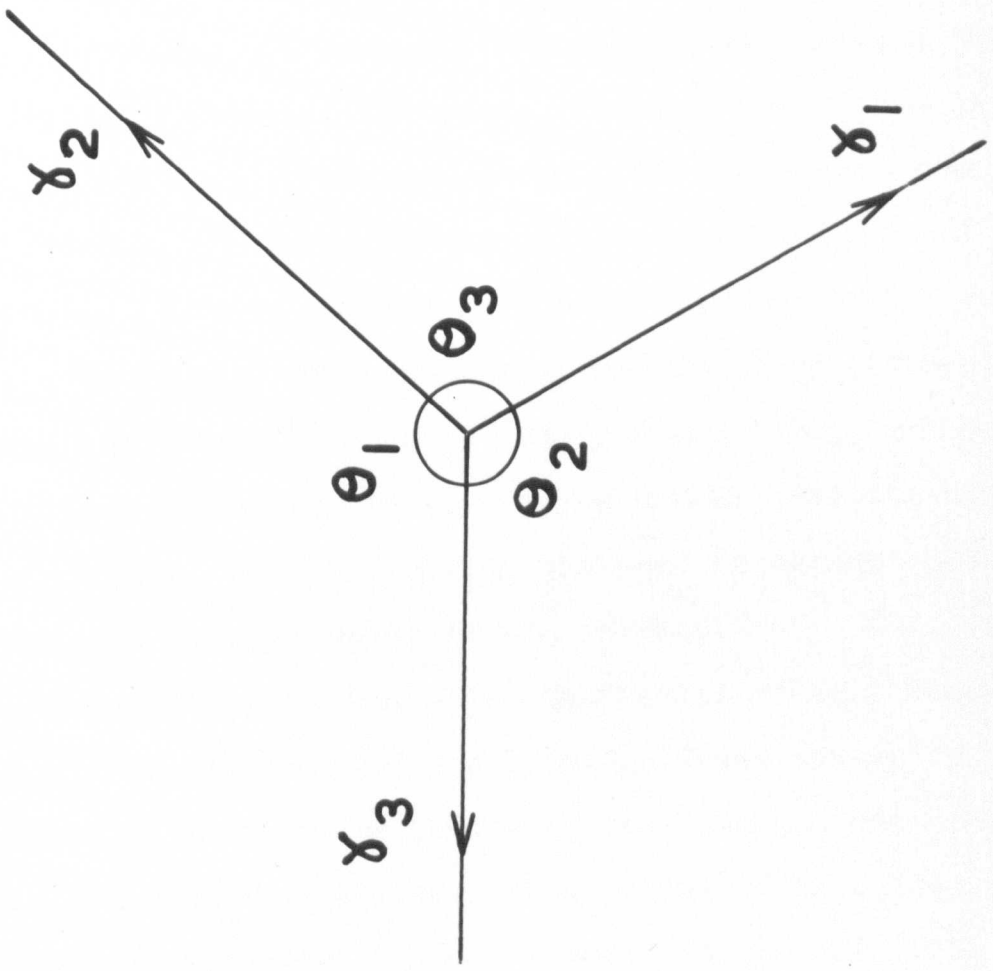

Figure 2.2. Intersection of three isotropic interfaces.

of a coincidence boundary, the torque terms are small and they are usually neglected for the purpose of measuring relative interfacial energies. (Further discussion of this point will be given in section 3.1.1.)

Techniques based on equation (2.20) or (2.21) can be applied over a relatively wide temperature range to a variety of systems. Thus, they can to some extent fill the gap between zero creep and controlled cleavage methods for solid surface energies. They also provide a means of measuring solid/liquid interfacial energies and are the easiest methods of measuring grain boundary energies. Measurements of the profiles formed at the intersections of grain boundaries and twin boundaries with the solid/gas interface were the basis of the present work and will be discussed fully in Chapter 3. Other workers have studied twin boundary/grain boundary interactions, for example Murr and co-workers [eg 1968 and 1970], who have used electron microscopy to give three-dimensional pictures of intersections thus eliminating the need to assume that boundaries are perpendicular to the surface.

By the choice of a suitable combination of equilibria it is possible to characterise a solid-liquid-gas system in terms of interfacial energies by measuring one absolute and several relative interfacial energies. This technique is called the multiphase equilibration technique and is described fully in a paper by Hodkin, Mortimer, Nicholas and Poole [1970] which is reproduced as an Appendix to this Thesis.

2.3 Segregation

The Gibbs adsorption isotherm, equation (2.17), shows how the decrease in interfacial energy provides a driving

force for solute segregation to the interface. (If the solute atoms cause an increase in interfacial energy then negative adsorption at the interface is predicted.) In the following sections the experimental evidence for segregation to grain boundaries and surfaces in solid metals will be summarised and some effects of equilibrium segregation on materials properties indicated. Effects which are caused by other, non-equilibrium, types of segregation will not be considered except where they are directly relevant to the present work.

2.3.1 Evidence for Segregation

There have been several reviews on this topic in the literature (Inman and Tipler [1963], Westbrook [1964] and Gleiter and Chalmers [1972]) so only a brief summary of their findings will be given here. The methods used to detect solute segregation fall into two groups: direct methods in which a difference in composition is measured between the interfacial regions and the grain interiors; and indirect methods in which some property which is thought to be dependent on solute concentration is measured. The latter type of techniques are the more numerous but usually only give qualitative results because the exact form of the dependence of the measured property on segregation is uncertain. The direct methods provide at least a semi-quantitative measurement of the amount and species of segregation but are more difficult experimentally and often have limited applicability.

The earliest direct measurements of segregation employed some means of selectively etching material from the grain boundaries and analysing the resulting solution. The sensitivity of this type of approach was increased by incorporating

radioactive tracers of the segregating element into the sample. Another method using radioactive tracers is autoradiography in which the distribution of tracer atoms is recorded by photographic or counting techniques. This technique can be applied only to a limited number of systems and its limitations in terms of resolution have been discussed by Stein [1967]. Attempts have been made to use electron probe microanalysis to detect equilibrium segregation but the volume of solid analysed by this technique ($\sim 10^{-18}$ m^3 or $\sim 10^{10}$ atoms) is in general too large to detect the segregation which typically occurs over a layer of material only a few atom diameters wide.

Two recent techniques which do have a sufficiently high resolution to detect segregation to such narrow regions near grain boundaries and surfaces are field ion microscopy and Auger spectroscopy. The field ion microscope has the highest resolution of any instrument at present available in that individual atoms at lattice plane edges on the specimen surface are imaged. It is thus also able to provide valuable information on the detailed structure of grain boundaries and surfaces. Unfortunately it is still limited to systems of high melting point. Nevertheless, it has been applied successfully to the study of grain boundary segregation of oxygen in iridium and tungsten and of other, unidentified, impurities in tungsten. The impurity atoms show up as bright spots on the FIM image. An 'atomprobe' modification of the microscope introduced by Brenner and McKinney [1968] should enable individual impurity atoms to be identified.

Auger spectroscopy (described in Chapter 6) enables the

analysis of the top few atom layers of a surface to be undertaken. It has been applied in the last few years to a variety of systems. For example Hondros [1972] showed segregation of Bi to the surfaces of Cu-Bi alloys and Bishop and Rivière [1970] found segregation of boron, nitrogen and sulphur to the surface of dilute iron alloys after treatment at different temperatures. In systems which exhibit intergranular fracture the exposed grain boundary surfaces can be examined. The results of some studies of this type will be discussed in section 2.3.3.

The most frequently used of the indirect methods for detecting interfacial segregation are the measurement of interfacial energies as a function of solute concentration and, for grain boundaries, the measurement of microhardness profiles across the boundary. The effects of segregation on interfacial energy are considered in the next section. Microhardness determinations of segregation have been discussed thoroughly by Westbrook [1964]. As they are often associated with non-equilibrium segregation they are of only passing interest here. Other indirect methods which have been used in attempts to detect grain boundary segregation include the measurement of electrochemical potentials, lattice parameters, electrical resistivities, internal friction, and grain boundary diffusion. These techniques have all been discussed in the reviews mentioned above and will not, therefore, be given further consideration here.

2.3.2 Effects of Segregation on Interfacial Energies

The free energy of an interface is a fundamental property which reflects the structure and cohesion of the interface.

It is thus an important materials parameter and has been measured for many systems. Interfacial energy measurements as a function of solute concentration have been successfully interpreted in terms of equilibrium solute segregation for a number of binary systems using Gibbs' adsorption equation. However, it is more difficult to interpret the measurements if more than one segregable solute is present, as is the case in most 'real' materials.

Several studies of segregation effects on interfacial energies have been conducted for free surfaces. Hondros and McLean [1968] collected the available data on surface energies in pure metals and binary alloys and attempted to find a correlation between the surface activity of solutes and some other physical properties. In most alloys in which surface segregation of the solute occurs the surface energy initially falls rapidly with increasing solute concentration then approaches a constant value corresponding to saturation coverage of the surface with solute atoms. Application of Gibbs' adsorption equation indicates that this saturation coverage is usually of the order of 1/4-1 monolayer of solute atoms on the surface. In many systems the solute saturation of the surface occurs at very low bulk solute concentrations, for example, 0.7 at% P in γ- and δ-Fe (Hondros [1965]), 0.3 at% Sb in Cu (Inman, McLean and Tipler [1963]). This is not always the case, however, as shown by the system Cu-Au studied by White, Adams and Wulff [1960] in which the surface energy goes through a minimum at a copper concentration of about 50%.

The effect of solute additions on surface energy can usefully be described by the surface activity of the solute,

defined as $(\frac{\partial\gamma}{\partial X})_T$ where X is the bulk solute concentration and $\partial\gamma/\partial X$ is measured for very dilute solutions, in other words $\partial\gamma/\partial X$ is the initial, steep slope of the surface energy versus bulk solute concentration curve. The values of $\partial\gamma/\partial X$ for various systems span a very wide range from 28 mJ m^{-2} per at% X for Cu-Au to 10^7 mJ m^{-2} per at% X for δFe-O. Hondros and McLean found a correlation between log $(\partial\gamma/\partial X)$ and log (maximum atomic solubility), solutes with a very low solid solubility having a very high surface activity. This is explained on the basis of atomic mismatch between solvent and solute. A low solubility indicates a high degree of mismatch and hence a large driving force causing the solute to migrate to an already disturbed region where the atoms will cause less distortion of the lattice, such as surfaces and grain boundaries. A high solubility on the other hand indicates a low degree of misfit and hence little tendency for the solute atoms to segregate.

Effects of solutes on grain boundary energies similar to those on surface energies have been found in several systems. An example of these effects taken from Hondros [1965] is shown in Fig 2.3. Here the rapid fall in γ_{sv} and γ_{gb} with increasing phosphorus concentration and the subsequent flattening of the curve as saturation occurs can be clearly seen. In that work the surface energies were determined by the zero creep technique and the grain boundary energies from the grain boundary groove angles. The same approach was used by Hilliard, Cohen and Averbach [1960] on the Cu-Au alloys at 850°C. They found that γ_{gb} went through a minimum of 300 mJ m^{-2} at about 40 at% Cu which was lower than the grain boundary energies of pure

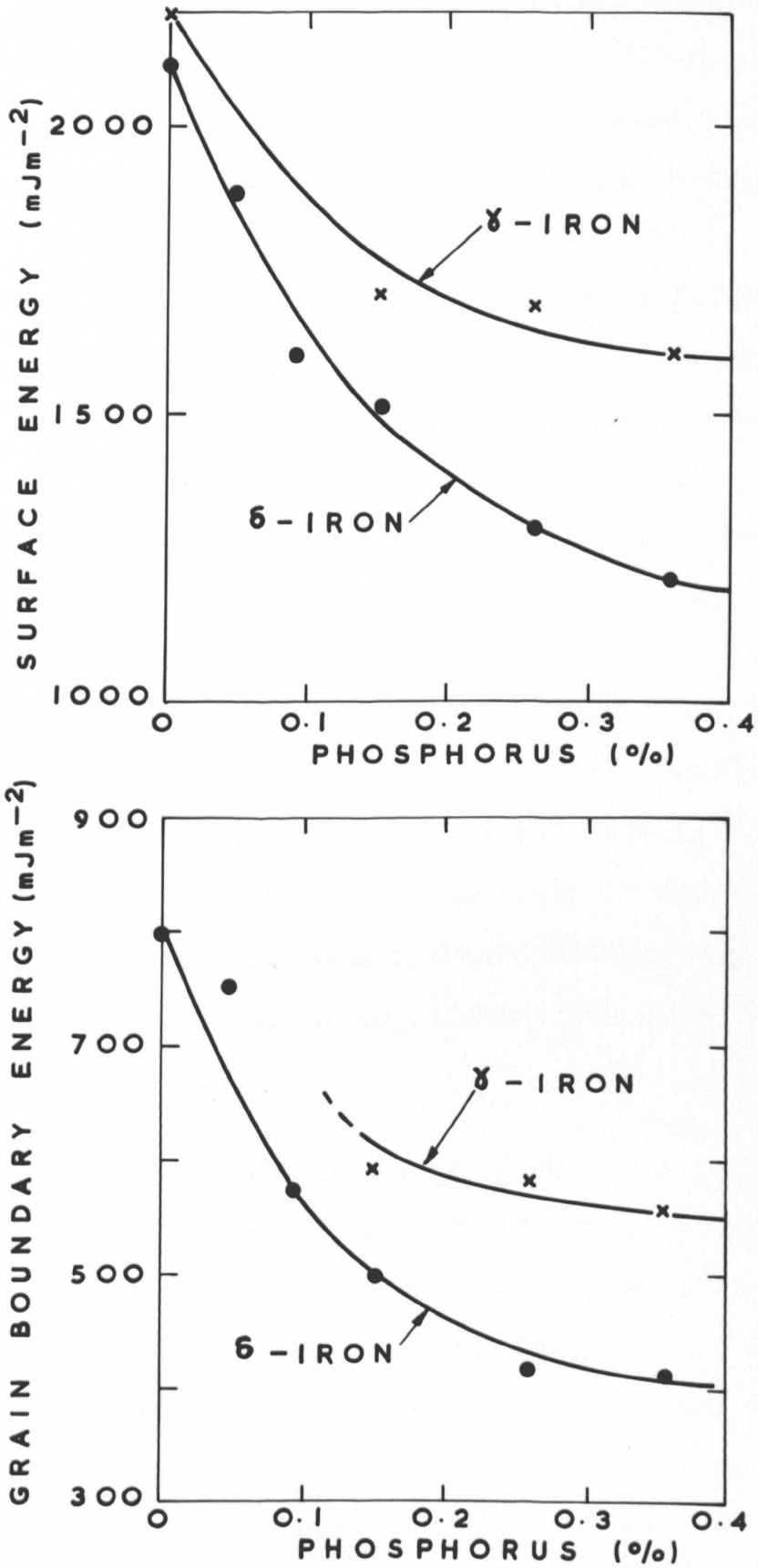

Figure 2.3. The effect of phosphorus on the surface and grain boundary energies of γ- and δ-iron.

gold (360 mJ m^{-2}) and pure copper (600 mJ m^{-2}). Inman, McLean and Tipler [1963] also used the technique on Cu-Sb alloys and found a 50% reduction in γ_{gb} with 0.26 at% Sb. Hondros [1970] found a reasonable correlation between grain boundary activity and the maximum bulk atomic solubility plotted on a log-log scale.

Hodgson [1972] in her investigation of the effects of boron in nickel used a similar approach to that adopted in the present work, namely using the twin boundary energy as a substandard against which to compare both surface and grain boundary energies. The ratios so obtained were then converted to absolute values by making use of the surface energy of pure nickel. She found that 0.01 wt% B reduced γ_{sv} by 30% and γ_{gb} by 50% of the values for boron free nickel at 1000°C. She derived a surface activity of 3×10^4 mJ m^{-2} (at% B)$^{-1}$ and a grain boundary activity 2×10^4 mJ m^{-2} (at% B)$^{-1}$. She quotes as a probable value for the solubility of boron in nickel 0.15 at% and thus her data fit onto Hondros and McLean's activity vs solubility correlation (as shown in Fig 5.10).

2.3.3 Mechanical Properties and Segregation

Impurity effects on mechanical properties have been known to metallurgists for a very long time. As the sensitivity of analytical techniques has improved over the years, so it has been realised that smaller and smaller concentrations of impurity can still have profound effects on properties. These can be brought about by segregation of the impurities to surfaces and internal interfaces so that a much higher concentration is produced in these localised areas. Westbrook

[1964] has reviewed the mechanical property effects which have been attributed to grain boundary segregation as well as some physical and chemical property effects.

Effects of small concentrations of solute have been found at both low and high temperatures. Low temperature intergranular embrittlement is very sensitive to the presence of certain elements. In certain cases the embrittlement is caused by a readily detectable second phase such as grain boundary carbide precipitates which form in some steels after particular heat treatments. However, there are numerous examples of low temperature intergranular embrittlement where no such second phase has been detected. Low [1969] discussed the available experimental data on this phenomenon in terms of equilibrium segregation to grain boundaries. In this way the grain boundary energy is lowered but so may be the surface energy, after fracture along the grain boundary, relative to the surface energy of a newly formed transcrystalline fracture surface. Intergranular fracture may then require much less energy to be supplied for the creation of new surfaces. Trace amounts of N or P have been found to embrittle bcc Fe; C, N and O embrittle the refractory metals W, Mo and Cr to various degrees; and of the fcc metals Cu is embrittled by Sb. It will be noticed that several of these systems have already been mentioned as showing reductions in interfacial energies. This embrittlement can be manifested as a reduction in the fracture energy or another toughness parameter or as an increase in the ductile-to-brittle transition temperature.

If more than one solute element is present in the metal, complex interactions can occur. An example which has been

studied by several workers is the Fe-C-O system. Honda and Taga [1968] and Low, among others, have presented evidence that the addition of carbon to iron containing oxygen reduces the embrittlement of the iron which was presumed to be caused by the oxygen. Tsukahara and Yoshikawa [1971] have, however, made measurements on alloys with much lower oxygen and carbon concentrations. They found that either 4 ppm oxygen is sufficient to embrittle iron or that iron grain boundaries are inherently weak, carbon strengthens them and, at higher concentrations than 4 ppm, the oxygen interacts with the carbon to prevent it segregating to the grain boundaries. From measurements on specimens quenched from the γ or δ phase, they concluded that the second possibility is the more likely.

More recently Powell et al [1973] have studied the fracture surfaces of some 'pure' irons using Auger spectroscopy. They found strong evidence for segregation of sulphur to grain boundaries as well as smaller amounts of carbon and nitrogen. However, they did not obtain clear evidence for segregation of oxygen to grain boundaries and postulated that the segregated sulphur was responsible for grain boundary embrittlement in their materials. Both Honda and Taga, and Tsukahara and Yoshikawa had sulphur present in their irons at about the same concentration as Powell et al. This then could account for the 'inherent' weakness of iron grain boundaries suggested by Tsukahara and Yoshikawa.

Another phenomenon which illustrates multiple element interactions is the reversible temper embrittlement of alloy steels. In this case the elements causing embrittlement are trace amounts of Sb, P, Sn or As and amounts of the order of a percent of Mn or Si. However, the effect only occurs in

the presence of alloying elements (Ni, Cr) and is absent from plain carbon steels. Temper embrittlement occurs in certain low alloy steels when they are heated for any appreciable length of time in the temperature range 350-550°C and disappears on reheating at higher temperatures. It appears as a marked increase in ductile-to-brittle transition temperature and a change in fracture mode from transgranular to intergranular. It is a very complex subject, by no means fully understood, despite a great deal of study.

Auger spectroscopy promises to be a very powerful tool for this purpose and has already been used by a few workers. Stein, Joshi and Laforce [1969] showed segregation of not only Sb but also Ni and Cr to grain boundaries in temper embrittled steels. Marcus and Palmberg [1969] also found segregation of Sb and of P in embrittled steels containing a few hundred ppm of either of these elements. Joshi and Stein have also used Auger spectroscopy to study other systems and have found grain boundary segregation of P in W [1970] and Bi in Cu [1971] associated with embrittlement. In some of these systems, however, the amount of segregation is more than can be accounted for by equilibrium adsorption.

At high temperatures solute segregation can affect creep failure by grain boundary cavitation and wedge cracking. For instance Tipler and McLean [1970] showed that Sb reduced the creep ductility and increased the occurrence of grain boundary cavities in copper. The lowering of the cavity surface energy by segregated impurities reduces the energy required to increase the size of the cavity. It may also sharpen the dihedral angle at the edge of the lenticular void, thus aggravating the notch effect there.

2.4 Boron in Iron and Steels

Boron has a very low solubility in iron, nickel and alloys based on them. Four groups of workers have published measurements on the low boron end of the iron-boron system and portions of their phase diagrams are shown in Fig 2.4. Although they differ in detail, all indicate a low maximum solid solubility of boron of 0.026 wt% or less in both the α and γ phases of iron. The most recent study by Garnish and Brown [1972] used autoradiography to study the lattice solubility and discount the boron segregated at grain boundaries. In their specimens quenched from the γ-phase the grain sizes were large so that they found that the fraction of boron segregated to the grain boundaries was insignificant. However, they still found boron solubilities much lower than any of the previous workers. They attributed this to the lower impurity content of their alloys. At higher boron concentrations, according to Hansen [1958], two boride phases, Fe_2B and FeB, have been identified and there is a eutectic point at 3.8 wt% boron with a melting temperature of 1149°C. The solubility of boron in nickel is similar to that in iron, the preferred estimate of the maximum solubility being 0.15 at% according to Elliot [1965].

Goldschmidt [1971a and b] has measured the solubility of boron in several austenitic steels and his results are summarised in Fig 2.5. He obtained very low maximum solid solubilities in the range 0.006-0.016 wt% B. The importance of additional alloying elements is indicated by the differences between the two 20% Cr 25% Ni steels with and without Nb, Mo and Si additions. In the latter case the solubility is almost three times what it is in the former.

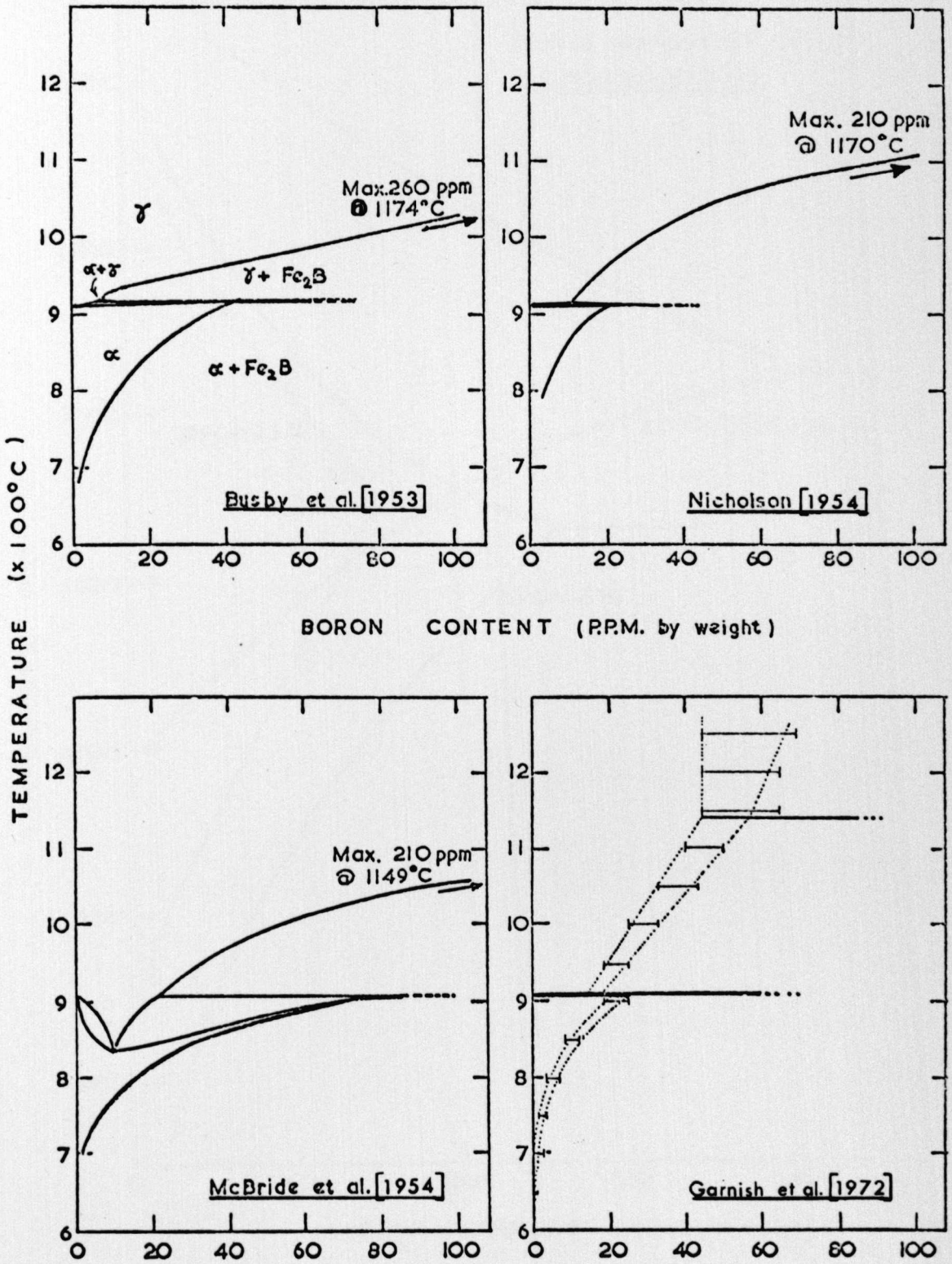

Figure 2.4. Partial phase diagrams for the iron-boron system.

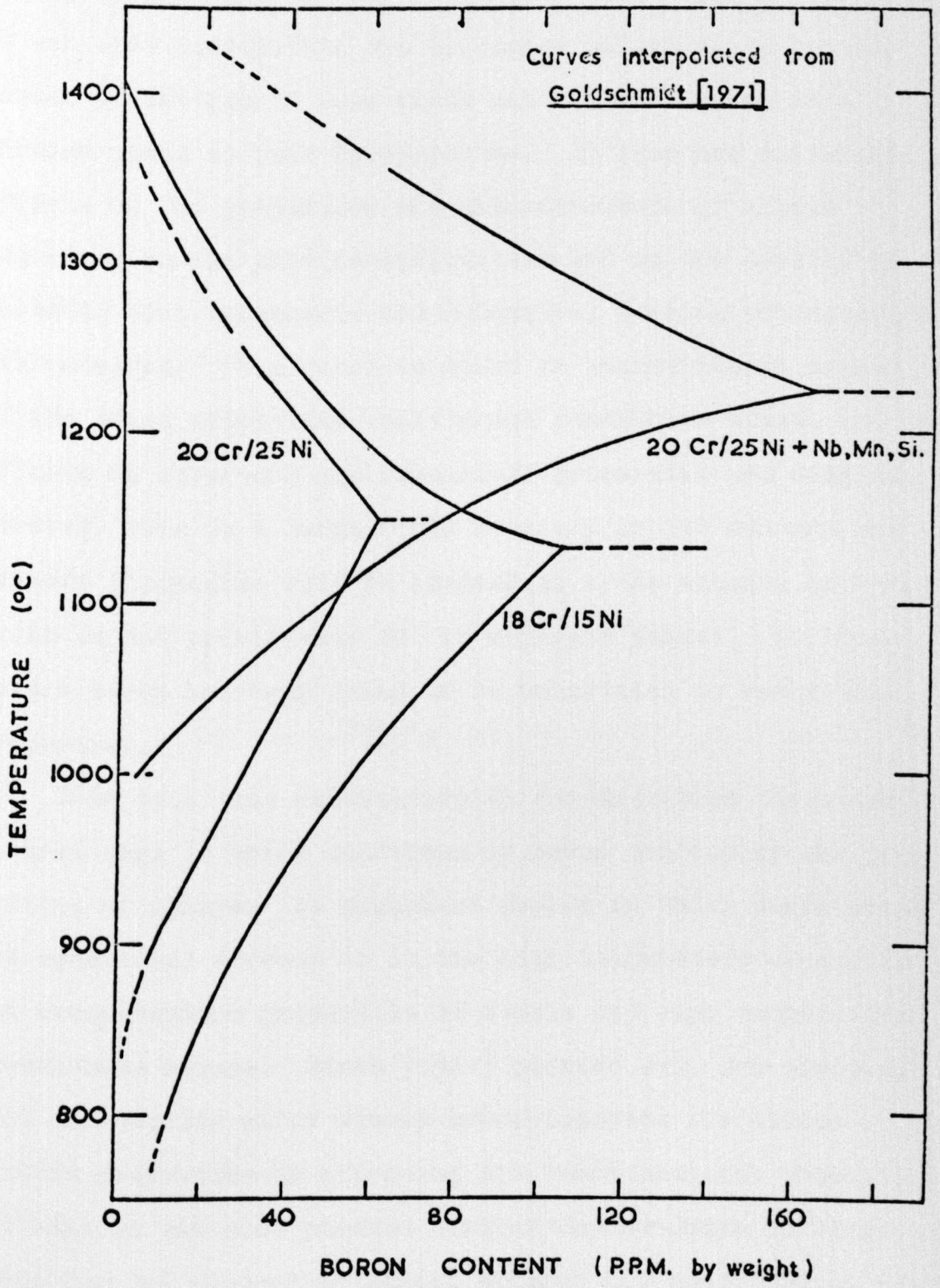

Figure 2.5. Partial phase diagrams for boron in several austenitic steels.

Because of its low solubility in these materials it is to be expected that boron will have a strong tendency to segregate from dilute solid solutions to available interfaces. It can also precipitate out of richer solutions as various boride phases and in some cases can replace carbon in a carbide phase to form borocarbides. It thus has different effects on the properties and microstructure of alloys depending on the precise composition and on the details of whatever heat treatments and mechanical working the material has received. When boron is added in quantities in excess of its solid solubility, multiphase structures occur, and the effects on structure and mechanical properties are complex. However, this is a large field of study on its own and the present discussion will be limited to trace amounts of boron which do not precipitate out as separate phases. At these levels boron has been found to be beneficial to mechanical properties.

Even with this restriction on concentration there are several ways in which additions of boron can modify the properties of alloys. An important region in which boron often has beneficial effects is in the high temperature ductility and creep-rupture properties of steels and high temperature nickel-base alloys. Stone [1967] pointed out, for example, that in some low alloy steels boron improves the stress rupture properties by affecting the transformation product, but that it can also produce similar improvements in other cases (eg 316 austenitic steel) without any modification of transformation product.

Williams, Harries and Furnival [1972] have found boron segregation to $M_{23}C_6$ type carbides in 316 steel during creep

testing at 600 and 700°C as well as a reduced tendency to sigma phase formation with increasing boron concentration in the range 0.0003-0.0050 wt%. This was correlated with a reduction in intergranular cracking associated with increased creep-rupture ductility and hence creep-rupture life when boron was added. The suppression of sigma phase formation was known to be beneficial to creep-rupture life and they also suggested that the boron would increase the lattice parameter of the $M_{23}(C,B)_6$ precipitates thus improving the coherency between these precipitates and the matrix. This should then reduce the tendency to fracture along the precipitate/matrix interface. However, further work by Williams and Talks [1972] indicated that the increase in lattice parameter is rather small (<0.1%).

Williams [1972] has also looked at the distribution of boron in 316 steel after solution treatment at 1050°C and quenching, using autoradiography. He showed that after a very fast quench no grain boundary segregation of boron could be detected but that after a slower quench segregation was present. He thus concluded that the only form of boron segregation occurring at this temperature was a non-equilibrium vacancy-induced type. This point will be considered in more detail in Chapter 6. Jandeska and Morral [1972] investigated the distribution of boron in a low alloy steel using auto-radiography. They found that boron segregated to grain boundaries during annealing in the austenite range and that the amount of grain boundary adsorption of boron decreased at higher temperatures corresponding to a decrease in hardenability of the steel.

Other mechanisms of hardening by boron have been suggested.

For example, Hasegawa and Okamoto [1965] found that additions of boron to pure iron produced hardening after quenching from annealing temperatures in the austenite range. They showed that in the hardened condition the alloy was a supersaturated solution of boron in α-iron. The boron additions increased the tensile strength of the alloys at room temperature but reduced their ductility.

At low temperatures boron can still have a beneficial effect on properties. Taga and Yoshikawa [1971] have studied its effects on fracture of iron at -196°C. They found that the fracture stress increased with boron additions up to a certain level (<0.01 wt%) dependent on the heat treatment, after which it was almost constant. Associated with the increase in fracture stress was a change in type of fracture from intergranular to transgranular. They considered the most probable explanation of their results, that increased strengthening occurred with increased annealing temperature in the range 600-850°C, to be that boron captures oxygen atoms thus stopping them embrittling the boundaries. This is analogous to the system of iron containing oxygen and carbon discussed in the previous section.

CHAPTER 3 EXPERIMENTAL TECHNIQUES

This Chapter will first of all describe in detail the methods used in the present work to obtain grain boundary and surface energies from measurements of the profiles of grooves (and ridges) formed at the intersections of grain and twin boundaries with the specimen surface. Then the specimen preparation techniques will be outlined and the equipment used for the profile measurements described.

3.1 Relative Energy Measurements

3.1.1 Grain Boundary Grooves

When a metal specimen is heat treated at a temperature greater than about half its melting point grooves form on the surface of the metal along the lines of intersection of grain boundaries with the surface. The equilibrium angle at the base of such grooves is determined by Herring's equation (2.21). For the grain boundary groove depicted in Fig 3.1 the equilibrium condition is

$$\gamma_{gb} = \gamma_1 \cos \theta_1 + \gamma_2 \cos \theta_2 + \frac{\partial \gamma_1}{\partial \theta_1} \sin \theta_1 + \frac{\partial \gamma_2}{\partial \theta_2} \sin \theta_2 \qquad \ldots (3.1)$$

where γ_1 and γ_2 are the surface free energies of grains 1 and 2 respectively. In order to make use of this equation, which as it stands has five unknown parameters, certain simplifying assumptions are usually made. These are

i. that the grain boundary is normal to the specimen surface

ii. that the anisotropy of surface energy is negligible ie $\gamma_1 = \gamma_2 = \gamma_{sv}$ and $\frac{\partial \gamma_1}{\partial \theta_1} = \frac{\partial \gamma_2}{\partial \theta_2} = 0$, and

iii. that the grooves are symmetrical.

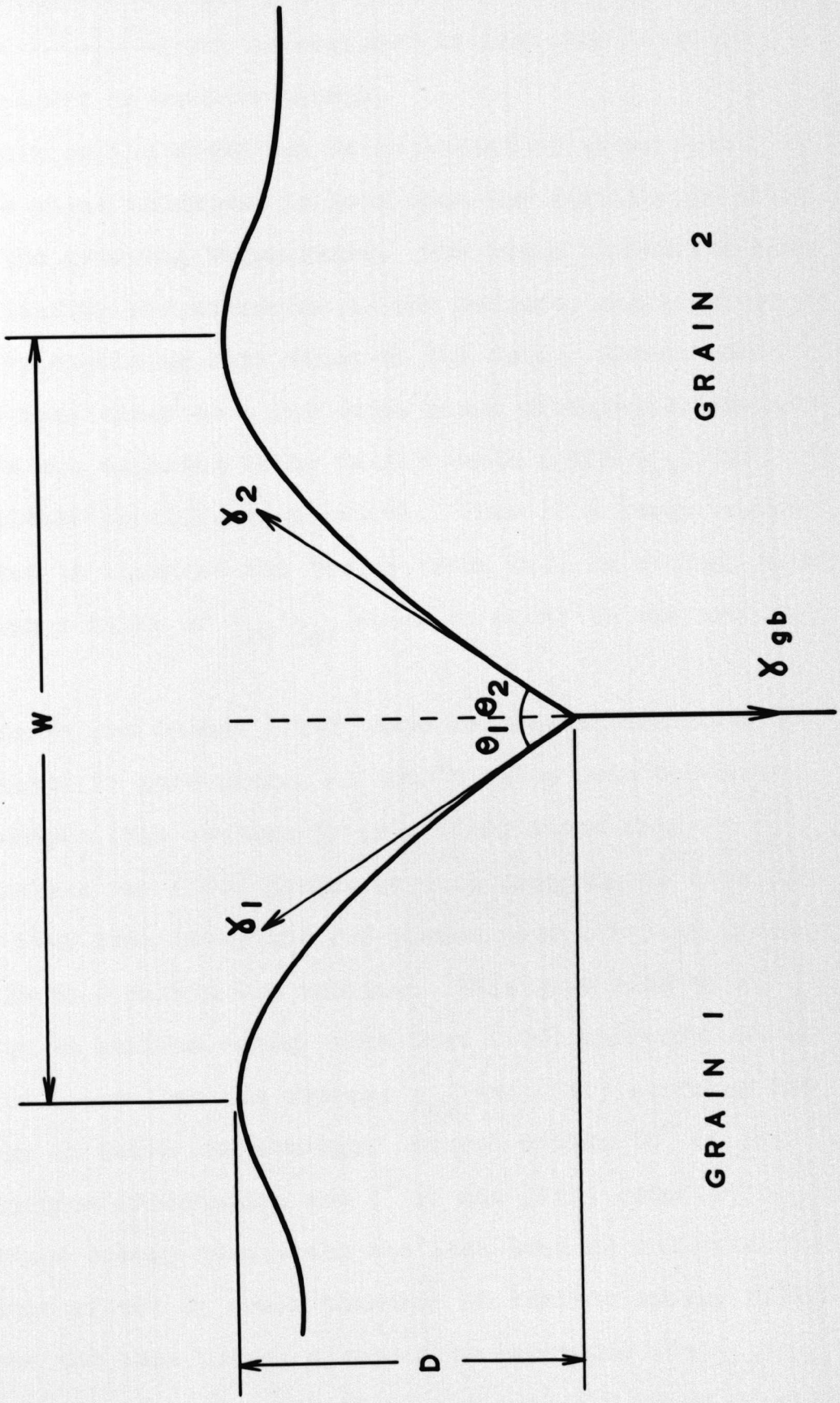

Figure 3.1. Schematic grain boundary groove profile.

These assumptions lead to the simplified equation

$$\gamma_{gb} = 2\gamma_{sv} \cos\left(\frac{\theta_1 + \theta_2}{2}\right). \qquad \ldots (3.2)$$

The angle $\left(\frac{\theta_1 + \theta_2}{2}\right)$ can be measured to give the ratio of grain boundary to surface energy.

Condition (i) above can be satisfied by using foil specimens whose thickness is less than the equilibrium grain size at the grooving temperature. The grain boundaries then tend to line up perpendicular to the surface, and this can be checked by examining both sides of the foil. Except for surfaces very close to a low index plane orientation the torque terms are expected to be fairly small ($\lesssim$10% γ_{sv}) and may be either positive or negative. Thus if a large number of grooves is measured the torque terms will on average cancel out giving a value of γ_{gb}/γ_{sv} which is equal to the true mean value.

Hodgson and Mykura [1973] have made measurements of the torque terms in pure nickel at 1000°C using twin boundary groove shapes (see section 3.1.2). They found that $\frac{1}{\gamma_s}\frac{\partial\gamma}{\partial\alpha}$ was a maximum for (100) planes at 0.24 dropping to zero 0.5 radians away from (100) and for planes near (111) it dropped from 0.20 to 0 within 0.5 radians. This gave rise to a variation in surface energy such that (100) surfaces had an energy 6% lower than the average γ_{sv} and (111) surfaces had an energy 4% below the average. Except within 10° of the (100) surface orientation and 5° of the (111) orientation the surface energy anisotropy was less than 2% and hence had negligible effect on grain boundary to surface energy ratios. They used the same nickel specimen to determine the γ_{gb}/γ_{sv} ratio, first using equation (3.2) and secondly using equation (3.1) with their calculated torque terms. The second set of

measurements had a slightly narrower spread than the first but the ratios obtained, 0.41 ± 0.04 from equation (3.2) and 0.38 ± 0.05 using torque term corrections, agreed well within the experimental error thus amply justifying assumption (ii) above. They attributed the remaining spread in the results to a combination of the genuine variation of grain boundary energy with misorientation across the boundary, errors due to the boundary not being perpendicular to the specimen surface, and some residual torque term errors due to the simplifying assumptions in the analysis they used.

3.1.2 Twin Boundary Grooves and Ridges

Along the line of intersection of a twin boundary with a metal surface a groove can be formed on equilibrating at a high temperature or sometimes a ridge. In the frequently occurring case of parallel pairs of coherent twin boundaries in face centred cubic metals it is usual to find one grooved and one ridged line of intersection. Figure 3.2 represents a cross-section of such a groove-ridge pair. Traces of low index, low energy planes are indicated in Fig 3.2a and the surface energy and torque term forces in Fig 3.2b. It can be seen from these diagrams that the torque terms act so as to rotate the surfaces towards the orientation of the low index planes, thus deepending the groove on the left and, because the coherent twin boundary energy is very low, converting the right hand 'groove' into a ridge.

Mykura [1957 and 1961] considered the application of Herring's equation (2.21) to this situation. Considering each intersection in turn gives

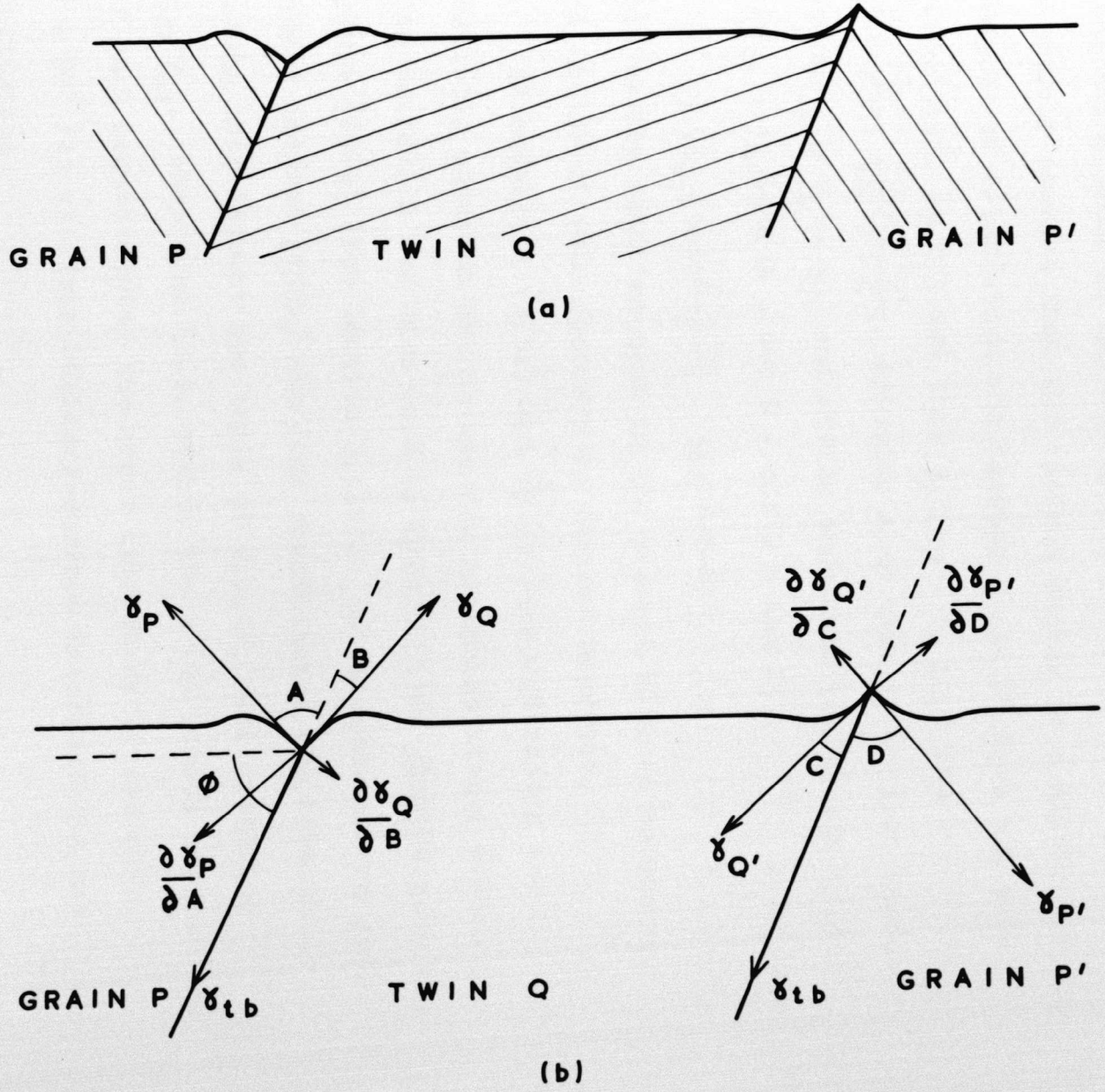

Figure 3.2. Schematic twin boundary groove-ridge pair.

$$\gamma_{tb} = \gamma_P \cos A + \gamma_Q \cos B - \frac{\partial \gamma_P}{\partial A} \sin A - \frac{\partial \gamma_Q}{\partial B} \sin B \quad \ldots (3.3a)$$

$$\gamma_{tb} = -\gamma_{P'} \cos D - \gamma_{Q'} \cos C + \frac{\partial \gamma_{Q'}}{\partial C} \sin C + \frac{\partial \gamma_{P'}}{\partial D} \sin D \quad \ldots (3.3b)$$

using the symbols as defined by Fig 3.2b. If it is then reasonably assumed that the surface energy is a slowly varying function of orientation and because P and P' have the same orientation, it follows that $\gamma_P \simeq \gamma_{P'}$, $\gamma_Q \simeq \gamma_{Q'}$ and $\frac{\partial \gamma_P}{\partial A} \simeq \frac{\partial \gamma_{P'}}{\partial D}$, $\frac{\partial \gamma_Q}{\partial B} \simeq \frac{\partial \gamma_{Q'}}{\partial C}$. Assuming also that to a first approximation $\gamma_P = \gamma_Q = \gamma_{sv}$ and adding equations (3.3a) and (3.3b)

$$2\gamma_{tb} = \gamma_{sv}(\cos A + \cos B - \cos C - \cos D) \quad \ldots (3.4)$$

$$\simeq 2\gamma_{sv}[\cos(\tfrac{A + B}{2}) - \cos(\tfrac{C + D}{2})]. \quad \ldots (3.5)$$

This is the equation used in the present work to determine the ratios of twin boundary to surface energies.

If equations (3.3a) and (3.3b) are subtracted the resulting equation can be used to determine torque terms. This technique has been used by Mykura [1961] and Hodgson and Mykura [1973] (see section 3.1.1). In measurements on pure nickel Hodgson [1972] has also investigated the effects of taking into account the angle of dip, ϕ, when measuring γ_{tb}/γ_{sv}. She found that, within the $\pm$ 10% limits of accuracy of such measurements, the error introduced by assuming $\phi = 90^\circ$ for all twin boundary-surface intersections was negligible.

3.1.3 Mullins' Analysis of Grain Boundary Grooves

Mullins [1957 and 1960] has considered the mechanism and kinetics of growth of grain boundary grooves on metal surfaces at elevated temperatures where rapid diffusion can take place. The possible mechanisms causing growth are surface

diffusion, volume diffusion through either the solid or the vapour phase, and evaporation-condensation, and Mullins considered each of these in turn assuming negligible effect from the others. The equilibrium contact angle means that a groove forms when mass transfer is possible. In the case of diffusion the transfer of mass away from the boundary, and the conservation of mass, causes ridges to form on either side of the groove. In the case of evaporation-condensation the mass is uniformly redeposited so no ridges form.

Mullins' theory is based on the assumption that the surface energy and diffusion coefficients are constant for the range of crystallographic orientations exposed by the groove surfaces. This is a good approximation for high angle grain boundaries. He considered a plane grain boundary intersecting the initially flat surface at right angles and chose a set of cartesian co-ordinates, as shown in Fig 3.3. He then used the Gibbs-Thomson formula to relate the chemical potential of an atom on the groove surface to the local curvature. The transport of matter induced by differences in chemical potential, and the concomitant development of groove topography, were calculated for each mechanism in turn. He used an approximation that depends on the groove surfaces always having small slopes. The grain boundary enters the theory as a mathematical boundary condition requiring a fixed discontinuity of slope at the groove root.

When surface diffusion is operating alone the groove profile at time t is described by

$$y_s(x,t) = m(Bt)^{1/4}\, Z[x/(Bt)^{1/4}] \qquad \ldots (3.6)$$

where $B = D_s \gamma_s n \Omega^2/kT$ in which n denotes the number of

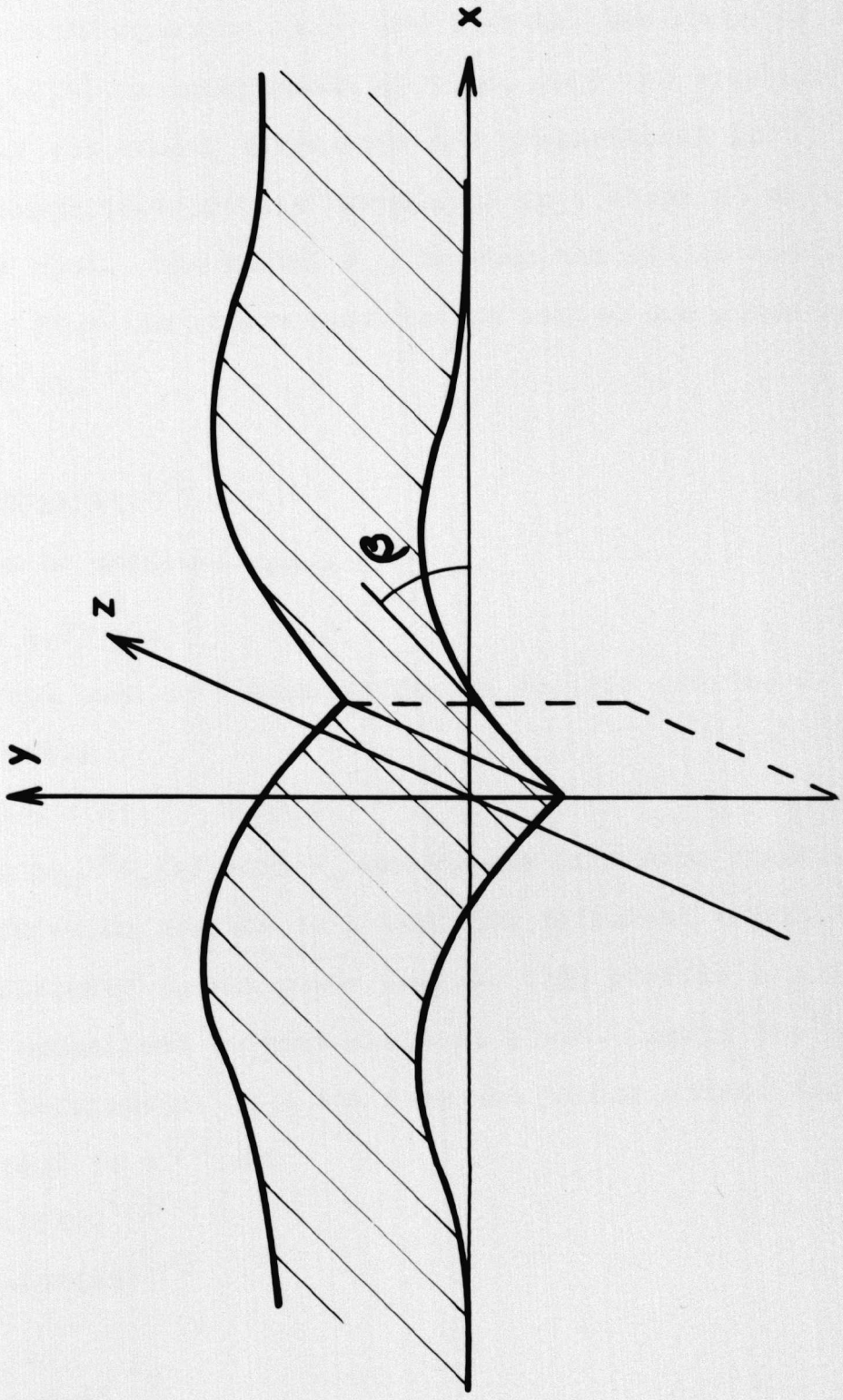

Figure 3.3. Cartesian coordinates used by Mullins.

atoms/cm^2 of surface, Ω is the atomic volume and kT has its usual meaning; $m = \gamma_{gb}/2\gamma_s$ is the slope at the groove root and Z is a function defined by a certain power series. Two consequences of equation (3.6) are that (a) the shape of the profile $y_s(x,t)$ is independent of time, only the size changes, and (b) all the linear dimensions are proportional to $t^{1/4}$. Fig 3.4a shows this profile normalised to a slope of unity at the groove root. The width, W_s, between the maxima and the depth, d_s, from the groove root to the maxima are given by

$$W_s = 4.6(Bt)^{1/4} \qquad \ldots (3.7a)$$

and

$$d_s = 0.973m(Bt)^{1/4} \qquad \ldots (3.7b)$$

from which we obtain

$$\tan \frac{\Psi}{2} = 4.73 \frac{W_s}{d_s}. \qquad \ldots (3.8)$$

For the case of volume diffusion Mullins derived a groove profile

$$y_v(x,t) = m(At)^{1/3} X[x/(At)^{1/3}] \qquad \ldots (3.9)$$

where $A = n\gamma_s \Omega^2 D_v/kT$ with D_v the volume diffusion coefficient and X a function similar to Z but with different values of the coefficients in the power series. The profile is shown in Fig 3.4b normalised to unit slope at $x = 0$. Again the profile shape is independent of t but here the linear dimensions are proportional to $t^{1/3}$ and

$$W_v = 5.0(At)^{1/3} \qquad \ldots (3.10a)$$

$$d_v = 1.01m(At)^{1/3} \qquad \ldots (3.10b)$$

so that

$$\tan \frac{\Psi}{2} = 4.95 \frac{W_v}{d_v}. \qquad \ldots (3.11)$$

If the groove grows by an evaporation-condensation mechanism Mullins [1957] showed that no ridges are produced

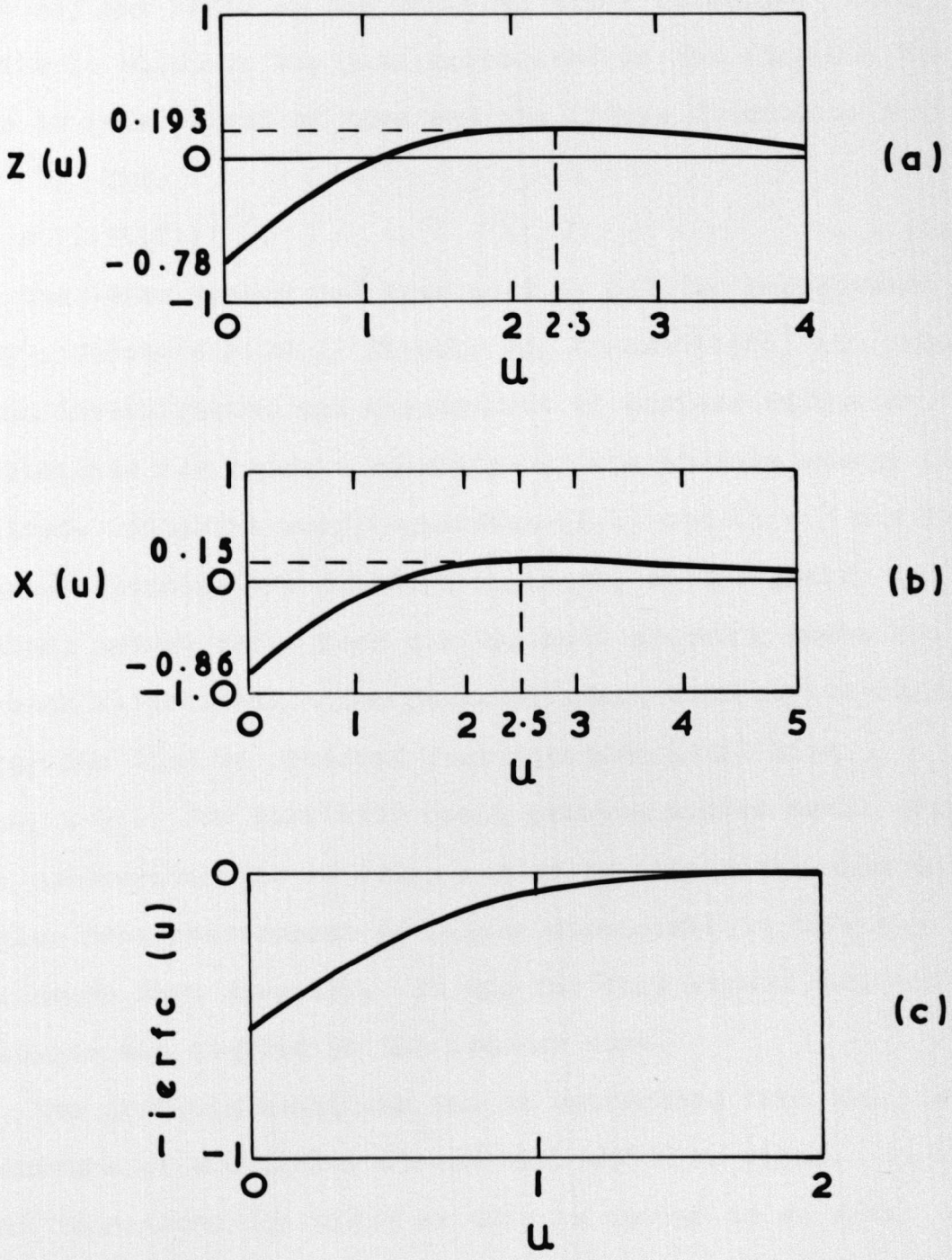

Figure 3.4. Grain boundary groove profiles formed by (a) surface diffusion, (b) volume diffusion and (c) evaporation-condensation.

and the profile is described by

$$y_e(x,t) = -2m(Ct)^{1/2}\ \text{ierfc}[x/2(At)^{1/2}] \qquad \ldots (3.12)$$

where $C = P_o\gamma_s\Omega^2/(2\pi M)^{1/2}(kT)^{3/2}$ with P_o the vapour pressure in equilibrium with a plane surface and M the weight of a molecule, and ierfc is the integral error function. This profile is shown in Fig 3.4c normalised as the others. The shape is independent of time and the linear dimensions increase as $t^{1/2}$. Thus

$$d_e = 1.13m(Ct)^{1/2}. \qquad \ldots (3.13)$$

The above theory has been used by Mullins and Shewmon [1959], Gjostein [1961], Blakely and Mykura [1963] and others in the investigation and measurement of surface diffusion coefficients for which a knowledge of the surface energy is required. Alternatively, equations (3.8) and (3.11) can be used to determine the dihedral angle, Ψ, at the grain boundary groove root, once the dominant grooving mechanism has been established. The ratio of grain boundary to surface energy can then be obtained from equation (3.2) with $\Psi = \theta_1 + \theta_2$. For work with small grooves and/or small grain size polycrystals it is often easier to obtain the dihedral angles from measurement of linear dimensions in this way than to measure them directly. It was for this reason that the technique was adopted in the present work.

The grooving mechanism can be determined from the time dependence of the groove dimensions, width or depth. It is usual to measure the width as this is easier to do with accuracy. Thus if a graph is plotted of log W vs log t the result should be a straight line whose slope is equal to 1/4, 1/3 or 1/2 if either surface diffusion, volume diffusion or evaporation-condensation accounts entirely for the groove

growth. An intermediate value of the slope indicates that more than one mechanism is operative and Mullins and Shewmon [1959] showed how data on grooves formed predominantly by surface diffusion can be corrected for a volume diffusion contribution if the volume diffusion coefficient is known.

Mullins' theories of grooving do not take account of the initial stages of growth when the mechanism may be different and where the atomic nature of the surface will certainly be important. Instead he assumes that the details of the initial groove formation will have negligible influence on the later development of the groove during which any effects arising from the atomistic nature of the crystals are ignored. McAllister and Cutler [1969 and 1970] have pointed out that a groove may have a significant width before Mullins' formulae become applicable. They therefore suggest adding a finite width at time zero to compensate for the transient conditions of initial growth of the groove to an equilibrium configuration. Such a non-zero initial width condition makes conclusions based on the slopes of log-log plots suspect as discussed by several authors, eg Mistler and Coble [1968], in connection with grain growth measurements.

McAllister and Cutler's suggested alternative for interpreting thermal grooving data is to plot W vs $t^{1/n}$ directly and accept the value which gives a positive width at time zero. They have reanalysed the data of Mullins and Shewmon [1969] and Gjostein [1961] on this basis, and reject the $t^{1/4}$ dependence simply on the basis of a negative value of W at $t = 0$. However, they give no indication of whether the initial stages of growth should be faster or slower than the later stages, and as the data they are considering is based

on zero time being the start of groove formation their statement that W must be positive for t = 0 would seem to be questionable.

A further practical difficulty with McAllister and Cutler's arguments is that when the groove is very small (ie for small t) it is difficult to detect grain boundary migration. Once a boundary groove has grown to some depth, the groove acts as an anchor against grain boundary migration. Thus the true time of start of growth is likely to be somewhat after t = 0 experimentally. Gjostein [1970] has also challenged their reinterpretation of his data on the grounds that they have not allowed for any minor contributions to groove formation from other diffusion mechanisms. Their graphs of W vs $t^{1/n}$ use only two points for each temperature thus hiding the curvature which Gjostein shows to be present. Because of the doubts raised about the simple use of log-log plots, however, both types of graphs were considered when interpreting the kinetic data obtained in the present work.

3.2 Specimen Preparation

3.2.1 Metallography

The steels were received as strips which had been cold rolled to their thickness of ~0.5 mm. There were, consequently, rolling marks in the form of ridges on the surfaces of the material which it was found didnot completely disappear during the thermal grooving treatments so that they interfered with the measurement of the groove shapes. The iron alloys were received as cast billets which were sliced and cold rolled, again to ~0.5 mm thickness, thus posing the same problem. This was overcome in both cases by metallographically polishing

one side of each specimen.

The specimens were cut from the sheet materials approximately 1 cm^2 which is a rather large area over which to obtain a uniform, scratch free metallographic polish, so that great care had to be exercised in the polishing process. The specimens were mounted in bakelite with a backing piece of 0.16 mm thick aluminium foil the same size as the specimen to facilitate removal from the mount after polishing. If the piece of foil was big enough to overlap the edges of the specimen and thus have its edge polished it tended to pick up small particles during one part of the process and deposit them at a later stage causing severe scratching of the specimen surface. If the aluminium was dispensed with or was too small, the bakelite bonded strongly to the specimen and it could not be removed from the mount without damage.

After mounting the specimens were first ground flat on a Lapmaster* which uses 600 grade silicon carbide grit on a cast iron lap and gives a surface which is flat to within about 1/2μm on a 1 1/4 inch diameter specimen. The second stage was to lap with 6μm diamond paste and a plywood lap on a 'Harwell' lapping machine (manufactured by Kristalap Ltd) for one or two periods of 5 mins each until none of the surface damage due to the Lapmaster could be seen on examination with a bench microscope.

Stage 3 was to polish on a Hyprocel Pellon pad K, which has a fairly hard finish, again using 6μm diamond grit and Hyprocel lubricant for one or two 5 minute periods. The scratches left after this step were removed by polishing with 1 μm diamond grit and Hyprocel lubricant on a Hyprocel Pellon

---

*Registered trade mark of Payne Products International Ltd.

Pan K pad, which has a fairly soft fibrous texture, for one or two periods of 1 minute. In between each polishing or lapping period the specimen was thoroughly cleaned with detergent and then ultrasonically agitated in methylated spirits for 5-10 minutes. Except in the case of the Lapmaster, which has a continuous flow of grit suspended in lubricant over the lap, the lap or pad was thoroughly cleaned of debris and fresh diamond and lubricant applied between each polishing period.

If at any stage during this process a satisfactory finish for the step could not be obtained - sometimes for instance large scratches would mysteriously appear after the 6μm pad, probably due to some contamination of the pad by dust or insufficiently thorough cleaning of the specimen - the specimen was taken back to an earlier stage until satisfactory results were obtained. At the end of this procedure the specimens usually had a few small scratches on them which were just detectable on an interference microscope and which were completely smoothed out during the heat treatments to produce grooves on the surfaces.

3.2.2 Vacuum Annealing Equipment

In the investigation of surface effects it is necessary that the surface of interest should not become contaminated with impurities from the test environment which might alter the effects being studied. This means that any solid material with which the surface may be in contact must be clean and chosen such that it is inert with respect to the specimen material. The commonest form of surface contaminants, however, come from the surrounding gas phase. It is for this

reason that almost all surface studies are conducted in vacuo or in a purified inert gas atmosphere.

The present work was conducted on surfaces prepared in a vacuum of better than 10^{-6} Torr. This was achieved in a water cooled stainless steel vacuum chamber with metal sealed flanges. An overall view of the vacuum chamber is shown in Fig 3.5 and a schematic representation of the layout of the pumping system in Fig 3.6. The large horizontal flanges were sealed using gold wire gaskets and the smaller ones had knife edges which sealed against copper gaskets. Inside the chamber was a molybdenum platform with a thermocouple in its centre placed so that the hot junction was close to the top of the platform. The thermocouple was calibrated by melting drops of metal on alumina plaques on the platform which could be observed through the viewing ports which were lined up with small holes cut in the radiation shields and the heating element. Around the platform was a one inch diameter tantalum split cylindrical resistance heater which was suspended from two water cooled copper electrodes. Surrounding the heating element were six cylindrical tantalum radiation shields and above and below were placed packs of 4 horizontal radiation shields to cut down the heat losses to the chamber walls. The specimen was loaded into the chamber through a port in the top flange into which an ionisation gauge was fitted.

The chamber was pumped through the side arm by a four inch diffusion pump, a two inch diffusion pump and a rotary backing pump connected in series. This arrangement has been found to give high evacuation rates and a good ultimate vacuum. Between the 4 inch pump and the chamber a thermo-electrically cooled chevron baffle to prevent back diffusion

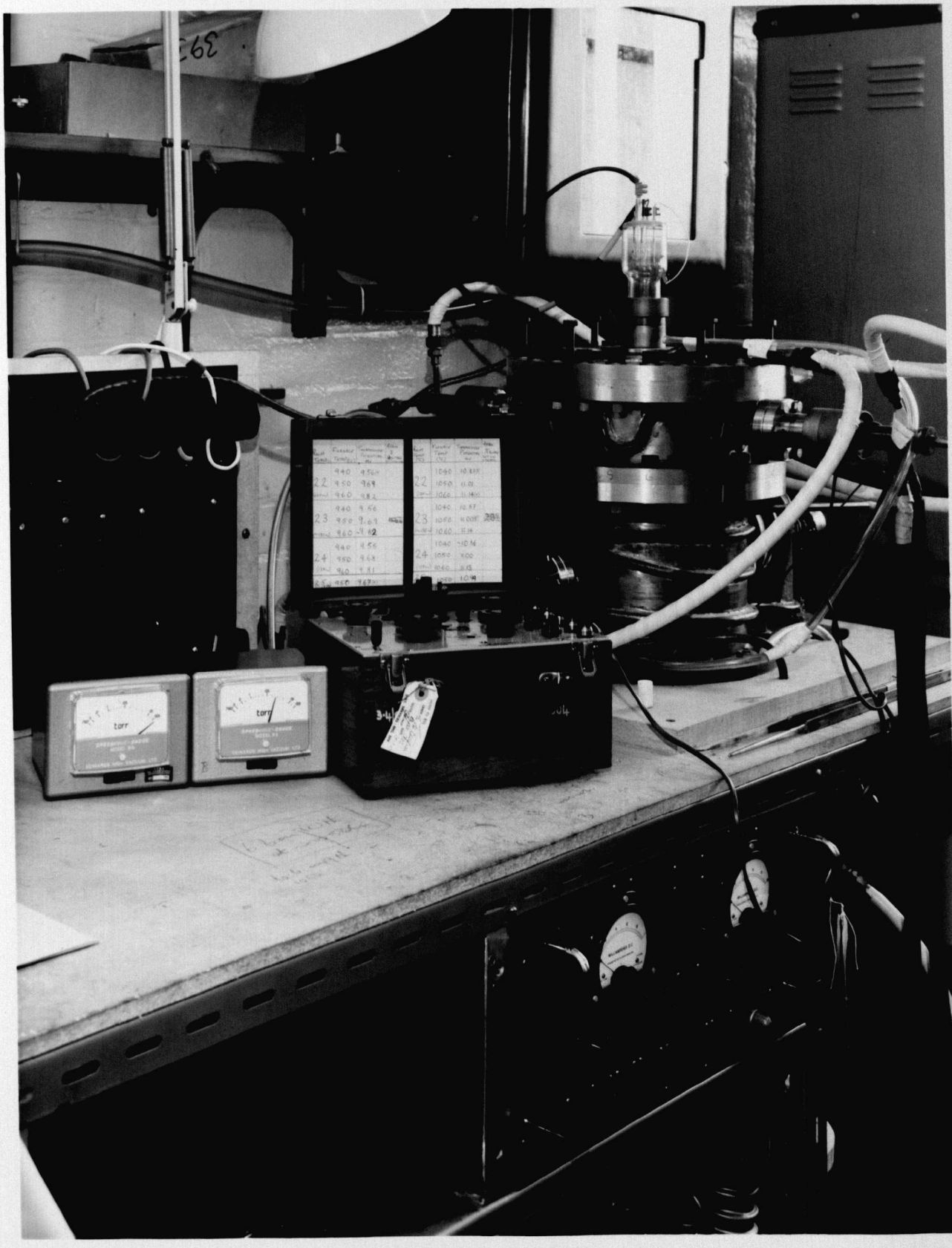

Figure 3.5. Vacuum furnace.

of the silicone oil vapour into the chamber and a butterfly isolation valve were positioned between stainless steel spacers to allow room for the valve to operate and facilitate connection to the rotary pump for rough pumping of the chamber.

Power was supplied to the resistance heating element from a constant power unit designed and manufactured by Hirst Electronics Ltd. This provided a low dc voltage (up to 6v) and high current (max 10^3 amps) and had a feedback system to a comparison unit which ensured that the power output of the unit was held constant for a given setting. With this power supply the temperature inside the furnace could be held constant to $\pm 5^{o}C$. The variation was due mainly to fluctuations in the temperature of the laboratory and the cooling water.

3.3 Groove Profile Measurements

The grain boundary groove profiles were quite easily measured using a Zeiss-Linnik interference microscope (section 3.3.1). However, because twin boundary energies are much lower than grain boundary energies the profiles formed at their intersection with the surface are much shallower. It was found that measurements of twin boundary profiles made on the interferograms were not accurate enough for the determination of interfacial energy ratios. This was particularly serious in the case of the steel specimens where the annealing times were deliberately kept fairly short. The twin boundary profile measurements were therefore made using a Talystep* II instrument (section 3.3.2) which is capable of much higher vertical magnifications than can be obtained by interferometry.

---

*Registered trade mark of Rank Taylor Hobson Ltd

3.3.1 Interference Microscope

A Zeiss Linnik-type interference microscope was used for the measurements on grain boundary groove profiles. This instrument and its principle of operation are illustrated in Fig 3.7. Monochromatic 'thallium' light of wavelength 0.54μm is supplied by the source Q. The light passes to a beam splitting prism P whence half the light goes to the reference surface S_R and the other half to the specimen surface S_P. O_1 and O_2 are identical objective lenses enabling images of S_R and S_P to be superimposed and viewed through an eyepiece E. If the path lengths of the two beams from the prism P to S_R and S_P then back to E are exactly equal, or differ by λ, and S_R and S_P are accurately perpendicular to their respective incident beams, bright images of the two surfaces are seen through E, superimposed on each other. If now S_R is tilted interference bands appear on the image seen at E because the path lengths of rays forming each part of the images are no longer equal for both S_R and S_P. For the same reason irregularities in the specimen surfaces produce localised sets of fringes if S_R and S_P are exactly perpendicular or deviations of the straight, parallel set of interference bands if S_R or S_P is inclined to the incident beam.

By changing the inclination of S_R the spacing and direction of the interference fringes can be varied. However, this method of adjusting the fringes hss the disadvantage that only a few fringes can be sharply focussed. The fringes can be adjusted more simply by tilting a plane-parallel plate G_1 in the beam while S_R is kept perpendicular to the beam. In this way all the fringes in the field of view can be sharply in focus. A second plate G_2 is placed in the path of the

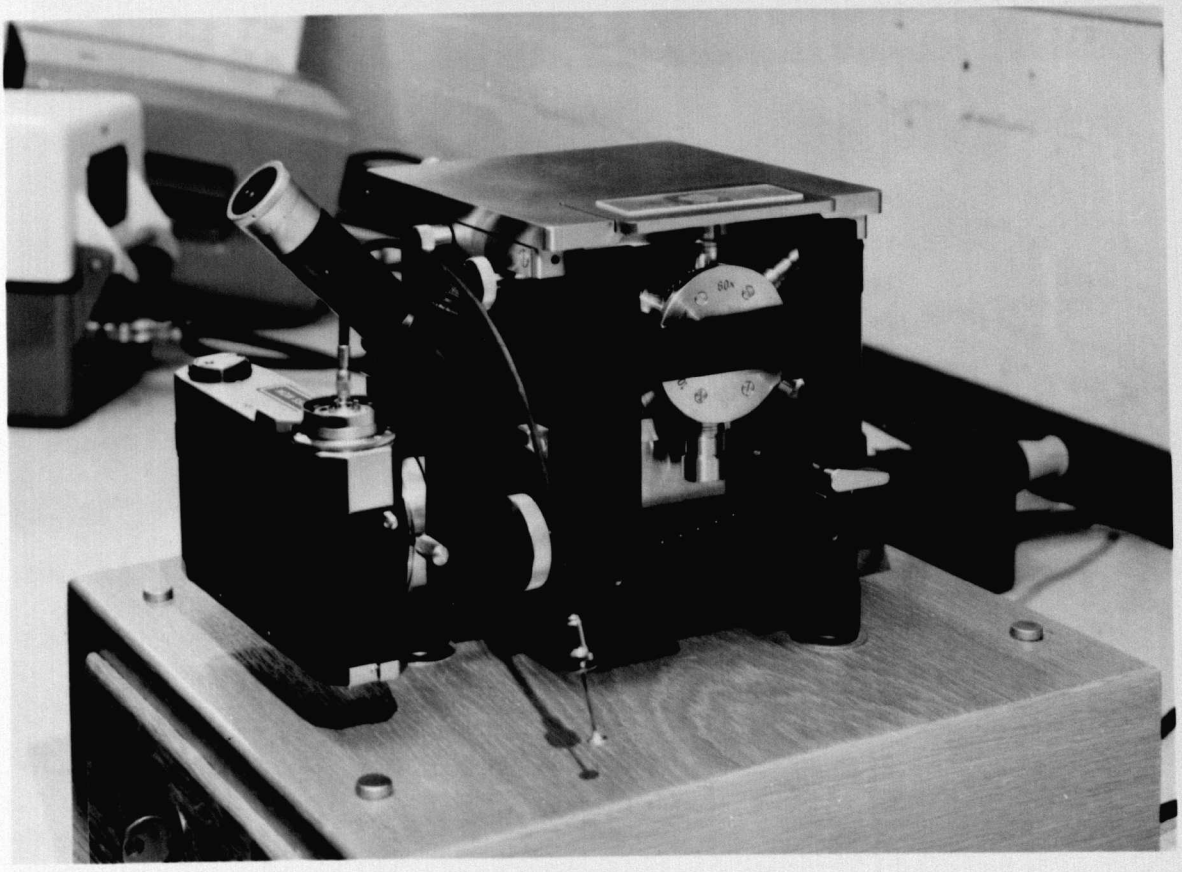

(a)

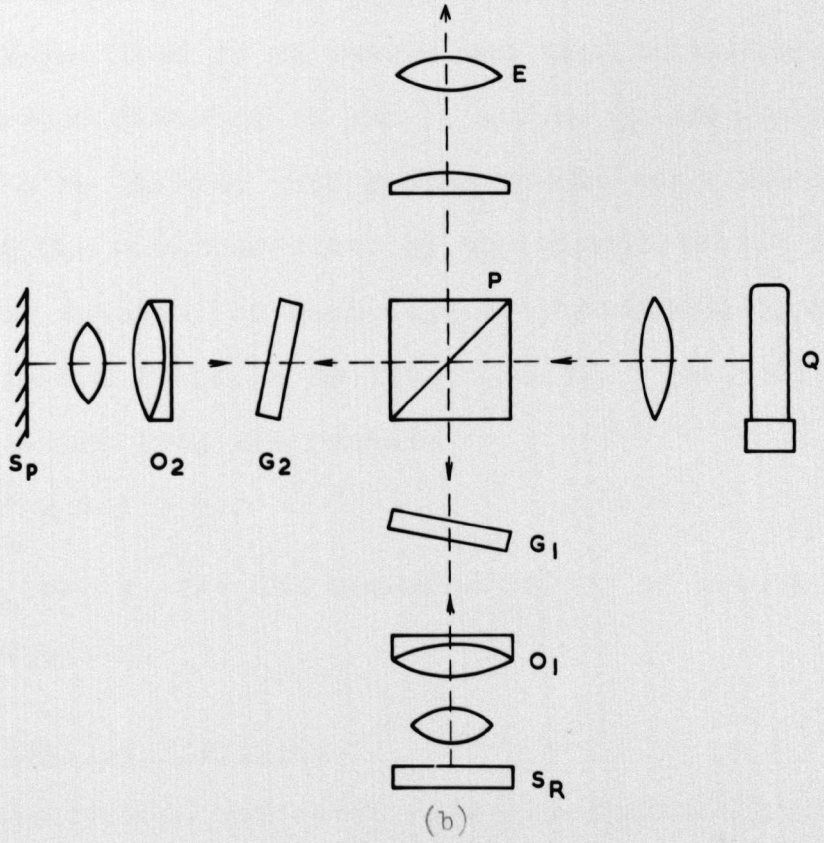

(b)

Figure 3.7(a) Zeiss interference microscope and (b) its principle of operation.

other beam, as shown, in order to equalise the two beams.

The spacing of the interference fringes represents a change in the height of the specimen surface (assuming S_R to be perfectly flat) equal to half the wavelength, λ, of the incident light, or 0.27 μm. This statement is accurately true for parallel, normal illumination and therefore objective lenses of small numerical aperture. However, for lenses with larger apertures a correction must be applied to account for the wide range of angles of incidence. Tolman and Wood [1956] first investigated the effect of using high aperture objectives and they found experimentally that for numerical apertures of about 0.6 the fringe spacing was equal to $1.1\lambda/2$. As a cross check for the particular arrangement used here, with an objective lens of numerical aperture 0.63 used at not quite full aperture, a calibrated step of height 0.39 μm was measured. The step height was found to be equal to 1.3 fringes indicating a fringe spacing of 0.30 μm ($\simeq 1.1 \times 0.27$).

A Zeiss Ikon 35 mm camera was used to photograph the interference patterns on Pan F, a fine grained black and white film made by Ilford. The groove widths were obtained by dividing the measured width by the magnification on the film which was checked for each film by photographing a standard graticule and found to be 116.1 ± 0.5X. The groove depths were obtained from the formula

$$d = \frac{d_m}{s_m} \times 1.1 \times \frac{\lambda}{2}$$

where d_m and s_m are the measured values of groove depth and fringe spacing.

3.3.2 Profile Projector

Measurements were made directly from the 35 mm films

(a)

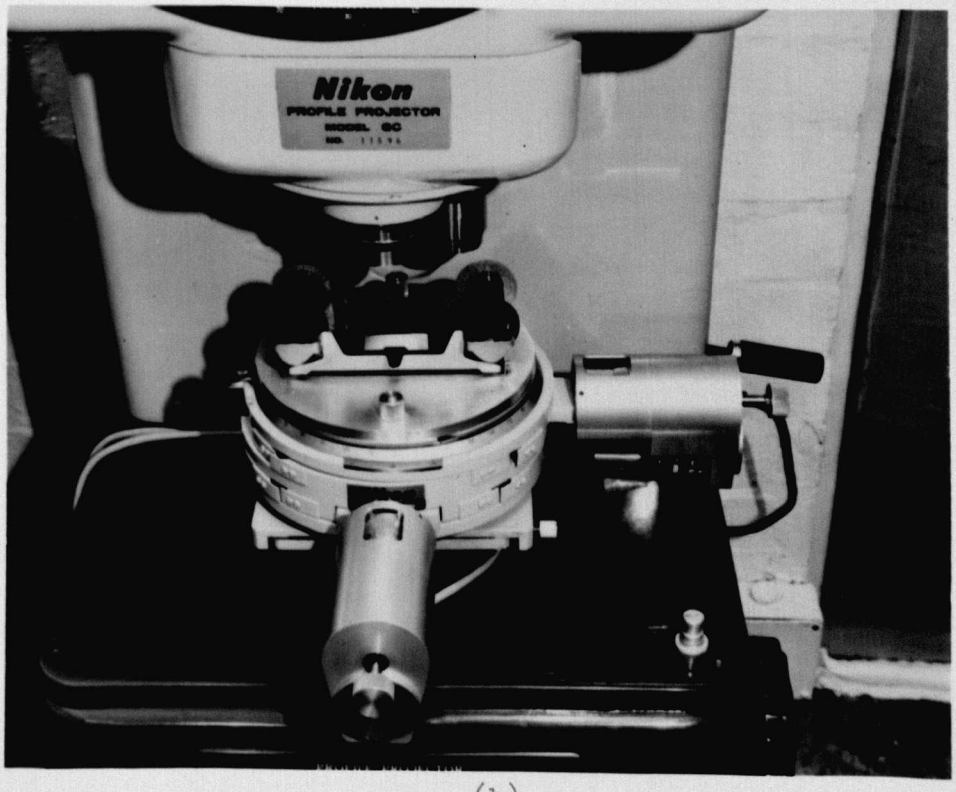

(b)

Figure 3.8. Nikon profile projector (a) overall view and (b) close up of micrometer stage.

using a Nikon Profile Projector illustrated in Fig 3.8. The projector has a graduated rotatable viewing screen on which cross-lines are marked and this was used for direct angular measurements. A rotatable micrometer stage (with movement in two mutually perpendicular horizontal directions) was specially adapted by Electronics Division, AERE Harwell to be controlled by two linear stepping motors. These were arranged so that one step of the motor advances the stage through a distance of 1 micron. Electric pulses are fed to each motor from a control unit and simultaneously counted on a bi-directional scalar unit. Thus the number of pulses gives the distance in microns moved by the stage holding the film and hence distances on the film can be measured directly without need for enlarged prints. Distances measured in this way, using forward and reverse directions on the stepping motors were found to be reproducible to $\pm$ 1 μm at a sharply defined edge. The major inaccuracies in measuring the interferograms thus arose from the lack of sharpness of the fringes.

3.3.3 Talystep

3.3.3.1 Basic Instrument

The Talystep is a stylus-type surface profile measuring instrument designed and manufactured by Rank Taylor Hobson Ltd for measuring the thickness of thin film deposits important in, for example miniature and micro-miniature electronic circuitry. It is thus designed to measure the heights of very small surface steps or grooves cut in such deposits. The complete instrument is shown in Fig 3.9. It works by traversing a sharp diamond stylus across the specimen surface at a constant speed and measuring the vertical displacement

Figure 3.9. Talystep instrument.

of the stylus by means of a variable air gap differential inductance transducer. The output from the transducer is amplified electronically to give the required vertical magnification of between 5000X and 10^6X on a rectilinear chart recorder. The marking on the chart is made electrically, giving a fine line from which to make measurements. The pick-up and stylus are carried on a vertical slide on a bracket which is hinged vertically to a column of the machine so that the stylus traverse is an arc of radius about 50 mm and length 2 mm. The horizontal magnifications are provided by varying the traverse speed and are 50X, 200X and 2000X.

A simple viewing microscope of magnification X 10 is provided to facilitate positioning of the specimen and is useful for seeing when the stylus comes into contact with the specimen surface. Lighting of the stylus area is provided by a small fibre optic assembly and an adjustable reflector mounted underneath the pick-up. This arrangement keeps the heating effect of the light down to a minimum while making it effective for viewing. Means are provided for tilting the platform to level the specimen surface. The measuring unit sits on an antivibration platform and is located in a ground floor laboratory because the pick-up is sensitive to vibrations - at the highest magnifications it will even pick up acoustic vibrations from an animated conversation.

The normal stylus provided with the instrument is conical with a tip radius of 12.5 μm which is adequate for simple step height measurements. However, for the twin boundary profile measurements a sharper stylus which is also suitable for surface roughness measurements was obtained. This is chisel-shaped and its end face is a rectangle 2.5 x 0.1 μm.

It is mounted in its holder so that the short edge is always parallel to the traverse direction. This makes it very suitable for measuring small grooves which run perpendicular to the traverse direction.

3.3.3.2 Modifications

In order to be able to use the Talystep to measure the profiles of twin boundary grooves and ridges (or indeed any other very small features) it is necessary to be able to locate the feature under the stylus and to align it with respect to the stylus traverse. In this way a profile can be measured in a direction perpendicular to the line of intersection of a twin boundary with the surface. The viewing microscope on the instrument was not powerful enough to resolve the grain structure of the specimens and to replace it with a powerful enough one was not possible because the focal length of the objective would have had to be so short that the microscope and stylus would be too close together. Instead, a special transferable 'nest' was designed in collaboration with Rank Taylor Hobson's Special Applications Department.

This 'nest' is shown located on a bench microscope in Fig 3.10a. The specimen is seen attached to a flat cylindrical holder which can be moved relative to the nest in two perpendicular directions, by means of the two pairs of screws visible on the sides of the nest and can be rotated. The nest is located in a particular position and orientation on the microscope stage and the specimen viewed through the microscope at a magnification suitable to pick out the twin boundaries (~ 100X). The specimen holder is then moved within the nest until a suitable pair of twin boundaries is located

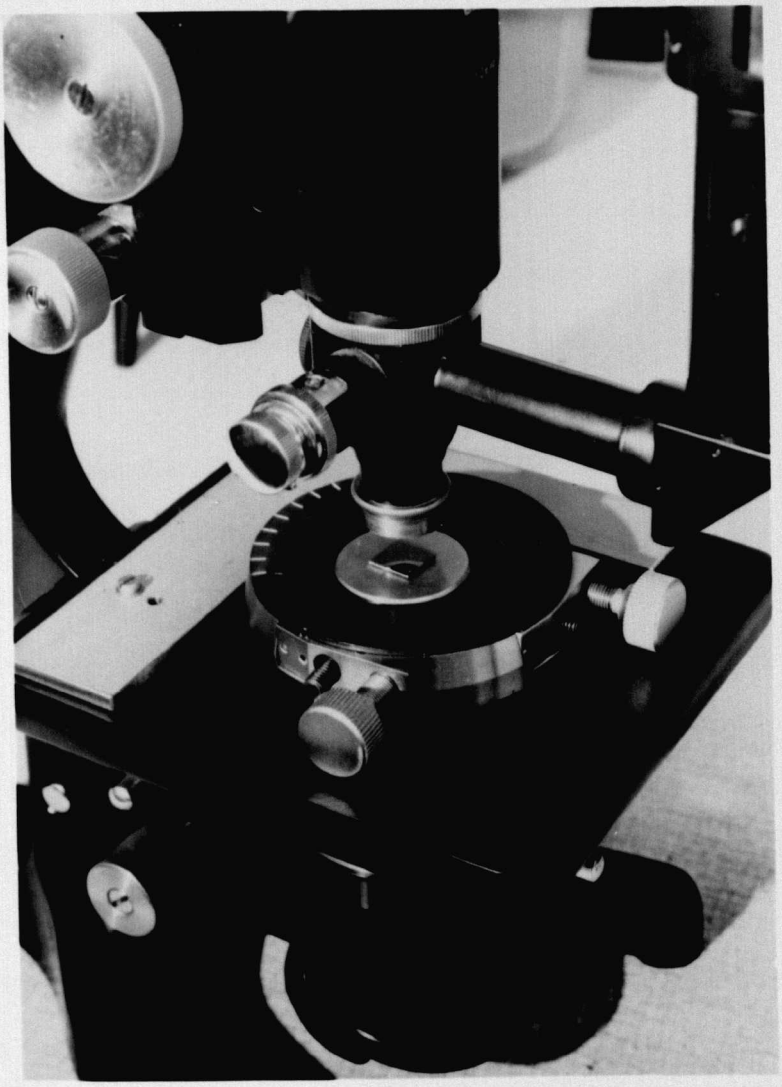

(a)

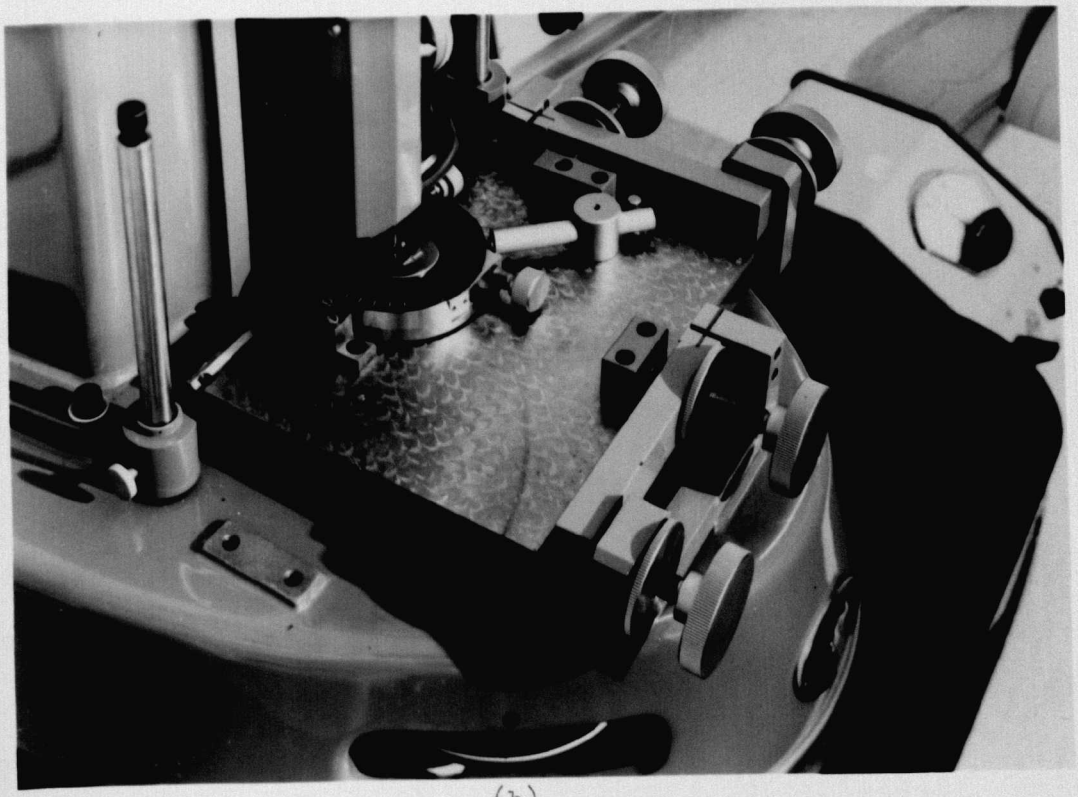

(b)

Figure 3.10. Talystep "nest" (a) on bench microscope and (b) in position on Talystep workstage.

and lined up parallel to one of the cross lines in the microscope eyepiece. The complete nest is then transferred to the Talystep workstage (see Fig 3.10b) and again located in a set position so that the stylus can be made to traverse the twin boundaries previously located under the bench microscope.

In order to set up the workstage precisely, fine adjustment screws were attached to it in place of the original coarser micrometers. A microscope eyepiece graticule with deposited cross lines was mounted on a specimen holder in the nest and lined up at ~45° to the microscope cross lines and cocentral with them. The nest was then transferred to the Talystep and the position of the workstage adjusted so that the stylus traversed the intersection of the cross lines. The traverse indicator dial was then zeroed at this intersection point. It was found that, with care, a linear displacement error of less than 1 μm could be achieved in the transfer operation. A further modification supplied by Rank Taylor Hobson at our request was a slower speed traverse motor to provide a horizontal magnification of 5000X instead of the 2000X on the standard instrument.

3.3.3.3 Accuracy

King et al [1972] have compared the Talystep with multiple beam interferometry and photoelastic shearing interferometry for the determination of film thicknesses by measuring the step height at the edge of the film. They found excellent agreement between the three methods on films with thicknesses ranging from 100 to 2000 Å, the difference in measured thickness rarely being more than 10 Å from one instrument to another. An accuracy of the same order was

indicated (both in their experience and ours) by the reproducibility of measurement of the calibration standards provided with the instrument.

The twin boundary traces were taken with a vertical magnification of X 200,000 which usually gave a depth of groove of between 30 and 50 mms on the graph. This depth could be measured to ± 0.5 mm with a ruler which is equivalent to an accuracy of ± 25 Å or ± 1%. The horizontal magnification was checked using a standard ruled grating with 100 divisions in 1 mm (ie each division 10 μm wide). The accuracy at X 5000 magnification was found to be ± 0.6 μm, this being no worse than the accuracy of the rulings on the grating.

A Talystep trace across a pair of twin boundaries is shown in Fig 3.11 with, for comparison, a normal and an interference micrograph of the same pair of boundaries taken on the Zeiss interference microscope. A check was made for possible distortion of the profiles due to plastic deformation of the specimen by the stylus, by moving the stylus backwards and forwards several times across the same twin profile. No measurable change occurred in the recorded profile shape. The dihedral angles were measured from the Talystep traces and the true dihedral angles calculated from the formula

$$\tan \frac{\Psi}{2} \text{ actual} = 40 \times \tan \frac{\Psi}{2} \text{ measured.}$$

Because of the finite width of the diamond stylus it cannot reach the bottom of sharply pointed grooves. On the steepest grooves measured (included angle 160°) the depth of groove below the stylus when it bottomed would be about 60 Å, equivalent to about 1 mm on the recorder chart. It was considered, however, that the angular measurements would not be affected by this problem when the lower portions of the

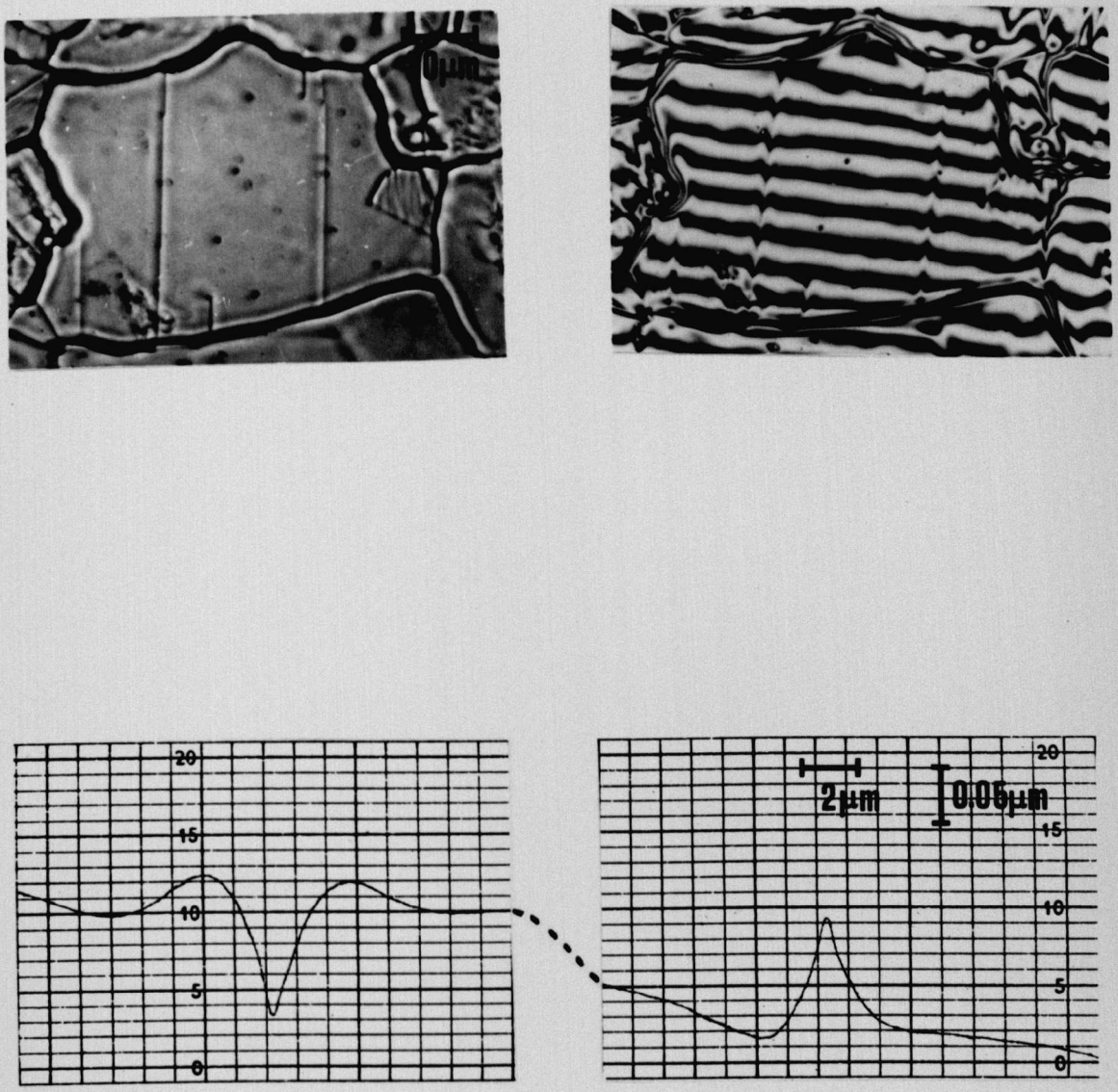

Figure 3.11. Twin boundary groove-ridge pair.

grooves were straight sided, which they usually were over about half their depth. Similarly the ridges might be expected to show a flat portion on the top of about 1/2 mm at 5000X horizontal magnification but this was never unambiguously observed.

A more serious source of error in the angular measurements arises from any inaccuracy in the alignment of the boundary trace with respect to the stylus traverse direction. In an extreme case if the misalignment was 5° and the groove angle was 83° this could lead to an error in the dihedral angle of $+ 1\,1/2^{\circ}$ and thus in its cosine of - 0.0004, comparable in magnitude to many of the twin boundary ratios obtained. However, the situation is not in fact as bad as would at first appear for two reasons. First, the alignment error is unlikely to be as much as 5° - probably $\pm 2^{\circ}$ is a more realistic estimate - and second, the error would be in the same direction for both the groove and the ridge thus tending to cancel out when the two cosines are subtracted.

It was found in practice that the angles could be measured on the traces to an apparent accuracy of usually better than $\pm 2^{\circ}$, giving an error of about $\pm$ 20% in tan $\frac{\Psi}{2}$ measured, somewhat greater than the inherent errors indicated in the above paragraphs. This could lead to an inaccuracy of $\pm$ 15-25% in the cosine of $\frac{\Psi}{2}$ actual and thus to a maximum error in γ_{tb}/γ_{sv} of 30-50%. This of course would be the error on each individual value of the ratio and the uncertainty on the mean of about 50 values was much less.

3.3.4 Statistical Treatment of Results

The energies of grain boundaries and surfaces vary with their orientation with respect to the bulk crystal lattice. The effects of surface energy variations have been discussed in Sections 3.1.1 and 3.1.2. Another important parameter in the case of grain boundaries is the difference in orientation between the grains on either side of the boundary. When the misorientation is low the boundary can be represented by an array of well spaced dislocations and has a low energy. However, in most cases the energy (and dislocation density) increases rapidly with increasing misorientation to reach either a plateau or a broad maximum. Gleiter and Chalmers [1972] have recently reviewed the experimental measurements and theoretical calculations of grain boundary energies as a function of orientation and other parameters.

In order to characterise the polycrystalline specimens used in the present work an 'average' high angle grain boundary energy was calculated for each specimen. To do this a large number (at least 50) of grain boundary grooves were measured and the mean taken. In doing this the surface torque terms were assumed to cancel out (see Section 3.1.1). A computer program was written to calculate the mean grain boundary to surface energy ratio, the standard deviation and standard error of the mean, from the measured values of groove width and depth and the interference fringe spacing. A large number of twin boundary to surface energy ratios were similarly averaged. Both the grain boundary and surface energies were expressed as multiples of the twin boundary energy, which was assumed to be independent of boron concentration. This assumption is considered to be reasonable as twin boundaries

are high density coincidence boundaries of very low energy and thus the driving force for solute segregation to them should be extremely low.

4.1 Materials and Annealing Treatments

AISI 316 is an austenitic steel containing approximately 16-18 wt% chromium, 10-14 wt% nickel and 2-3 wt% molybdenum plus several other minor constituents. Four casts* of steel originally from the same billet but with their carbon and boron concentrations systematically varied to give a set of alloys with two carbon and two boron levels were used for the present work. The detailed compositions of the steels are given in Table 4.1, from which it can be seen that the variations in all the constituents are minor except for the deliberately varied carbon and boron levels and the silicon level which was higher in steels I and IV than in steels II and III. In future the steels will be identified by the numbers I-IV as given in the first column of Table 4.1.

Specimens were prepared from these steels as described in Chapter 3 (3.2.1) and annealed in the diffusion pumped vacuum furnace for various times between 1 and 50 hours. For the energy ratio measurements the annealing times were chosen to correspond approximately to the times used in practice for the solution treatment of these steels. These times were fairly short (3 hours at 1050°C and 1 hour at 1150 or 1250°C) so that the grain sizes, initially 10-20 μm diameter, remained quite small (~100 μm). At 950°C the grain size stayed so small (~30 μm) that groove profile measurements could not be made satisfactorily, so these specimens were first annealed for 1 hour at 1050°C to approximately double the grain size

*Originally obtained from the Electrical Research Association.

TABLE 4.1

Compositions of Steels in Weight Percentages

Steel	I	II	III	IV
B	0.001	0.006	0.001	0.0065
C	0.06	0.05	0.12	0.12
Cr	17.60	17.20	17.40	17.40
Ni	11.60	11.55	11.50	11.50
Mo	2.69	2.63	2.56	2.63
Mn	1.32	1.39	1.34	1.46
Si	0.51	0.32	0.39	0.47
N	0.030	0.034	0.031	0.038
S	0.022	0.022	0.030	0.022
P	0.015	0.014	0.012	0.015

and then for 24 hours at 950°C to produce the equilibrium groove shape appropriate for this temperature.

4.2 Use of Mullins' Analyses

The small grain size and small groove size produced in the steels due to the short annealing times used in this work made accurate direct measurement of the dihedral angles from interferograms extremely difficult and it was found much easier to measure the linear dimensions of the grooves. Mullins' analysis of grain boundary groove shapes discussed in Chapter 3 applies strictly only to single component systems. It was therefore necessary to evaluate the applicability of Mullins' equations to the 316 steels. It was thought that this attempt was justified even though the chemical compositions of the steels are complex, because the temperatures used were such that the specimens were single phase. One specimen of steel I and one of steel IV annealed at 1050°C were therefore subjected to direct dihedral angle measurement and to groove dimension measurement so that the grain boundary to surface energy ratios obtained by the two techniques could be compared. The ratios obtained by the two methods are shown in Table 4.2 and it can be seen that they are the same within the experimental errors of the measurements, expressed in the table as the standard errors of the means. Thus it was concluded that Mullins' equation could be used to calculate the energy ratios from measurements of the linear groove dimensions.

The equation for determining the grain boundary groove angle, Ψ, from the measured width, W, and depth, D, of the

TABLE 4.2

Grain boundary to surface energy ratios: comparison of Mullins' equation with direct measurement of dihedral angles

Steel	Technique	
	Direct angle measurement	Mullins' equation
I	0.73 ± 0.04	0.70 ± 0.03
IV	0.56 ± 0.03	0.54 ± 0.02

profile is

$$\tan \frac{\Psi}{2} = C.\frac{W}{D} \qquad \ldots (4.1)$$

where C is equal to 4.73 if the grooves are formed by surface diffusion alone or 4.95 if volume diffusion is the dominant mechanism. Mullins also showed (see section 3.1.3) that the width or depth of a grain boundary groove increases as a function of time at temperature which is determined by the grooving mechanism dominating at that temperature, while the shape of the groove profile remains the same. The groove width or depth is proportional to the grooving time to the power 1/4 for surface diffusion, 1/3 for volume diffusion and 1/2 for evaporation-condensation.

4.3 Determination of Grooving Mechanism

At the temperatures of interest some grain growth takes place in the steels. Thus, before kinetic studies to determine the grooving mechanism were carried out, specimens were preannealed to stabilise the grain size. For the samples to be studied at 1250°C the preanneal was carried out at 1250°C (for 3 hours) as it was feared that at higher temperatures evaporation losses would be significant. For the lower temperatures the preanneals were carried out for 1 hour at a temperature 100 degrees higher than the subsequent kinetic study. The specimens were polished in the usual manner after being preannealed and then annealed for various times up to a total of 50 hours at the required temperature. The widths of at least 50 boundaries were measured after each anneal using the interference microscope, and then the specimen was ultrasonically cleaned in methylated spirits and returned to the furnace for a further anneal. In this way the time dependence

of the groove width and hence the dominant grooving mechanism was determined.

The measurement of grooving time was not absolutely straightforward as the furnace took a finite time to heat up and cool down, during which a small amount of groove growth (and shape variation because the dihedral angle and hence the groove shape are temperature dependent) must take place in the specimen. The total time taken from switching on the power to reach the annealing temperature was usually about 15 minutes, for the first 2 or 3 minutes of which the specimen was below 500°C and therefore no significant mass transport would be expected to take place during this time. The time taken to cool down to 500°C after switching off the power was 10-15 minutes. To a first approximation, therefore, the grooving time was taken to be equal to the time during which the power was switched on.

Kinetic studies were carried out on steel II at 950°C, steel IV at 1050 and 1150°C, and steel I at 1250°C. The graphs of log W vs log t (t = time in h) for these specimens shown in Fig 4.1 have slopes of 0.26, 0.25, 0.29 and 0.38 respectively. The obvious interpretation of these measured slopes is that the dominant grooving mechanism at 950 and 1050°C is surface diffusion, at 1250°C is volume diffusion and at 1150°C is a mixture of the two.

However, as discussed in Chapter 3 (3.1.3) McAllister and Cutler [1969] have suggested that simple deductions from this type of plot can be erroneous, and that more reliable conclusions are to be drawn from plots of the type shown in Fig 4.2. From these graphs of W vs $t^{1/n}$ it can be seen that at 950 and 1050°C the measured groove widths lie on a straight

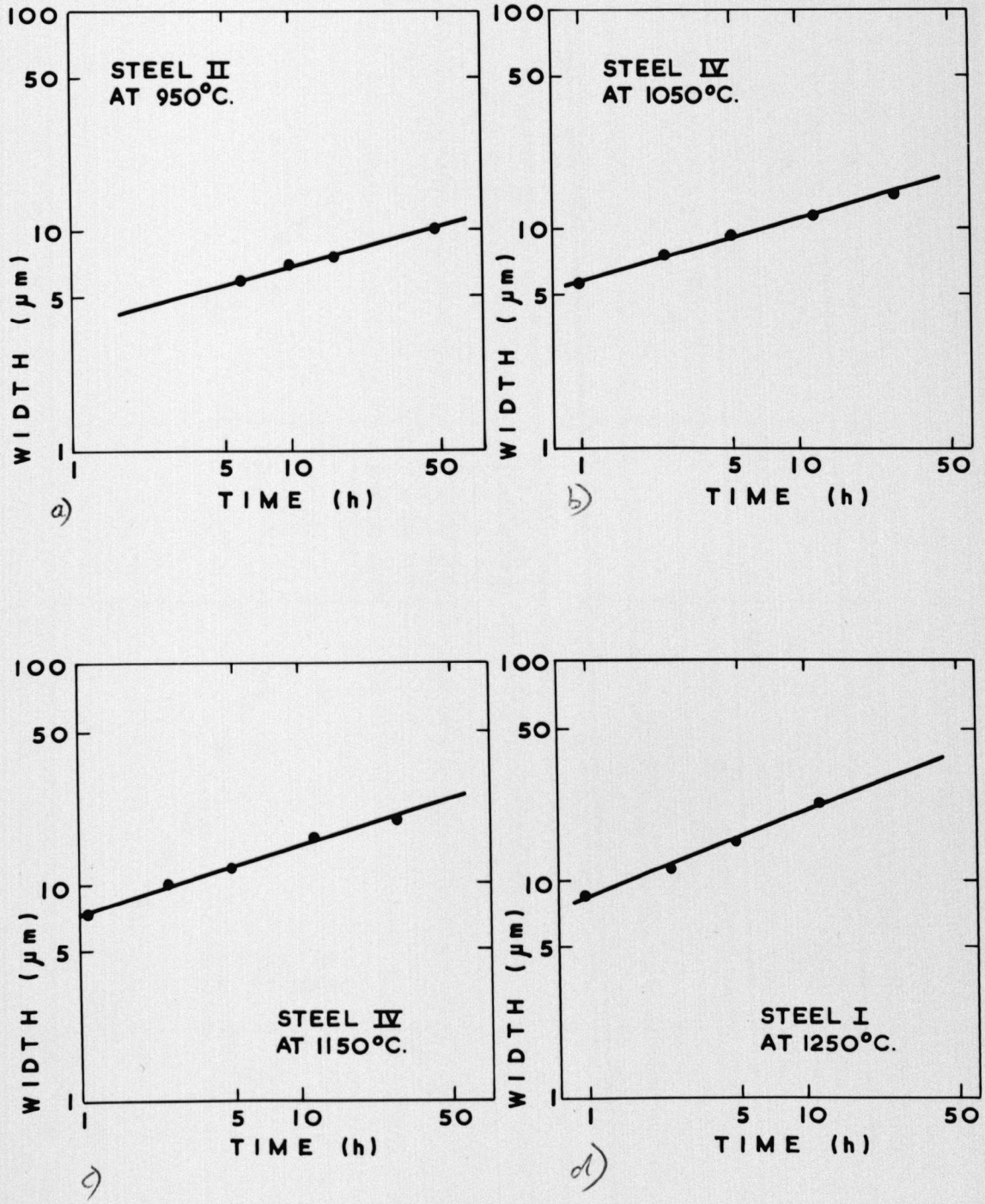

Figure 4.1. Grain boundary groove width in 316 steels vs. annealing time (log-log scale).

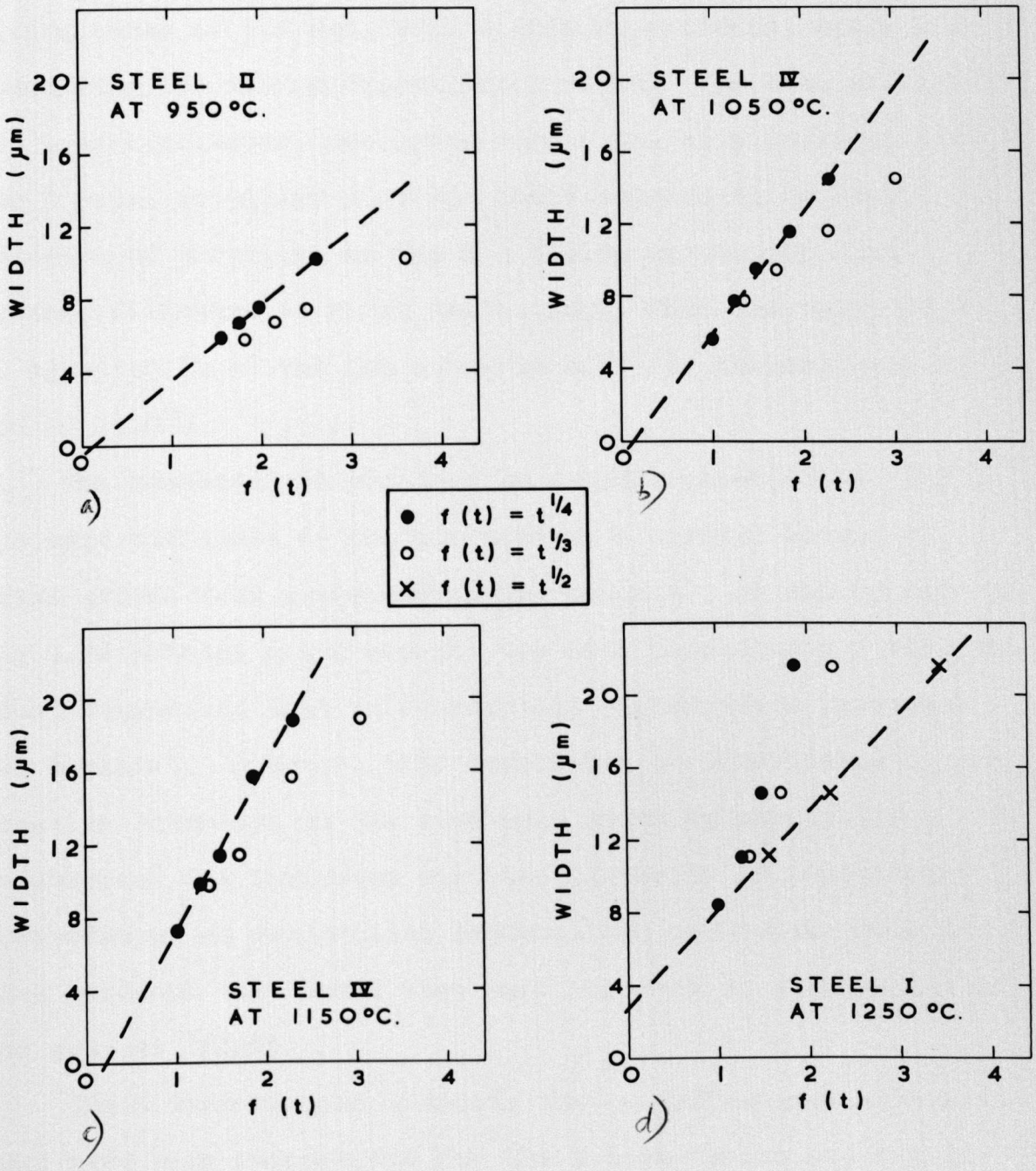

Figure 4.2. Grain boundary groove width in 316 steels as a function of (annealing time)$^{1/n}$.

line passing close to the origin for n = 4, indicating that surface diffusion is the dominant grooving mechanism. The 'best fit' line, as found by a least squares method, in both cases cuts the W = 0 axis at $t^{1/4} < 0.2$ which indicates a timing error of 5.8 sec, well within experimental error and justifying the timing approximation used. The data at 1150°C are less conclusive, not lying very close to a straight line for n equal to either 3 or 4. There appears to be less evidence of curvature on the n = 4 plot suggesting that surface diffusion is still dominating. Thus the value of C in equation (4.1) was put equal to 4.73 for temperatures of 950 to 1150°C.

The measurements obtained on samples annealed at 1250°C are more difficult to analyse because a certain amount of grain growth took place during the anneals. As can be seen in Fig 4.2d putting n = 2 brought the data points onto a straight line, suggesting that an evaporation condensation mechanism was dominant. However, this conclusion is invalidated by the negative intercept on the time axis which is physically meaningless and indicates that the linearity is fortuitous. Furthermore, an evaporation condensation mechanism could not have produced the ridges that were observed on either side of the grooves (Fig4.3).

These observations indicate that a diffusional mechanism must have been responsible for the groove formation, but it is not possible to establish the nature of this mechanism because of the curvature of the plots in Fig4.2obtained by putting n = 3 or 4. Volume diffusion will become increasingly important as the temperature is raised, but surface diffusion has been shown to be dominant up to 1150°C and there are no

specific grounds for assuming a complete change in mechanism at 1250°C. If it is assumed that surface diffusion is the controlling mechanism (ie C = 4.73 in equation (4.1)) the grain boundary to surface energy ratios obtained are about 3.5% lower than those calculated assuming volume diffusion to be dominant (C = 4.95). In view of the uncertainty over the identity of the grooving mechanism a compromise value of C = 4.85 was used for the calculations of grain boundary to surface energy ratios at 1250°C. This will introduce a systematic error of up to ± 2% in these ratios as presented in Table 4.3 and in the absolute values of grain boundary energy shown in Fig 4.7 but will not affect the relative values for different boron levels at this temperature.

4.4 Grain Boundary to Surface Energy Ratios

Measurements were made from interferograms on the Nikon profile projector of the width and depth of at least 50 grain boundary grooves on each specimen. Some interferograms are shown in Fig 4.3a-d. Some boundaries were curved like the right hand one in Fig 4.3a and these were not measured. Other grooves were asymmetrical like those in Fig 4.3c and these too were ignored. One possible reason for asymmetry is that the grain boundary was at a large angle to the normal to the specimen surface. Another possibility is that the surface torque terms were very different on the two sides of the boundary, which could happen if there was a large orientation difference between the two grain surfaces, especially if one surface was close to a low index plane when the torque term would be large. A grain boundary which is actively migrating will also produce an asymmetrical groove with a larger ridge in the grain into which it is moving. Another possible cause

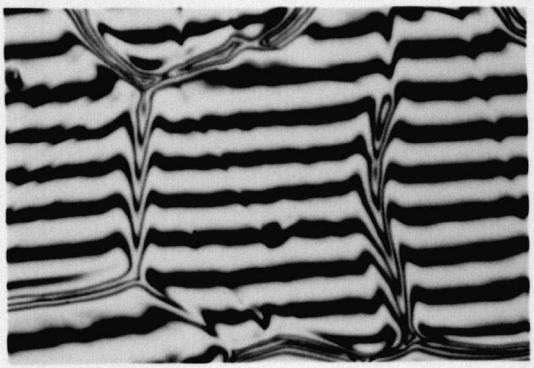

(a)

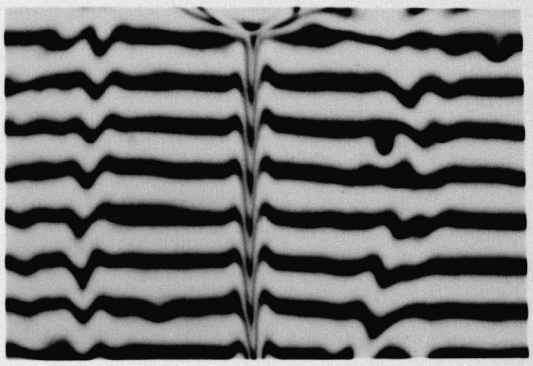

(b)

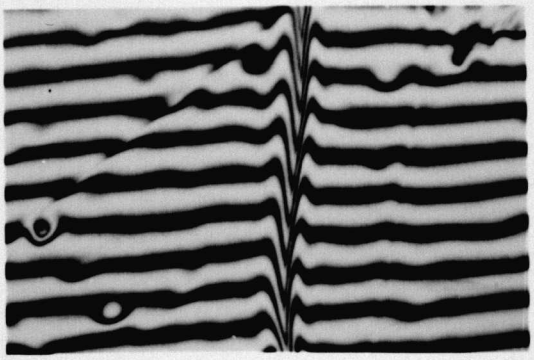

(c)

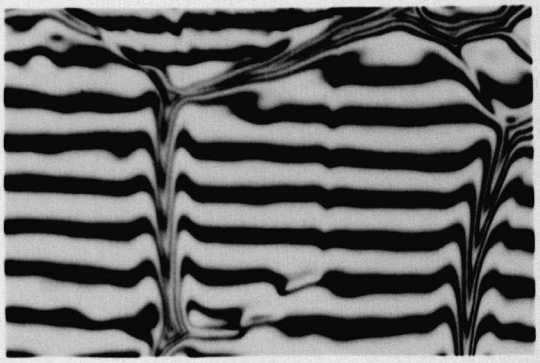

(d)

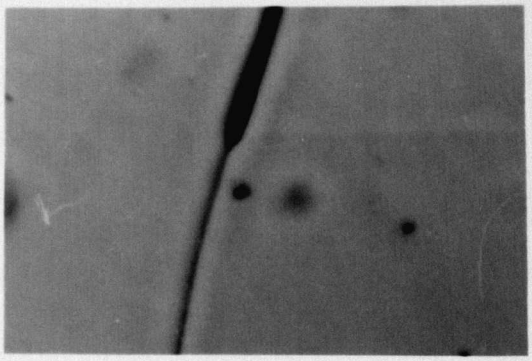

(e)

Figure 4.3. Grain boundary grooves in 316 steels, (a) to (d) interferograms showing groove shapes, (e) micrograph showing change in grain boundary groove width at twin boundary intersection. (X730)

of asymmetric grooves may be the dependence of the diffusion coefficient on the surface orientation.

Blakely [1961], for example, found variations of the surface diffusion coefficients with surface orientation on nickel, iron and platinum surfaces. He saw marked changes in scratch smoothing rate on crossing certain twin and grain boundaries. He found the lowest diffusion coefficients for surfaces with orientations near to a (100) plane where the activation energy for nickel was 1.7 eV compared to 0.78 eV for the average overall orientations. Other evidence for variations in diffusion coefficient with orientation seen in the present work was an occasional marked change in grain boundary groove size at the intersection with a twin boundary such as is shown in Fig 4.3e.

The ratio of grain boundary to surface energy was then computed from equation (3.2) for each boundary and the mean ratio calculated for each specimen. The spread of values obtained was quite large due to a combination of the errors introduced in the actual measurements and the inherent spread of angles caused by the surface energy anisotropy (torque terms) and grain boundary energy variations. A typical set of histograms for the measurements made at 1050°C are shown in Fig 4.4. The mean ratios are indicated by a vertical line on each histogram and this figure shows clearly a reduction in γ_{gb}/γ_{sv} produced on increasing the boron concentration of the steel from 0.001 to 0.006 or 0.0065 wt% at both carbon levels.

Similar results were obtained at the other temperatures employed and the ratios obtained are summarised in Table 4.3 which gives the mean ratio and its standard error for each specimen. It can be seen that the ratio γ_{gb}/γ_{sv} is reduced

Figure 4.4. Histograms of grain boundary to surface energy ratios measured on 316 steels annealed at 1050°C.

TABLE 4.3

Grain boundary to surface energy ratios of 316 steels

Annealing treatment	Steel	Wt percent of Carbon	Wt percent of Boron	γ_{gb}/γ_{sv}	% Reduction on increasing boron content
24 hrs at 950°C	I	0.06	0.001	0.66 ± 0.05	22.2
	II	0.05	0.006	0.54 ± 0.02	
	III	0.12	0.001	0.57 ± 0.03	5.5
	IV	0.12	0.0065	0.54 ± 0.04	
3 hrs at 1050°C	I	0.06	0.001	0.70 ± 0.03	9.4
	II	0.05	0.006	0.64 ± 0.04	
	III	0.12	0.001	0.76 ± 0.02	40.7
	IV*	0.12	0.0065	0.54 ± 0.02	
1 hr at 1150°C	I	0.06	0.001	0.81 ± 0.04	35.0
	II	0.05	0.006	0.60 ± 0.03	
	III	0.12	0.001	0.65 ± 0.05	12.1
	IV	0.12	0.0065	0.58 ± 0.02	
1 hr at 1250°C	I	0.06	0.001	0.83 ± 0.05	15.3
	II	0.05	0.006	0.72 ± 0.03	
	III	0.12	0.001	0.87 ± 0.06	42.6
	IV	0.12	0.0065	0.61 ± 0.03	

*This specimen annealed 4½ hours.

by the extra boron for all four temperatures used and for both carbon levels. There is also some indication that the higher carbon level causes a reduction in the ratio but the evidence for this is not conclusive as in 2 out of the 8 cases an increase occurs at the higher carbon concentration. What is noticeable, however, is that for each temperature the lowest ratio is obtained for steel IV, which has both a high carbon and a high boron content. No effect of the variations in silicon level can be deduced from the figures so we must conclude that if it has any effect, this is swamped by the other changes.

Ratios of grain boundary to surface energies have been measured by a number of workers in a variety of systems and all show similar amounts of scatter. Some examples are the measurements of Hilliard et al [1960] on gold-copper alloys, Williams and Barrand [1965] on copper-nickel alloys, and Hodgson [1972] on nickel-boron alloys, all of whom found experimental errors of $\pm \sim 10\%$ on their ratios. The errors incurred in the present measurements are thus very similar to those found by other users of these techniques. The only workers who are known to the author to have measured an effect of boron on interfacial energies in austenitic steels are Adair, Spretnak and Speiser [1955]. They investigated the effects on grain boundary groove angles of adding 0.0011 and 0.0013 wt% boron to two austenitic steels. They measured small increases in the angles on adding boron, equivalent to reductions in the ratio of 2-4% at temperatures of about 900 and 1000°C. These reductions are much smaller than those observed in the present work on increasing the boron content

from 0.001 to ~0.006 wt% (see Table 4.3). Their small variations could be because the low boron additions affect the surface and grain boundary energies by compensating amounts. There seems to be no justification for Adair et al's assumption that the surface energy is unaffected by boron additions which they use to calculate its effect directly on grain boundary energy.

4.5 Twin Boundary to Surface Energy Ratios

Measurements of the dihedral angles at pairs of twin boundary/surface intersections were made directly from Talystep traces taken perpendicularly across the boundary pairs. Some typical pairs of traces are shown in Fig 4.5. Photographs of the boundaries were taken on a bench microscope for identification purposes, as a check that the same boundaries were not measured several times. Though rather poor quality, the photographs were perfectly adequate for that purpose. As in the case of the grain boundary grooves, any obviously asymmetrical grooves were not measured as equation (3.5) could not be applied to them.

This equation was used to calculate the ratio γ_{tb}/γ_{sv} from the angular measurements and the mean ratio obtained for each specimen. The spread of values of this ratio was, in proportion, much larger than that of γ_{gb}/γ_{sv}. This was partly due to the fact that the ratio is derived from the difference of two quantities, each of which has a quite large error to produce a third quantity at least an order of magnitude smaller. Also because the twin boundary energy is very much smaller than the surface or grain boundary energy the effect of the torque terms is of much greater importance. This is

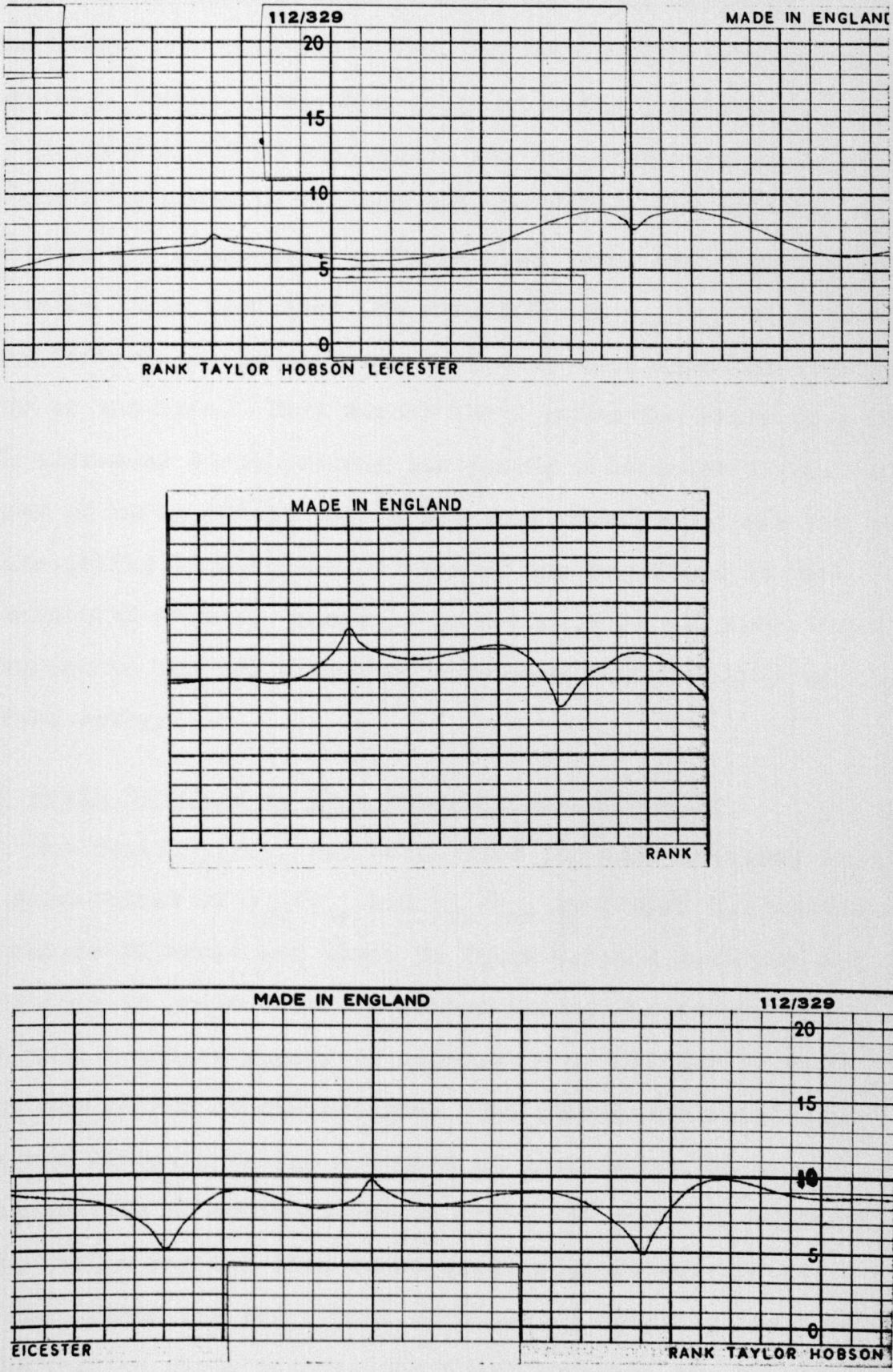

Figure 4.5. Talystep traces of twin boundary profiles in (a) steel IV annealed at 1250°C, (b) steel II annealed at 1150°C and (c) steel II annealed at 1050°C.

emphasised by the fact that one twin boundary in each pair formed a ridge instead of a groove. Thus the dihedral angles measured at twin boundaries are influenced much more by the (variable) torque terms than those at grain boundaries.

A typical set of histograms for the specimens annealed at 1050°C is shown in Fig 4.6 and the ratios for all the specimens are summarised in Table 4.4. From the figure and the table it is seen that the variation in γ_{tb}/γ_{sv} with boron concentration is, in all cases but one, less than the standard error of the mean. In 5 out of the 8 pairs the ratio goes up with increased boron content indicating a decrease in surface energy of up to 30% at 1050°C but this observation may not be statistically significant in view of the magnitude of the experimental errors. There is no evidence at all from these measurements for any effect of carbon or silicon level on the surface energy.

4.6 Grain Boundary to Twin Boundary Energy Ratios

The ratio γ_{gb}/γ_{tb} was calculated for each specimen from the mean values of γ_{gb}/γ_{sv} and γ_{tb}/γ_{sv} in Tables 4.3 and 4.4. The ratios obtained are shown in Table 4.5 and indicate the variations in grain boundary energy (using the assumption that twin boundary energy is constant - cf Chapter 3) with boron and carbon concentrations. The percentage reductions in grain boundary energy obtained on increasing the boron concentration at constant carbon level are shown in column 6 of the table and are seen to be quite significant amounts. For comparison the reductions obtained by doubling the carbon concentration while keeping the boron constant are given in column 7. On the whole these are considerably smaller,

Figure 4.6. Histograms of twin boundary to surface energy ratios measured on 316 steels annealed at 1050°C.

TABLE 4.4

Twin boundary to surface energy ratios of 316 steels

Annealing treatment	Steel	Wt percent of Carbon	Wt percent of Boron	γ_{tb}/γ_{sv}
24 hrs at 950°C	I	0.06	0.001	0.015 ± 0.003
	II	0.05	0.006	0.014 ± 0.002
	III	0.12	0.001	0.015 ± 0.003
	IV	0.12	0.0065	0.017 ± 0.004
3 hrs at 1050°C	I	0.06	0.001	0.010 ± 0.002
	II	0.05	0.006	0.014 ± 0.002
	III	0.12	0.001	0.012 ± 0.003
	IV*	0.12	0.0065	0.012 ± 0.002
1hr at 1150°C	I	0.06	0.001	0.009 ± 0.002
	II	0.05	0.006	0.011 ± 0.002
	III	0.12	0.001	0.008 ± 0.002
	IV	0.12	0.0065	0.010 ± 0.002
1 hr at 1250°C	I	0.06	0.001	0.011 ± 0.002
	II	0.05	0.006	0.012 ± 0.002
	III	0.12	0.001	0.013 ± 0.002
	IV	0.12	0.0065	0.012 ± 0.002

*This specimen annealed 4½ hours.

TABLE 4.5

Grain boundary to twin boundary energy ratios in 316 steels

Annealing treatment	Steel	Wt percent of Carbon	Wt percent of Boron	γ_{gb}/γ_{tb}	% Redn with B	% Redn with C
24 hrs at 950°C	I	0.06	0.001	44 ± 9	12	14
	II	0.05	0.006	39 ± 6		
	III	0.12	0.001	38 ± 8	16	18
	IV	0.12	0.0065	32 ± 8		
3 hrs at 1050°C	I	0.06	0.001	70 ± 14	34	10
	II	0.05	0.006	46 ± 7		
	III	0.12	0.001	63 ± 16	29	2
	IV*	0.12	0.0065	45 ± 8		
1 hr at 1150°C	I	0.06	0.001	90 ± 20	39	10
	II	0.05	0.006	55 ± 10		
	III	0.12	0.001	81 ± 21	29	- 5
	IV	0.12	0.0065	58 ± 12		
1 hr at 1250°C	I	0.06	0.001	75 ± 14	20	9
	II	0.05	0.006	60 ± 10		
	III	0.12	0.001	68 ± 11	25	15
	IV	0.12	0.0065	51 ± 9		

*This specimen annealed 4½ hours.

particularly at the temperatures where boron has its biggest effect and at 1150°C, the high boron pair of steels actually show an increase in grain boundary energy on increasing the carbon concentration, though it is so small that it is probably not statistically significant.

4.7 Absolute Energy Values

The absolute surface energy of steel III at 1050°C was determined by the multiphase equilibration technique described in the Appendix. A different, but similar, vacuum furnace was used for these measurements than for the energy ratio anneals and silver was chosen as the liquid phase. The measured dihedral angles are shown in Table 4.6, where the symbols are the same as those used in the Appendix. A value of 735 mJ m^{-2} was obtained for the surface energy of steel III at 1050°C and from this a twin boundary energy of 8.8 mJ m^{-2} was obtained for steel III at 1050°C. It is often found that the twin boundary energy of a material is approximately equal to half the stacking fault energy. The room temperature stacking fault energies of austenitic steels are low (Dulieu and Nutting [1964]), typically 10-25 mJ m^{-2}, so the low twin boundary energy found here is reasonable, though it must be remembered that both stacking fault and twin boundary energies may have significant temperature coefficients.

This value of the twin boundary energy was then used to give absolute values of the surface energies and grain boundary energies of all 4 steels at all the temperatures used. These values are shown in Table 4.7 and plotted in Figure 4.7 as a function of temperature.

TABLE 4.6

Dihedral angles measured on silver - 316 steel system

Ψ	84°
Ψ^{*}	85°
ϕ	13°
θ	29°

TABLE 4.7

Absolute values of surface and grain boundary energies in 316 steels

Annealing treatment	Steel	Wt Percent Carbon	Wt Percent Boron	Surface energy mJ m^{-2}	Grain boundary energy mJ m^{-2}
24 hrs at 950°C	I	0.06	0.0010	590 ± 120	390 ± 80
	II	0.05	0.0060	630 ± 90	340 ± 50
	III	0.12	0.0010	590 ± 120	330 ± 70
	IV	0.12	0.0065	520 ± 130	280 ± 70
3 hrs at 1050°C	I	0.06	0.0010	880 ± 180	620 ± 120
	II	0.05	0.0060	630 ± 90	400 ± 60
	III	0.12	0.0010	730 ± 200	550 ± 140
	IV*	0.12	0.0065	730 ± 130	400 ± 70
1 hr at 1150°C	I	0.06	0.0010	980 ± 230	790 ± 180
	II	0.05	0.0060	800 ± 150	480 ± 90
	III	0.12	0.0010	1100 ± 290	700 ± 180
	IV	0.12	0.0065	880 ± 180	510 ± 110
1 hr at 1250°C	I	0.06	0.0010	800 ± 150	660 ± 120
	II	0.05	0.0060	730 ± 130	530 ± 90
	III	0.12	0.0010	680 ± 110	600 ± 100
	IV	0.12	0.0065	730 ± 130	450 ± 80

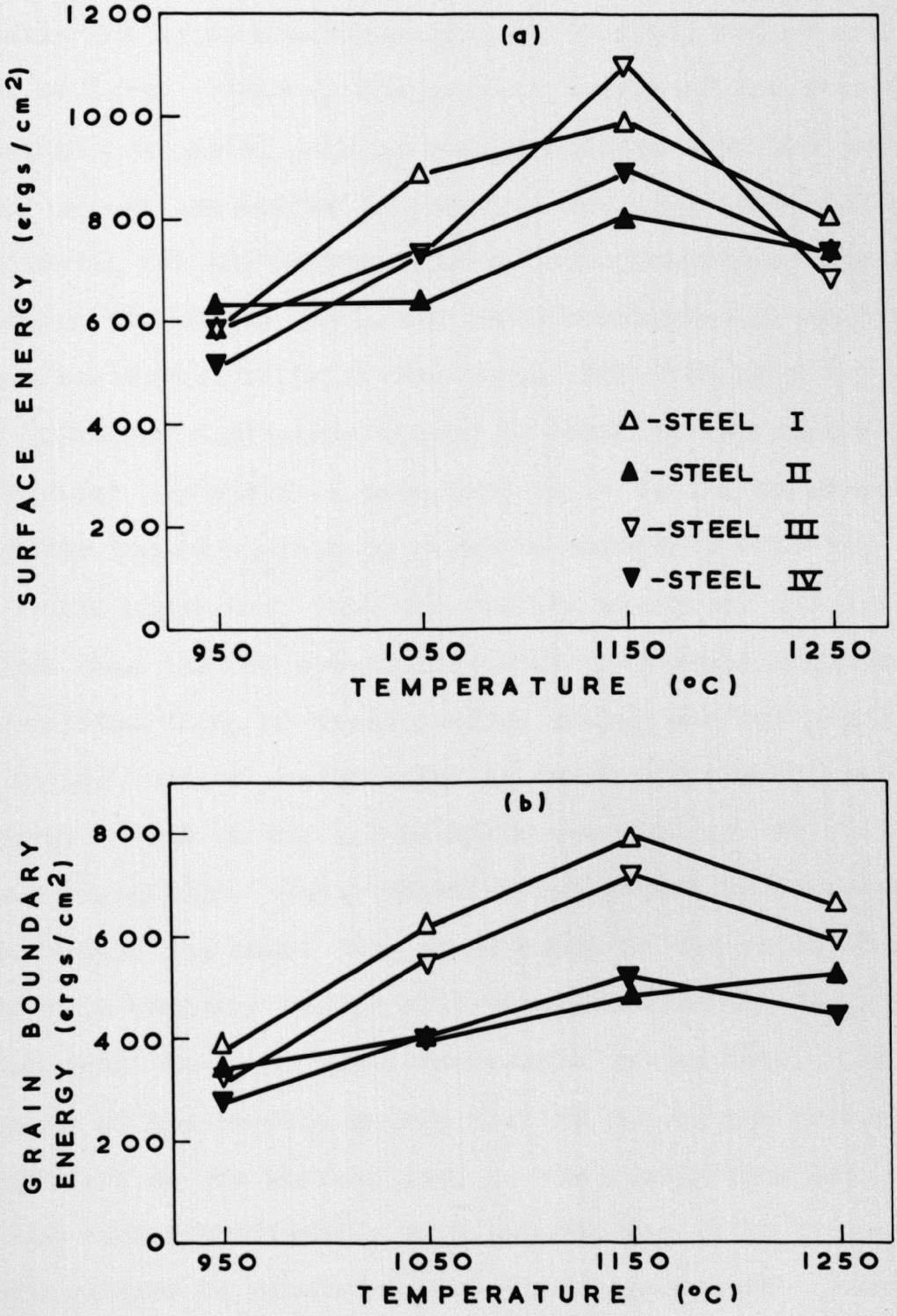

Figure 4.7. Absolute values of (a) surface energy and (b) grain boundary energy of 316 steels as a function of temperature and boron content.

4.8 Discussion

Energy Measurements

The data in Table 4.4 and Figs 4.6 and 4.7 show that increasing the boron concentration of 316 steel had no consistent or large effect on the surface energy of the steels. The absolute values of surface energy derived from the twin boundary energy are rather low, within the range 500-1100 mJm^{-2}, even allowing for the rather large errors incurred by the statistical techniques used, the surface energies of austenitic iron and nickel being in the range 1850-2150 $mJ\ m^{-2}$ (Jones [1971]). A possible source of error in the multiphase equilibration technique as used here could be the contamination of the liquid surface by elements dissolved from the steel. This might mean that the surface energy of the liquid was lower than that of pure silver, but this would mean that the calculated value of steel surface energy was too high. An error in the surface energy value obtained would mean that all the energy values in Fig 4.7 would be too high or too low by the same percentage. Their relative magnitudes would nevertheless remain the same. The correlation of the value obtained for the twin boundary energy with literature values for stacking fault energies lends confidence to the data. The depression of the surface energy must be due to the presence of impurities on the surface and, as the energy does not appear to vary significantly with composition it is probable that the surface is saturated with these impurities. They could either be adsorbed from the environment, or, more likely, be surface active elements segregated from the bulk of the material. Hondros and McLean [1968] have noted that the surface activity of solutes is higher for those which

have a low solubility in the matrix. Boron has a very low solid solubility in iron (Garnish and Brown [1972]) and austenitic steels (Goldschmidt [1971(a) and (b)])of up to about 0.02 wt% and 0.01 wt% respectively. It is therefore probable that boron plays a large part in the depression of the surface energy of these steels. Phosphorus and sulphur are also surface active elements with low solubilities in austenitic lattices and Auger spectroscopy experiments have shown large amounts of sulphur present on iron (Bishop and Rivière [1970]), nickel (Hodgson [1972]) and stainless steel (Rivière [1968]) surfaces at temperatures similar to those used in the present work.

The effect of boron on the grain boundary energy is seen very clearly in Fig 4.7b. As the grooves from which the energy ratios were derived were formed during solution treatment this effect is due to equilibrium segregation of boron at temperature and has nothing to do with the non-equilibrium segregation of boron, which takes place during slow cooling, reported by Williams [1972]. Increasing the boron concentration from 0.001 to ~0.006 wt% while other constituents were kept constant reduced the grain boundary energy in all the cases measured in the present work. The effect was greatest at 1050 and 1150°C and rather less at 1250°C and at 950°C.

The absolute values of γ_{gb} increased as the heat treatment temperature increased, levelling off above 1150°C. This implies that boron was desorbing from the grain boundaries at the higher temperatures. It is thus surprising that the effect of increasing the boron concentration had less effect at 950°C than at any of the higher temperatures. This is

probably explained by the observation (see section 6.1) that quite significant amounts of carbide were not taken into solution during the treatment at this temperature and remained within the bulk of the material. Thus those specimens were not completely equilibrated and a significant proportion of the boron may have been tied to the undissolved precipitates and consequently been unable to influence the grain boundaries. There is also the possibility that other interfacially active species were segregating more strongly in all the steels at the lower temperatures, thus keeping the absolute values of the grain boundary energies low and masking the effects of changing boron concentration.

It was observed during the present measurements that differences in grain size occurred between the different steels and temperatures. A rough estimate of grain size was made on each of the specimens measured. It was found (Fig 4.8) that the grain size increased with annealing temperature but that there was no systematic effect of composition on grain size. By grossly approximating the shape of the grains to a sphere, the minimum grain size for which 0.001 wt% boron would be sufficient to give a monolayer coverage of the grain boundaries was found to be about one third of the smallest grain size measured. It was therefore concluded that in none of the specimens measured were the grain boundaries necessarily being 'starved' of boron owing to too small a grain size.

The only other systematic study of interfacial energies in a steel has been that of Murr, Wong and Horylev [1973] on AISI 304 steel*. They used the zero creep technique to

---

*Austenitic steel containing by weight 18-20% Cr, 8-12% Ni and at most 0.08% C, 2.00% Mn, 0.045% P, 0.030% S and 1.00% Si.

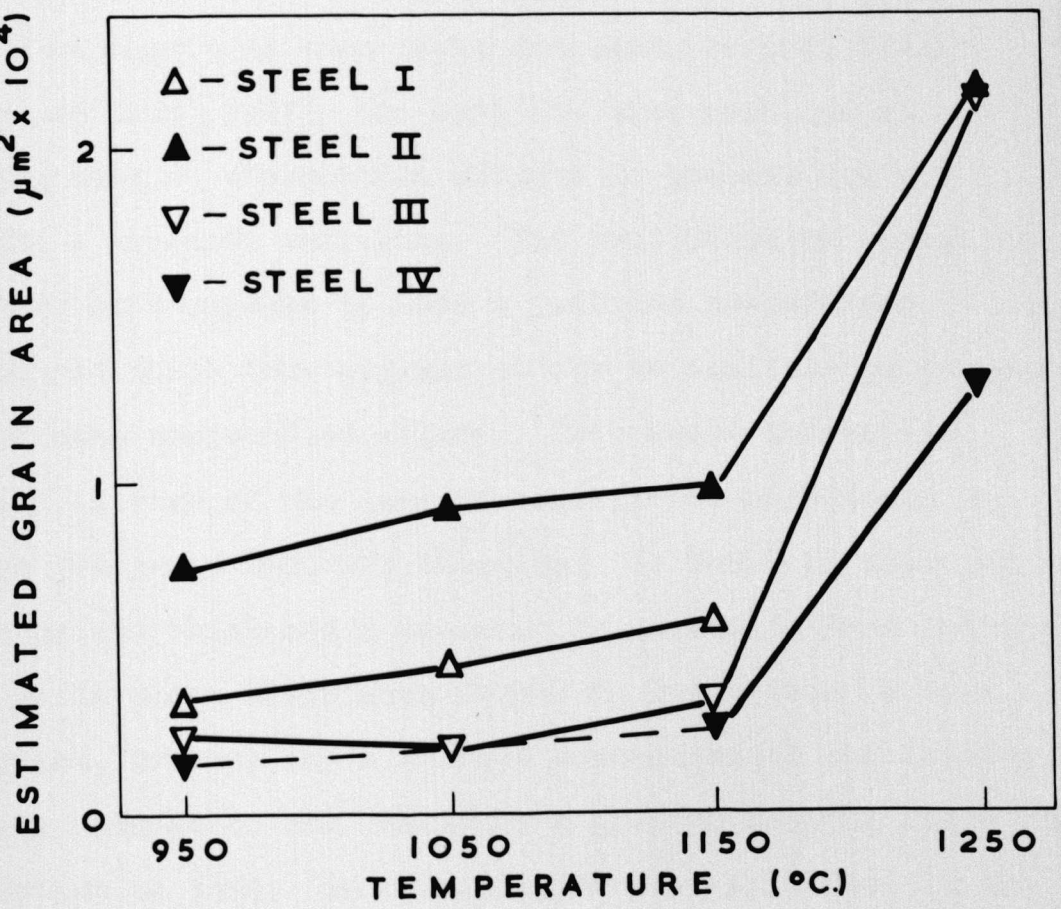

Figure 4.8. Grain size in the 316 steel specimens as a function of annealing temperature.

measure surface energy, grain boundary groove angles to give grain boundary energy and analysed twin-grain boundary intersections to obtain twin boundary energies over a temperature range from 910 to 1180°C. They obtained temperature coefficients of - 1.76 and - 0.89 mJ $m^{-2}\,°C^{-1}$ for the surface and grain boundary energies respectively. These values are greater in magnitude than those obtained for pure metals (Jones and Leak [1967]) but have the same negative sign, implying that no segregation effects if present are not exerting a dominant influence. The twin boundary energy on the other hand appears to have a positive temperature coefficient which they suggest is due to equilibrium segregation of some unspecified solute. This seems inherently unlikely in view of the lack of segregation effects on the surface and grain boundary energies. It would be expected that a solute which had a tendency to segregate from the matrix would go to these interfaces first, in preference to twin boundaries, because there is more distortion of the lattice at these interfaces and therefore a greater driving force for segregation to them. On examining Murr et al's data it is found that all except one of their twin boundary energy values are based on only 9 or 10 measured values of the ratio γ_{tb}/γ_{gb}. This is a very small number from which to take a statistical average. From their histograms an estimate of the standard error of the mean of these ratios can be obtained. When this is done it is found that the variation in twin boundary energy with temperature is within the experimental error arising from these ratios. Fig 4.9 shows their data plotted as a function of temperature with the error bars

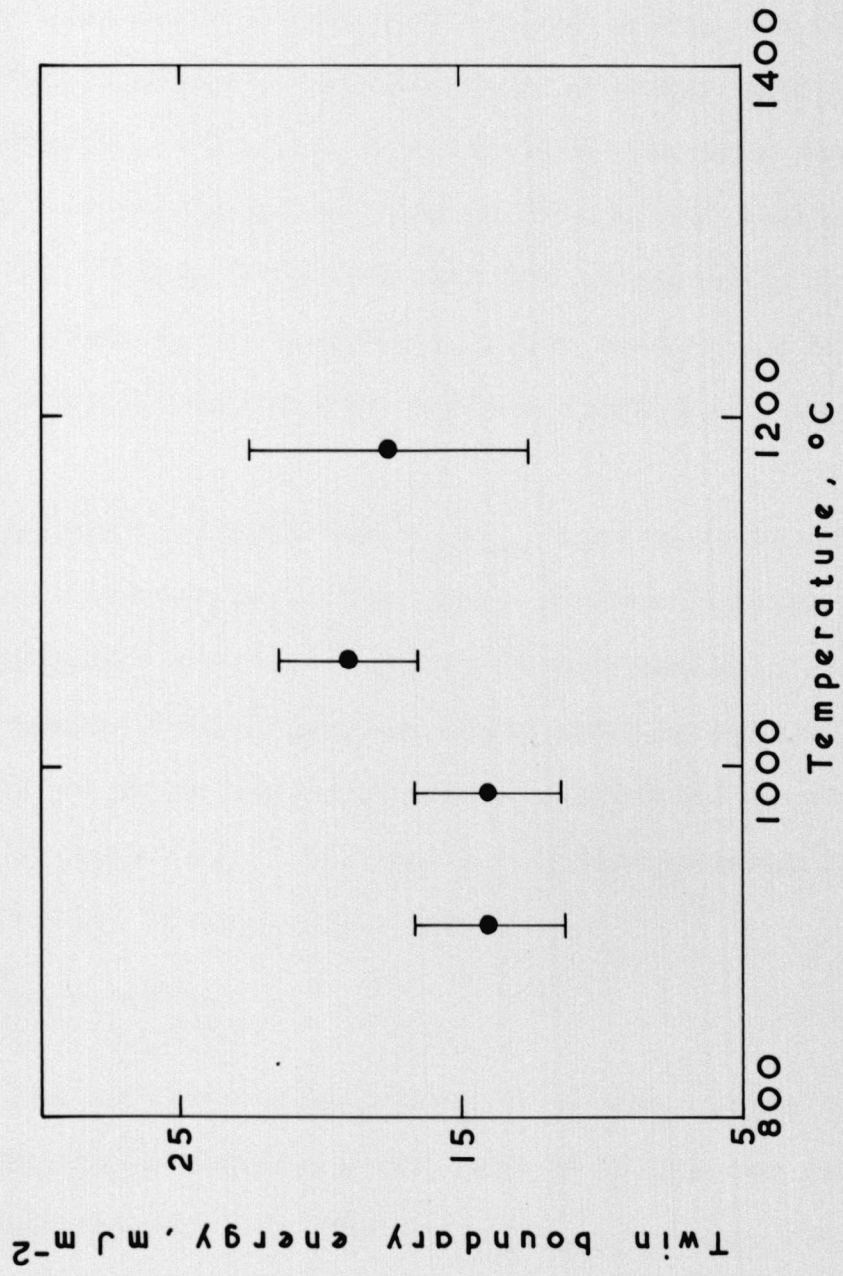

Figure 4.9. Twin boundary energies in 304 steel (Murr et al [1973]).

included and it can be seen that the temperature dependence of twin boundary energy in 304 stainless steel is slight.

Mass Transport Properties

The results of the kinetic studies indicated that, at most of the temperatures employed in this work, the dominant mass transport mechanism forming grain boundary grooves was surface diffusion. This is also the case for many other fcc metals over a wide temperature range though the detailed mechanism for surface diffusion may not necessarily be the same in all cases as is suggested by the wide range of activation energies quoted for surface diffusion (see Gjostein [1967]).

The agreement between the γ_{gb}/γ_{sv} ratios obtained from direct angular measurements and those derived through Mullins' equations indicate that the results of his analysis can be applied to these steels, despite their complex nature. From the analysis of grain boundary grooving produced by surface diffusion, Mullins [1957] derived a relation between D_s, the surface diffusion coefficient, and W:

$$D_s = \frac{W^4}{(4.6)^4} \times \frac{kT}{\gamma_{sv} \Omega^2 n t} \qquad \ldots (4.2)$$

where T is the absolute temperature, Ω is the atomic volume, n is the density of surface atoms, and k is the gas constant. From the measurements made for the γ_{gb}/γ_{sv} ratios, average values of groove width could also be obtained. These were therefore used to calculate approximate values of D_s from equation (4.2) for the specimens used in the present work at 1050°C to 1250°C. Values of D_s at 950°C were derived from widths measured on samples whose grain size had been stabilised

by a 1050°C anneal before they were polished then annealed at 950°C.

The values of D_s obtained using the values of γ_{sv} in Fig 4.7 are plotted on a logarithmic scale as a function of $\frac{1}{T}$ in Fig 4.10. It can be seen that the values obtained at 950 to 1150°C lie on a straight line but, as might be expected after the kinetic study results, the values obtained at 1250°C deviate significantly from this line. The slope of the best line calculated by a 'least squares' fit to the data excluding that for 1250°C gives an activation energy for surface self diffusion in the steels of 28 $\pm$ 8 kcal/mole. No literature values of surface diffusion coefficients of 316 steel are known to the author but measurements have been made by various workers on pure fcc metals. Neumann [1972] has collected together vast amounts of experimental data on diffusion coefficients. From his table 3 it is seen that activation energies for surface diffusion in the range 13.3 to 60.4 kcals/mole for iron and 13.8 to 47.7 kcals/mole for nickel have been obtained by a variety of techniques over a wide temperature range. It thus appears that the surface diffusion data obtained in the present work, though approximate because of the nature of the experiments and materials used, are not unreasonable. This adds to the justification of the use of Mullins' analysis to obtain grain boundary to surface energy ratios from grain boundary groove profiles.

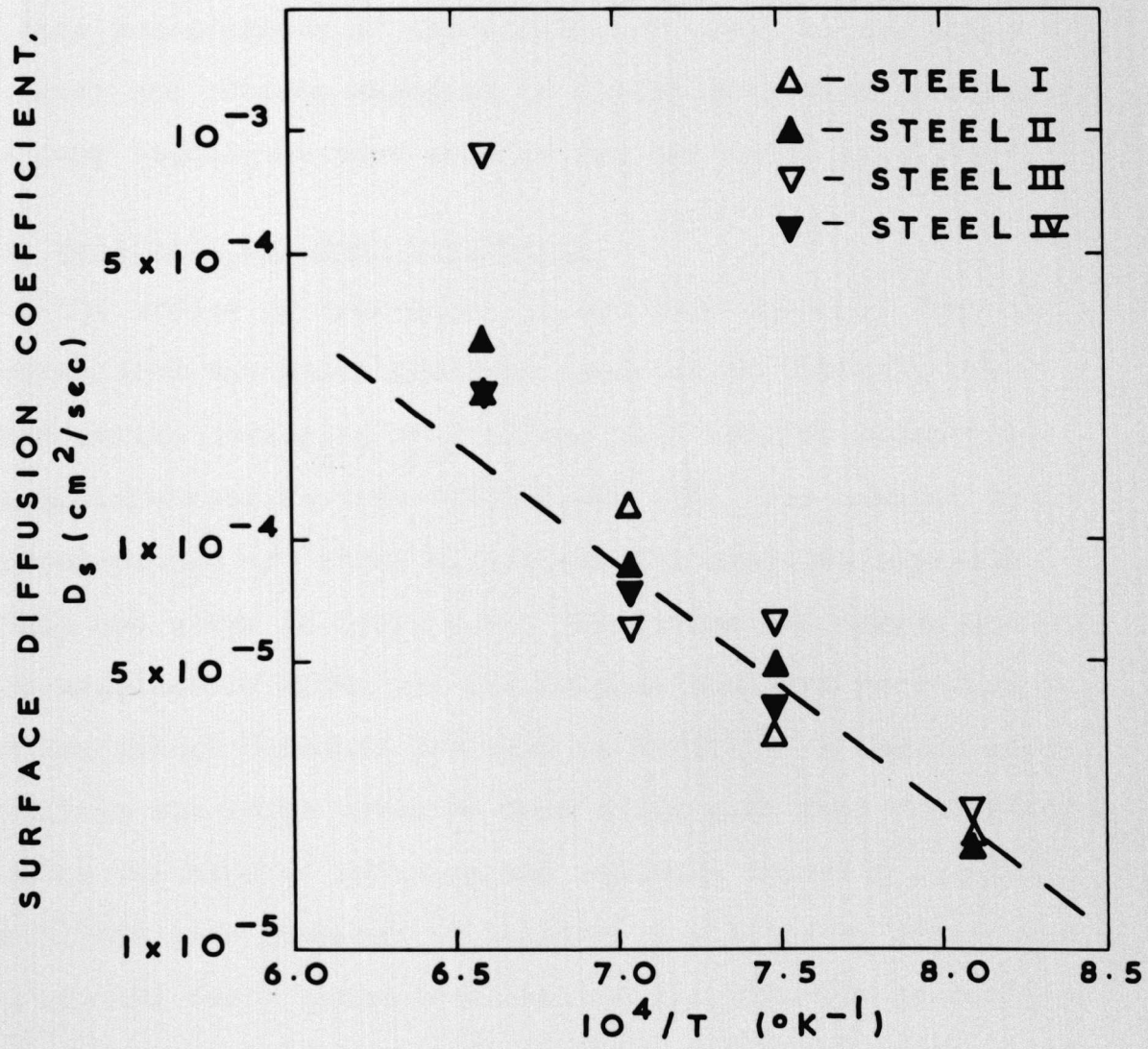

Figure 4.10. Surface diffusion coefficients in 316 steels.

CHAPTER 5 MEASUREMENTS ON IRON-BORON ALLOYS

The complex chemical composition of the steels makes interpretation in terms of the thermodynamic approach discussed in Chapter 2 impossible. The Gibbs adsorption equation (2.17, 2.19) can only be applied conveniently to data obtained for binary systems. It was decided, therefore, to make measurements of the effects of boron on the grain boundary and surface energies of binary iron-boron alloys. The same techniques were used as for the steel specimens.

5.1 Materials and Heat Treatments

Two series of iron-boron alloys were obtained from the British Iron and Steel Research Association (BISRA). The first series consisted of 7 alloys with nominal boron concentrations ranging from 0.000-0.020 wt%. The nominal boron concentrations of these alloys and the measured impurity levels are given in Table 5.1. The carbon and oxygen analyses were supplied by BISRA and the sulphur analyses were done by the Analytical Sciences Division at Harwell. A second series of alloys was later obtained from BISRA made from zone refined iron in the hope of reducing the residual impurity levels. The alloys were prepared by melting in a hydrogen atmosphere. The nominal boron concentrations and the impurity contents as measured at Harwell are given in Table 5.2. As can be seen from a comparison of the two tables, the oxygen and sulphur concentrations were considerably lower in the second series of alloys but the carbon levels were about five times greater. However, it was considered that if the results from both sets of alloys were in agreement then the dominant effects on interfacial energies must be from the boron in the alloys.

TABLE 5.1

Impurities in compositions of 'Series 1' alloys in weight percentages

Alloy	Nominal boron	Carbon	Oxygen	Sulphur
F1	0	0.005	0.005	0.006
F2	0.001	0.004	0.005	n d
F3	0.001	0.007	0.0025	n d
F4	0.003	0.009	0.003	0.005
F5	0.008	0.006	0.005	n d
F6	0.014	0.004	0.002	0.005
F7	0.020	0.003	0.004	n d

TABLE 5.2

Impurities in compositions of 'Series 2' alloys in weight percentages

Alloy	Nominal Boron	Carbon	Oxygen	Sulphur	Nitrogen
F8	0	0.037	< 0.002	< 0.002	0.002
F9	0.005	0.035	< 0.002	n d	0.002
F10	0.010	0.020	< 0.002	< 0.001	0.002

n d = not determined

Specimens were prepared from both sets of alloys as described in Section 3.2.1 and annealed in the austenitic phase (fcc) at either 950 or 1050°C for a week. On cooling to room temperature the alloys undergo a phase change to ferrite (bcc) at ~ 910°C. Associated with this phase change is a volume expansion of the crystal lattice of very nearly 1%. This volume change is too great to be accommodated by simple elastic strain and so plastic deformation and slip occurs, causing rumpling of the specimen surface. It was thus found necessary to grow large grooves at the grain boundaries in order to facilitate measurement of their shapes. Large grain sizes were obtained in the specimens during annealing at these temperatures so that large grooves could easily be measured. (This was in contrast to the small grain sizes in the steel samples which meant that large grooves would begin to interfere with each other in the centres of the grains.)

After the annealed specimens had been examined and measured their boron concentrations were determined by the Applied Chemistry Division at Harwell using boron autoradiography (see Section 6.1). This removed any uncertainties about the boron concentration in the specimens due to non-isotropic distribution of boron in the alloys or to boron loss during the annealing treatment, though the latter was expected to be low. The values of boron concentration for the individual specimens are given in Table 5.3. There was quite wide variation between samples taken from the same alloys indicating some inhomogeneity in the boron distribution.

TABLE 5.3

Grain boundary to surface energy ratios of iron-boron alloys

Annealing treatment	Alloy	Nominal B wt %	Actual B wt ppm	γ_{gb}/γ_{sv}
168 hrs at 1050°C	F1	0.000	6.6 ± 1.3	0.352 ± 0.008
	F3	0.001	16 ± 3	0.396 ± 0.009
	F4	0.003	33 ± 3	0.324 ± 0.009
	F5	0.008	45 ± 4	0.353 ± 0.012
	F6	0.014	178 ± 18	0.284 ± 0.009
	F7	0.020	214 ± 21	0.276 ± 0.005
	F8	0.000	4 ± 2	0.367 ± 0.007
	F9	0.005	16 ± 5	0.317 ± 0.011
	F10	0.010	50 ± 5	0.290 ± 0.007
168 hrs at 950°C	F1	0.000	4 ± 2	0.439 ± 0.016
	F2	0.001	7 ± 3	0.332 ± 0.007
	F3	0.001	14 ± 4	0.389 ± 0.011
	F4	0.003	34 ± 3	0.345 ± 0.009
	F5	0.008	56 ± 6	0.329 ± 0.007
	F6	0.014	35 ± 10	0.326 ± 0.007
	F7	0.020	208 ± 21	0.332 ± 0.006

5.2 Grooving Mechanism

Blakely and Mykura [1963] have shown that grain boundary grooves form by a surface diffusion mechanism in iron up to 1100°C. It is unlikely that the trace amounts of boron present in the alloys used in this work would radically change the grooving mechanism. However, as the boron is expected to segregate to the surfaces during annealing a cross check was made. Kinetic studies similar to those for the steel samples were undertaken for a sample of the 'zero' boron alloy F1 at 1050°C and one of the alloy F4 containing nominally 30 ppm boron at 950°C. The grain boundary groove widths were plotted against time on a log-log plot, Fig 5.1, which yielded straight lines of slopes 0.26 for alloy F1 and 0.25 for alloy F4. These slopes indicate that the grooves were formed by a surface diffusion mechanism but because of the doubts raised about the validity of using log-log plots in this way (see section 3.1.3) the widths were also plotted directly as a function of $t^{1/4}$ and $t^{1/3}$ (Fig 5.2). As can be seen in Fig 5.2, the groove widths lie on a straight line through the origin when plotted against $t^{1/4}$ but the plot of width vs $t^{1/3}$ shows pronounced curvature. Thus the deduction from the log-log plots was confirmed. Indeed, the fact that the W vs $t^{1/4}$ graph goes through the origin indicates that in this case a log-log plot is justified.

5.3 Grain Boundary to Surface Energy Ratios

The widths and depths of the grain boundary grooves were measured from interferograms. Grain boundary to surface energy ratios were computed from equation (3.2) for each boundary. Some typical interferograms from the iron-boron alloys are

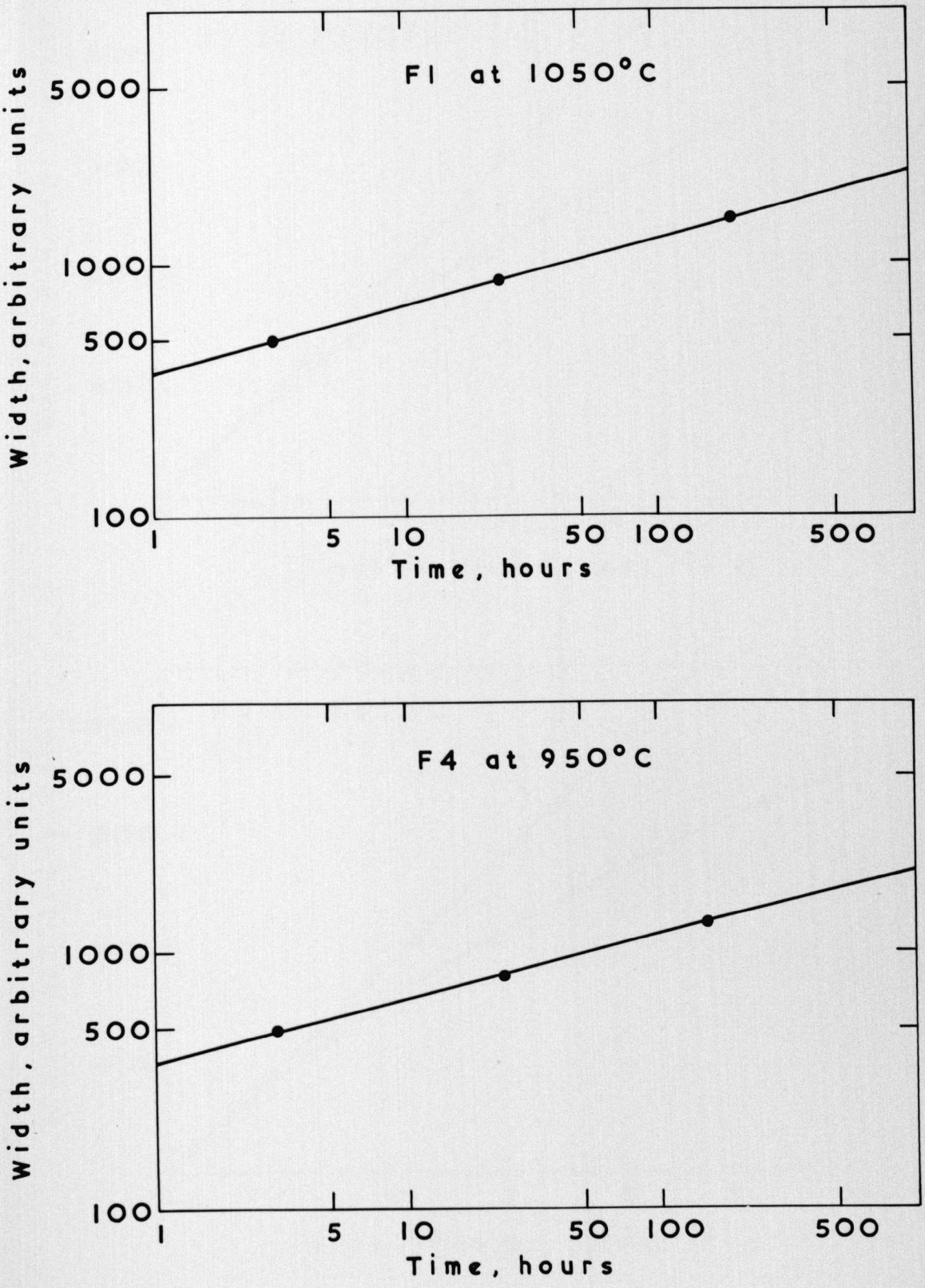

Figure 5.1. Grain boundary groove width in iron-boron alloys vs. annealing time (log-log scale).

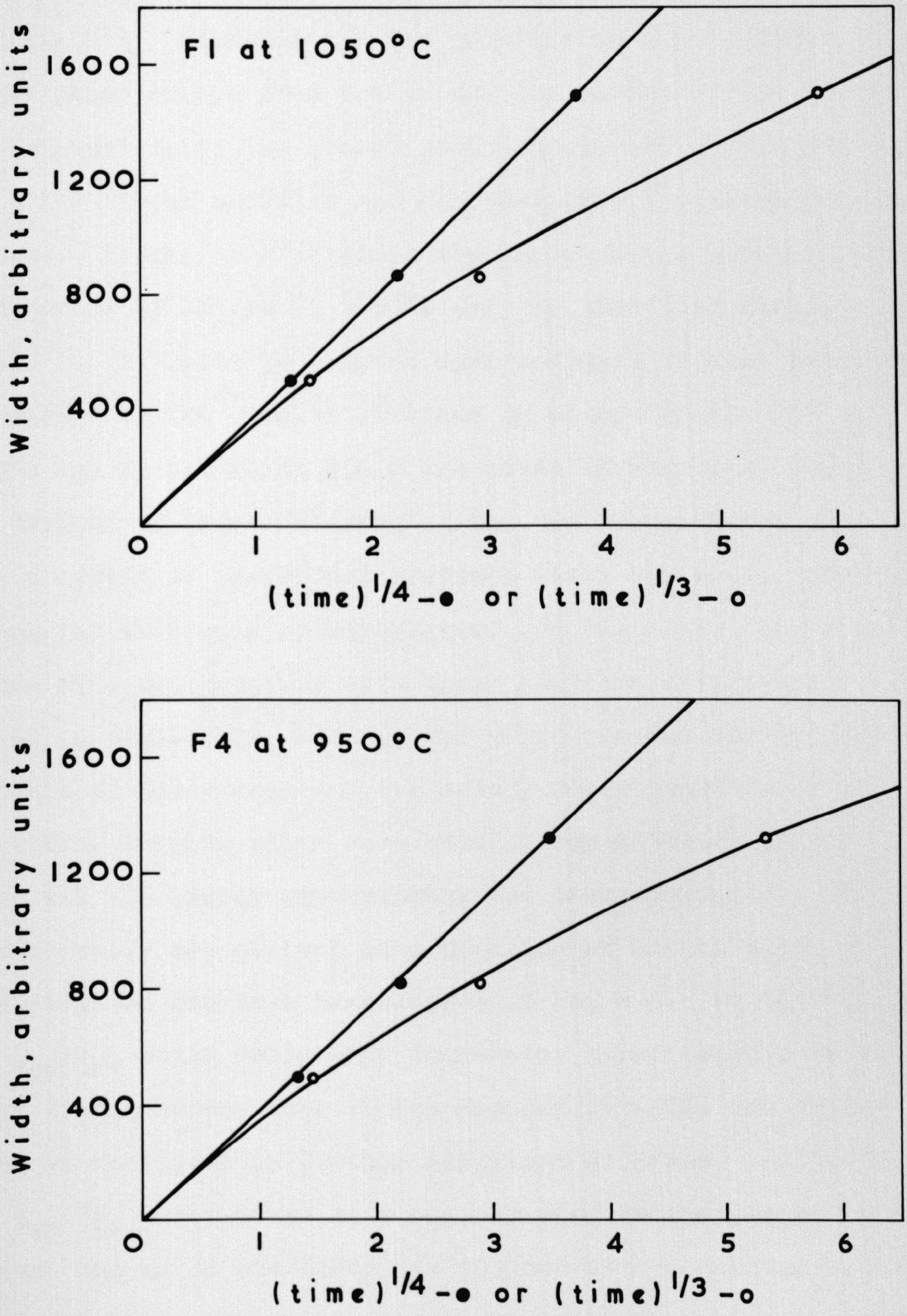

Figure 5.2. Grain boundary groove width in iron-boron alloys as a function of (annealing time)$^{1/n}$.

shown in Fig 5.3. The much larger groove size obtained in these specimens than the steel ones can be seen by comparison with Fig 4.3. Occasionally the rumpling of the surface caused by the phase change from fcc to bcc was severe enough to produce distortion of the groove profiles as, for example, in Fig 5.3d. These profiles and any that were lop-sided were ignored. Ratios were obtained from symmetrical grooves for both series of alloys at 1050°C and for the first series only at 950°C. At least 50 grooves were measured on each specimen. Histograms of the results obtained on alloys F5 and F10 at 1050°C and F3 and F7 at 950°C are shown in Fig 5.4. These are typical of those obtained at the two temperatures and show a spread of individual readings about the mean, which is normal for this type of measurement (cf Fig 4.4). The mean values obtained together with their standard errors are listed in Table 5.3. Also in the table are the nominal boron contents of the alloys and the actual boron contents of the individual samples which were obtained by autoradiography after all the energy measurements had been completed. The energy ratios are plotted as a function of actual boron concentration for each temperature in Fig 5.5. At 1050°C the γ_{gb}/γ_{sv} ratio drops with increasing boron content up to about 50 ppm boron, when it has dropped by $\sim$20%, and thereafter is unchanged by further additions of boron. At 950°C the γ_{gb}/γ_{sv} ratio drops more rapidly with increasing boron content and by 35 ppm boron has reached its saturation value about 20% below its value for the nominally boron free alloy.

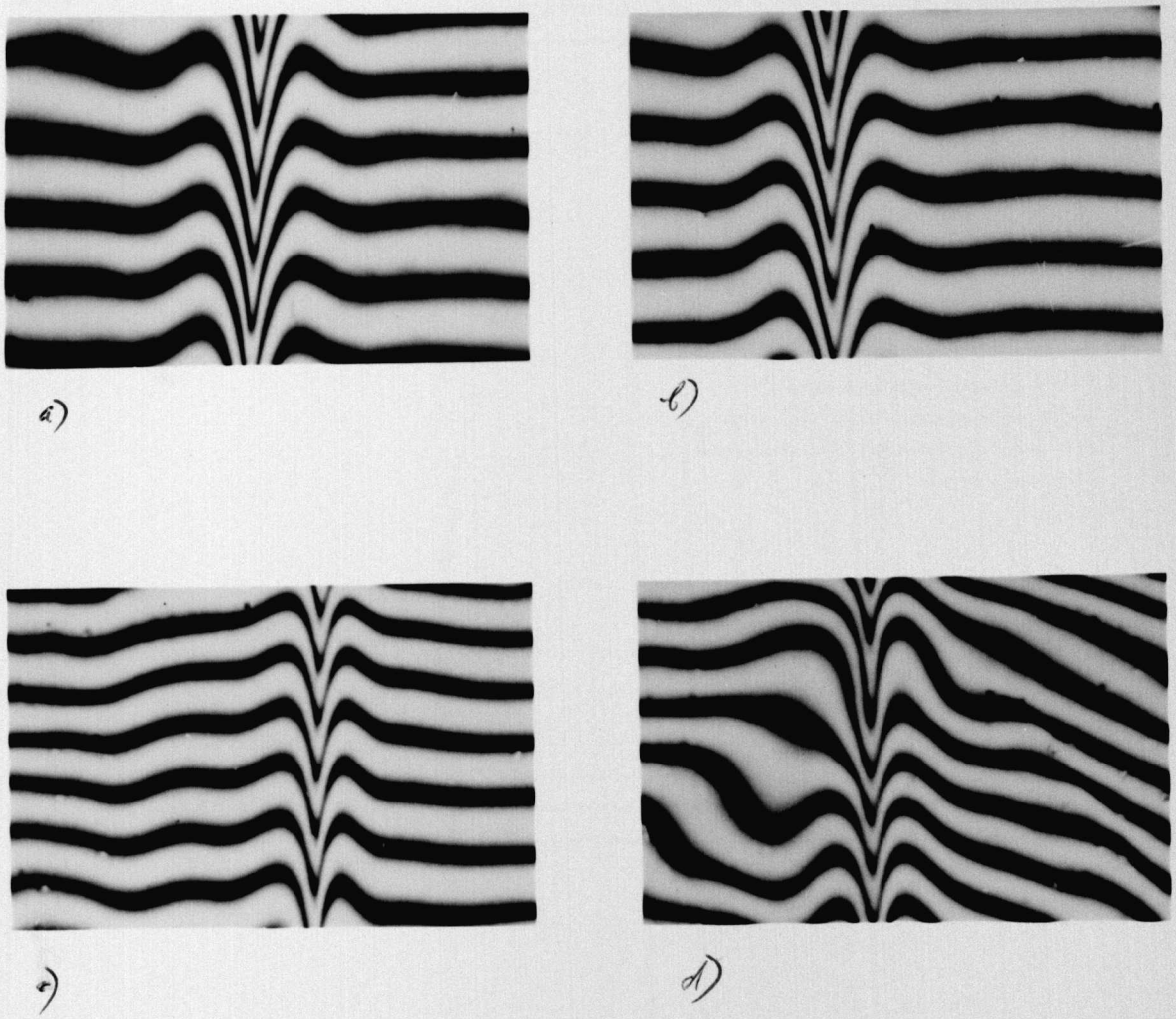

Figure 5.3. Interferograms of grain boundary grooves in iron-boron alloys. (X730)

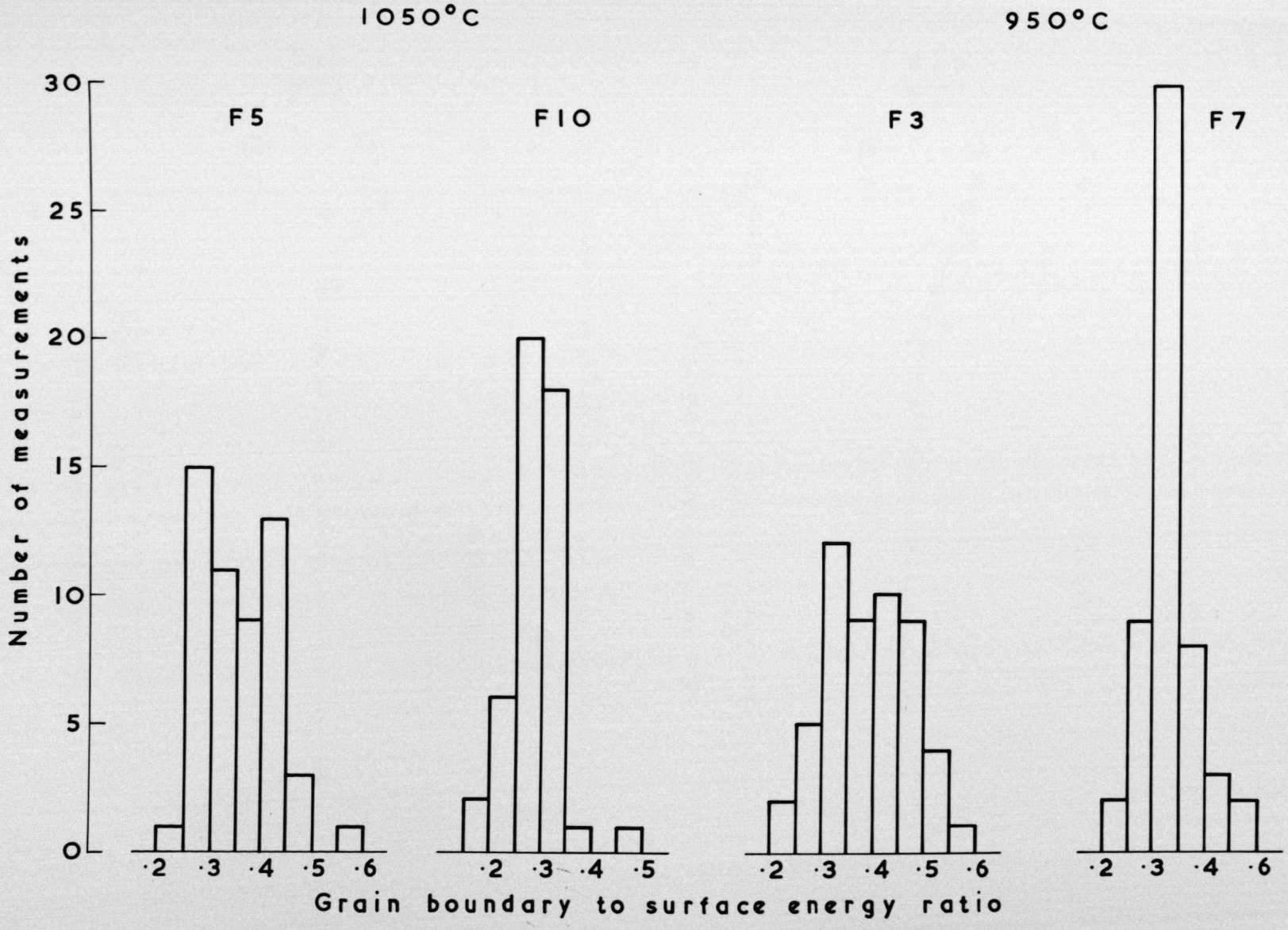

Figure 5.4. Histograms of grain boundary to surface energy ratios measured on iron-boron alloys.

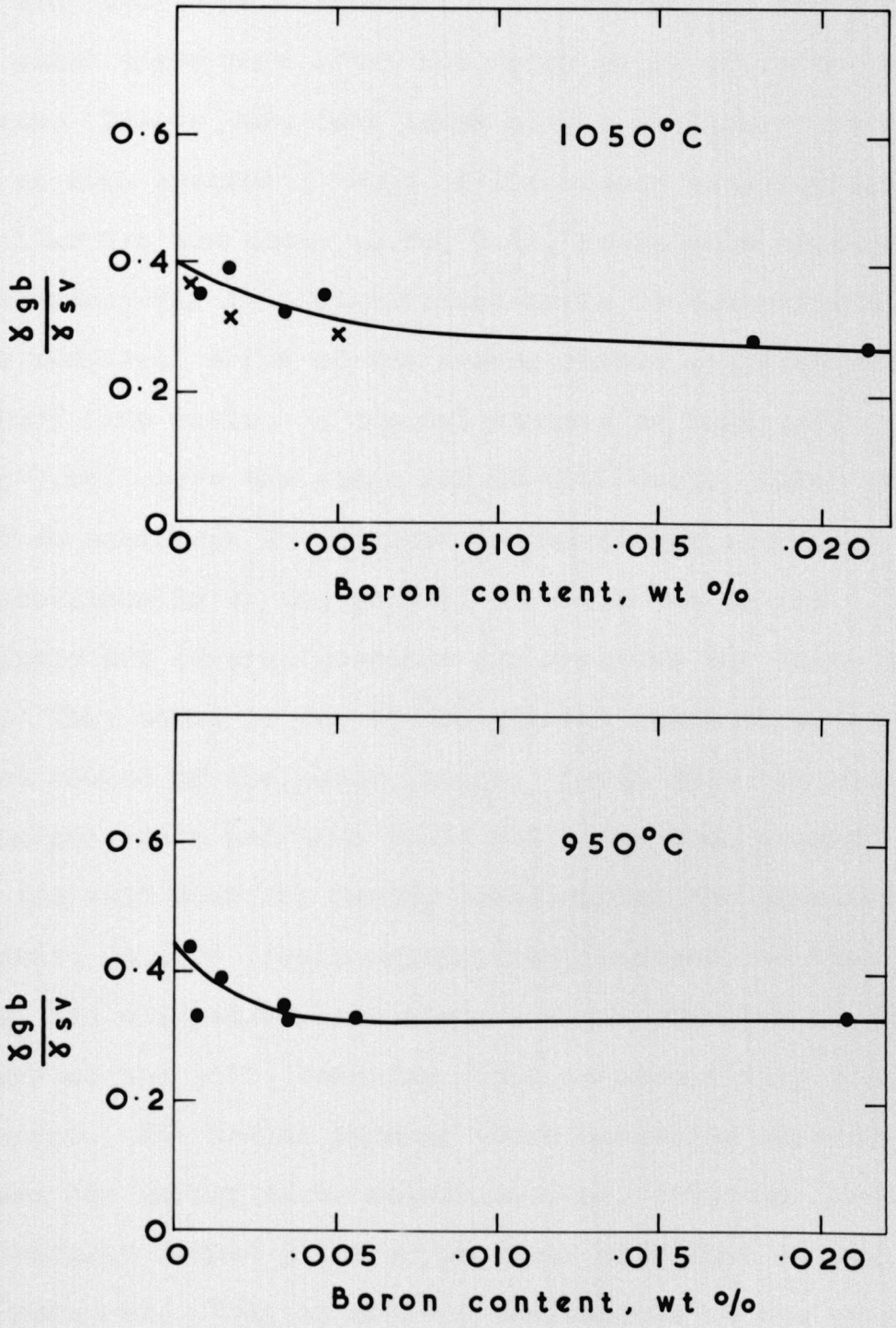

Figure 5.5. Grain boundary to surface energy ratios vs. boron content in iron-boron alloys.

5.4 Twin Boundary to Surface Energy Ratios

The ratios of twin boundary to surface energy were determined from Talystep traces of pairs of twin boundary groove and ridge profiles using equation (3.5). Because of the large grain sizes there were often not fifty pairs of twins on a specimen. Traces were thus taken of all available pairs of twins on each specimen. Some of the traces obtained were lop-sided like the one shown in Fig 5.6a, presumably because the twin boundary lay at a significant angle to the perpendicular to the surface. A few of the traces showed steps or ridges on a very fine scale. A typical example of this type is shown in Fig 5.6b; here the steps are 20-200Å deep. Other profiles showed an anomalous double peak on the ridged boundary (and very occasionally on the groove) like the one in Fig 5.6c.

There are several possible explanations for these extra peaks. They could be due to the general rumpling of the surface caused by the phase change, though this was usually on a larger scale and thus would not cause such a sharp peak, or to the twin boundary having moved during the grooving treatment. A more likely explanation, however, is that the crystal had slipped/sheared along a plane parallel to the twin boundary as the {111} twinning plane is also a slip plane in fcc metals. The traces showing these anomalous shapes were not used for energy ratio determinations, only the smooth, symmetrically shaped pairs of profiles like that in Fig 5.6d being measured. Thus on many of the samples it was possible to measure only quite small numbers of profiles. The mean γ_{sv}/γ_{tb} ratio values obtained for such samples were thus subject to rather large uncertainties (see Table 5.4).

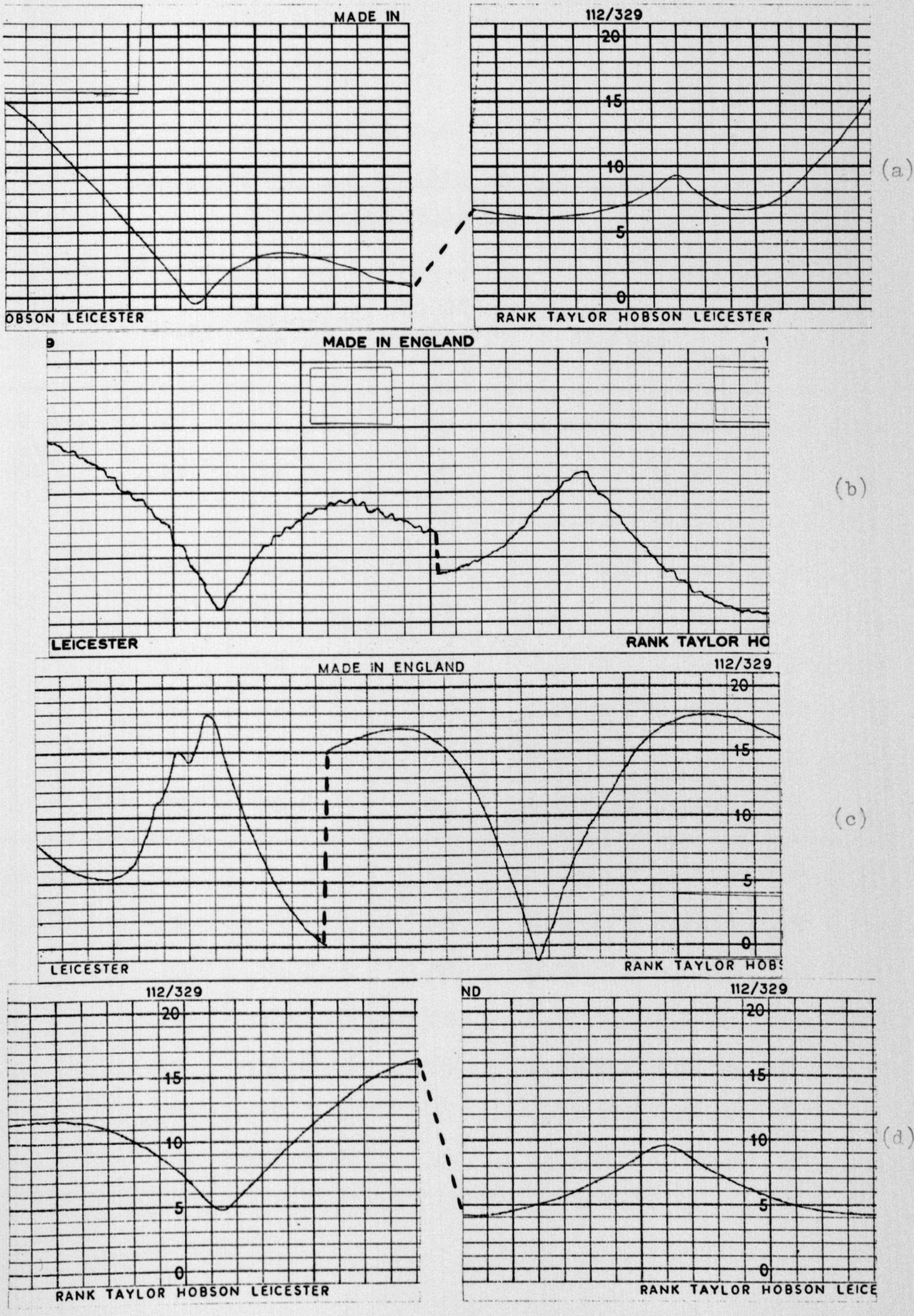

Figure 5.6. Talystep traces of twin boundary/surface intersections in (a) alloy F1 annealed at 1050°C (b) alloy F5 annealed at 950°C (c) alloy F1 annealed at 950°C and (d) alloy F7 annealed at 950°C.

TABLE 5.4

Twin boundary to surface energy ratios of iron-boron alloys

Annealing treatment	Alloy	Actual B wt ppm	No of measure-ments	γ_{tb}/γ_{sv}	γ_{sv}/γ_{tb}
168 hrs at 1050°C	F1	6.6 ± 1.3	33	0.0098 ± 0.0017	102 ± 18
	F3	16 ± 3	20	0.0101 ± 0.0023	99 ± 23
	F4	33 ± 3	30	0.0112 ± 0.0019	89 ± 15
	F5	45 ± 4	18	0.0119 ± 0.0019	84 ± 13
	F6	178 ± 18	27	0.0117 ± 0.0020	85 ± 15
	F7	214 ± 21	22	0.0118 ± 0.0017	85 ± 12
	F8	4 ± 2	20	0.0113 ± 0.0012	89 ± 9
	F9	16 ± 5	12	0.0102 ± 0.0035	98 ± 34
	F10	50 ± 5	14	0.0121 ± 0.0015	83 ± 10
168 hrs at 950°C	F1	4 ± 2	16	0.0099 ± 0.0027	101 ± 31
	F2	7 ± 3	33	0.0104 ± 0.0013	96 ± 12
	F3	14 ± 4	28	0.0107 ± 0.0015	93 ± 13
	F4	34 ± 3	22	0.0111 ± 0.0023	90 ± 19
	F5	56 ± 6	23	0.0098 ± 0.0014	102 ± 15
	F6	35 ± 10	27	0.0115 ± 0.0016	87 ± 12
	F7	208 ± 21	35	0.0104 ± 0.0009	96 ± 8

Some of the histograms of these ratios are shown in Fig 5.7. The spread of values obtained was similar to that for the steel specimens (Fig 4.6) but because of the smaller numbers of profiles measured the overall uncertainty in the mean value was greater.

The ratios obtained are listed in Table 5.4 together with the standard errors of their means, the number of pairs of twin traces measured and the actual boron concentration for each specimen. The results are plotted in Fig 5.8 as γ_{sv}/γ_{tb} vs actual boron concentration, for each temperature. At 1050°C there is a pronounced drop in this ratio with increasing boron content up to ~20% at 50 ppm boron. This indicates that the surface energy of the iron alloys was reduced to 80% of its value for 'pure' (ie very low boron) iron by the addition of 0.005 wt% boron. At 950°C, however, the effect of boron on the ratio γ_{sv}/γ_{tb} is not clear. Although a slight decrease in surface energy of up to about 10% is apparent on adding up to 0.003 wt% boron, the values for the higher boron concentrations are the same as for the nominally boron-free alloy. In fact, no differences between ratios were found that were bigger than the standard error of the mean for each specimen. Thus the effect of boron concentration on the surface energy at 950°C was too small to be satisfactorily determined from these measurements. This was probably due mainly to the large uncertainties in the ratio measurements. There may also be interference from the S, C and O in the material affecting the boron segregation. Normally segregation, and therefore its effect on the surface energy, would be expected to increase as the equilibrating temperature is lowered.

Figure 5.7. Histograms of twin boundary to surface energy ratios measured on iron-boron alloys.

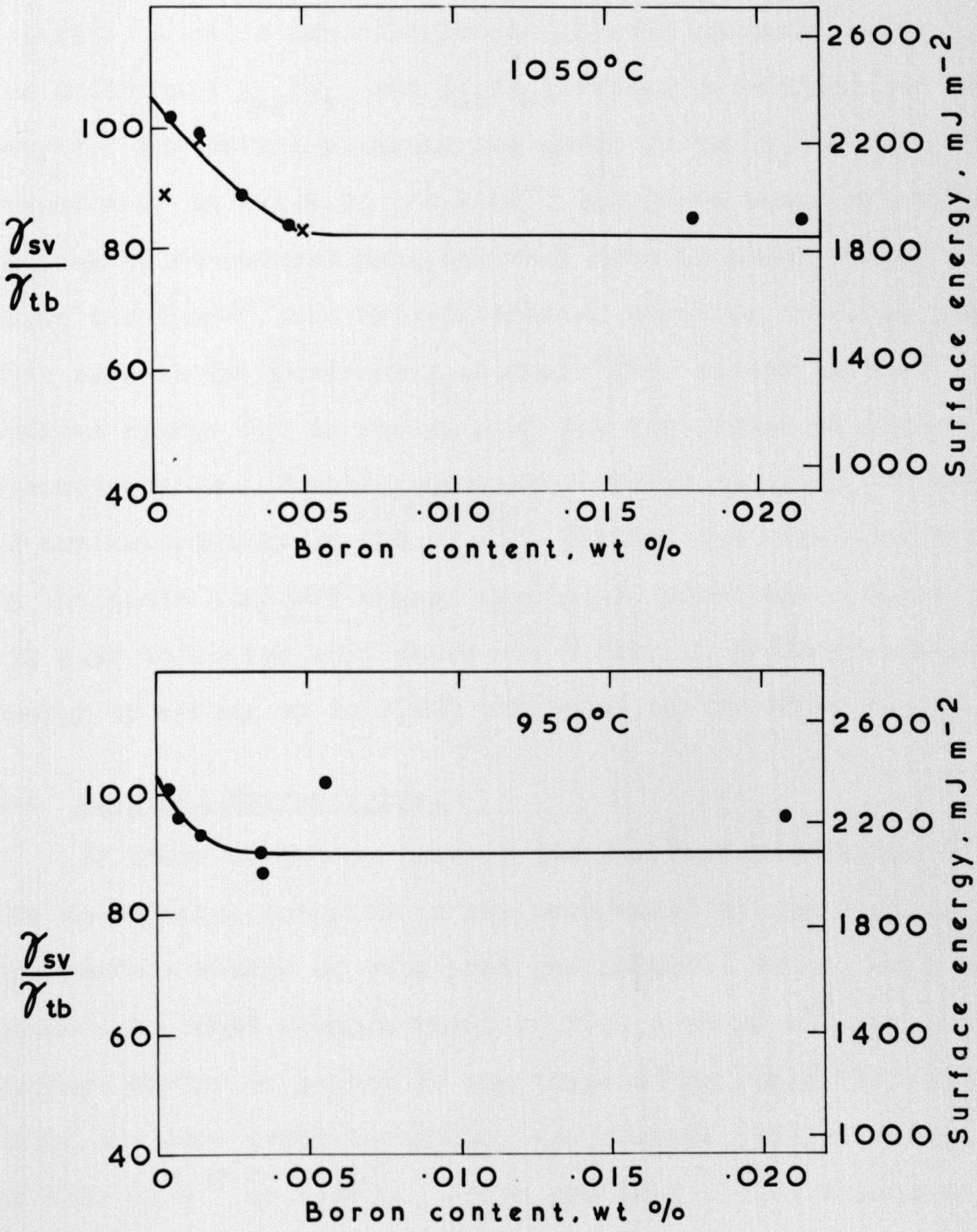

Figure 5.8. Surface to twin boundary energy ratios vs. boron content in iron-boron alloys.

5.5 Grain Boundary to Twin Boundary Ratios

In order to see the effect of boron concentration on the grain boundary energy (separate from its effect on the surface energy of these iron samples) the ratios γ_{gb}/γ_{tb} were calculated. A ratio was calculated for each specimen using the individual γ_{gb}/γ_{sv} and γ_{tb}/γ_{sv} ratios determined for that sample. The values obtained are given in Table 5.5 and graphically in Fig 5.9. At 1050°C the grain boundary energy is seen to be reduced progressively down to about 70% of its value for 'pure' iron by additions of boron up to 0.005 wt%. This is a larger percentage decrease than occurs in the surface energy but it occurs over the same range of boron concentrations. For the specimens treated at 950°C, because of the uncertainty in the γ_{tb}/γ_{sv} ratios, the effect of boron on the grain boundary energy was rather uncertain. However, Fig 5.9b indicates that there was a drop in grain boundary energy on adding up to 0.003 wt% boron of the order of 10%.

5.6 Absolute Energy Values

In order to get an idea of the absolute magnitudes of the interfacial energies in the iron-boron alloys a value for the surface energy of pure iron was needed. Price, Holl and Greenough [1964] found a value of 2150 ± 15 mJ m^{-2} for the surface energy of γ-iron in the temperature range 1360-1390°C using the zero creep technique, and Hondros [1965] found a value of 2140 mJ m^{-2} at 1380°C. Jones and Leak [1967] discussed the available experimental data on the temperature coefficients of solid metals. They concluded that, although the generally accepted value of - 0.5 mJ $m^{-2}\,°C^{-1}$ was not universally applicable (they estimated values up to - 3.0 mJ $m^{-2}\,°C^{-1}$ on

TABLE 5.5

Grain boundary to twin boundary energy ratios for iron-boron alloys

Annealing treatment	Alloy	Actual B wt ppm	γ_{gb}/γ_{tb}
168 hrs at 1050°C	F1	6.6 ± 1.3	36 ± 6
	F3	16 ± 3	39 ± 9
	F4	33 ± 3	29 ± 5
	F5	45 ± 4	30 ± 5
	F6	178 ± 18	24 ± 4
	F7	214 ± 21	23 ± 3
	F8	4 ± 2	32 ± 3
	F9	16 ± 5	32 ± 11
	F10	50 ± 5	27 ± 3
168 hrs at 950°C	F1	4 ± 2	44 ± 14
	F2	7 ± 3	32 ± 4
	F3	14 ± 4	36 ± 5
	F4	34 ± 3	31 ± 7
	F5	56 ± 6	34 ± 5
	F6	35 ± 10	28 ± 4
	F7	208 ± 21	32 ± 3

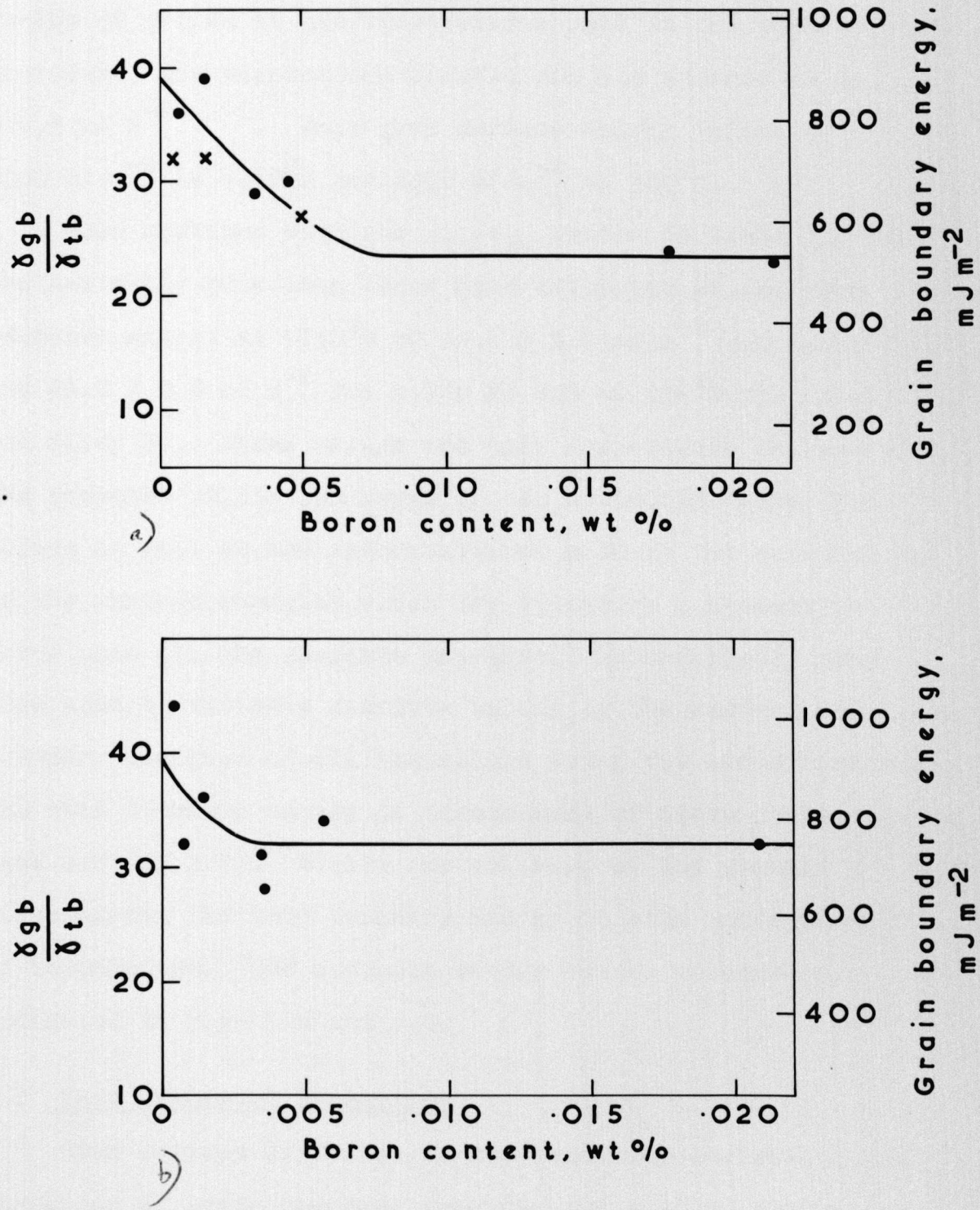

Figure 5.9. Grain boundary to twin boundary energy ratios vs. boron content in iron-boron alloys.

Cu, Ag, Au, Fe and Ni) the available data were not sufficiently accurate to provide reliable values of the coefficients for the five metals they considered. In order to estimate the surface energy of γ-iron at the temperatures used in the present work, therefore, the temperature coefficient was assumed to be -0.5 mJ $m^{-2}\,{}^{o}C^{-1}$. This gave surface energy values of 2300 mJ m^{-2} at 1050°C and 2350 mJ m^{-2} at 950°C.

When combined with the γ_{tb}/γ_{sv} ratios in Table 5.4 for the nominally pure iron these gave estimates of the twin boundary energy at 1050°C of 22.6 ± 3.9 mJ m^{-2} for Alloy F1 and 26.0 ± 2.8 mJ m^{-2} for alloy F8 and at 950°C 23.3 ± 6.3 mJ m^{-2} for alloy F1. These values are only approximate because of the presence of 4-6 ppm boron in the nominally boron free alloys as well as the approximations made in the calculation of the surface energies which may introduce a systematic error into all the absolute energies. Nevertheless, they were used to estimate absolute values of the surface and grain boundary energies of all the alloys using the assumption that the twin boundary energy is independent of boron concentration (see section 3.5). Within the accuracy of the present measurements the twin boundary energy is also independent of temperature. The absolute energy values obtained are indicated in Figs 5.8 and 5.9.

5.7 Mass Transport Properties

When surface diffusion is the mechanism dominating the formation of grain boundary grooves, the surface diffusion coefficients, D_s, can be calculated from Mullins' equation (4.1). Blakely and Mykura [1963] used this equation with $\Omega^2 n = d^4$, where d is the interatomic spacing and is equal to 2.6Å for

γ iron. As a further approximation for the present work it was assumed that d was unaffected by the small amounts of boron in the alloys. Equation (4.1) was rearranged slightly to give

$$D_s = \frac{W_s^4}{4.64} \times \frac{kT(\gamma_{tb}/\gamma_{sv})}{d^4 \; t \; \gamma_{tb}} \qquad \ldots (5.1)$$

and D_s values calculated using the values derived for γ_{tb}/γ_{sv} and γ_{tb}. The results are shown in Table 5.6 which also includes Blakely and Mykura's results. As can be seen the two sets of values are very similar. The effect of boron on the D_s values is not clear from the results in Table 5.6 which are again strongly dependent on the rather uncertain γ_{tb}/γ_{sv} ratios. It is nevertheless encouraging to note that the D_s values, particularly for the purer iron, are in good agreement with those of Blakely and Mykura which were measured under similar conditions of vacuum and temperature and using a value for γ_{sv} of 2000 mJ m^{-2}.

5.8 Discussion

Surface and grain boundary energies of iron-boron alloys have not previously been measured. However, two sets of workers have measured γ_{gb}/γ_{sv} and γ_{tb}/γ_{sv} ratios for pure iron. Blakely and Mykura [1963] obtained a value of γ_{gb}/γ_{sv} of 0.38 ± 0.04 for pure iron in vacuo at 1060°C. This is in good agreement with the values obtained in the present work at 1050°C which were 0.352 ± 0.008 and 0.367 ± 0.007 for alloys F1 and F8 respectively. Kudrman and Čadek [1969a] carried out measurements in hydrogen over a range of temperatures and obtained somewhat lower values than those in vacuo in the present work. At 1050°C their value was 0.318 ± 0.003.

TABLE 5.6

Surface diffusion coefficients

This work			
Annealed at 1050°C		Annealed at 950°C	
Alloy	D_s $cm^2\ sec^{-1}$	Alloy	D_s $cm^2\ sec^{-1}$
F1	2.2×10^{-6}	F1	1.1×10^{-6}
F3	2.7×10^{-6}	F2	1.0×10^{-6}
F4	2.0×10^{-6}	F3	8.6×10^{-7}
F5	2.6×10^{-6}	F4	8.9×10^{-7}
F6	3.5×10^{-6}	F5	1.5×10^{-6}
F7	3.9×10^{-6}	F6	1.4×10^{-6}
F8	4.5×10^{-6}	F7	1.4×10^{-6}
F9	3.6×10^{-6}		
F10	3.6×10^{-6}		

Blakely & Mykura 1963	
Annealing Temperature	D_s $cm^2\ sec^{-1}$
925°C	1.45×10^{-6}
975°C	1.9×10^{-6}
1060°C	7.7×10^{-6}
1100°C	2.24×10^{-5}

The same workers also measured γ_{tb}/γ_{sv} ratios on their materials. Blakely and Mykura obtained a value of 0.017 ± 0.006 at 1060°C which was an average of only a few measurements. McLean and Mykura [1964] re-examined the same sample and from 30 measurements obtained a value of 0.015 ± 0.004. This result agrees within the experimental errors with our values of 0.010 ± 0.002 for alloy F1 and 0.011 ± 0.001 for alloy F8 at 1050°C. Kudrman and Čadek [1969b] measured γ_{tb}/γ_{sv} ratios in vacuo at 1050 and 1150°C obtaining values of 0.0160 ± 0.0027 and 0.0136 ± 0.0015.respectively. The value at 1050°C is a bit higher than the present measurements but the difference is only just outside the experimental errors.

The measurement of grain boundary to surface energy and twin boundary to surface energy ratios was severely hampered in these iron samples because of distortions of the profiles which occurred during the phase change from austenite (fcc) to ferrite (bcc) on cooling from the annealing temperature. The uncertainties in the γ_{tb}/γ_{sv} ratios were also increased by the small numbers of symmetrical twin boundary profiles on each specimen. However, certain effects of boron concentration on the interfacial energies are evident.

The reduction in both surface and grain boundary energy on addition of boron is most clear at 1050°C. At this temperature additions of boron up to 0.005 wt% progressively decrease the surface energy down to ~80% of the 'pure' iron value and the grain boundary energy to ~70% of the 'pure' iron value. Further additions of boron do not change the energies any more, indicating that the interfaces are saturated with boron at a bulk concentration of 0.005 wt%.

At 950°C the situation is less clear. Due to the greater scatter of results no apparent effect of boron on the surface energy could be deduced from the measurements. However, a reduction in the ratio γ_{gb}/γ_{sv} of up to 20% was found with additions of up to 0.0035 wt% boron. This is the same percentage reduction as was seen in this ratio at 1050°C but the bulk concentration at which grain boundary saturation apparently occurs is lower. This indicates a stronger tendency for boron to segregate to the grain boundaries at the lower temperature as would be expected. On the other hand it makes the lack of detectable effect of boron on the surface energy more puzzling.

Boron is not the only interfacially active element present in the alloys, though it is the only one which was systematically varied. There were also significant amounts of C, O and S in all the alloys. All these elements are found to affect the fracture behaviour of iron (cf Chapter 3) and sulphur has been shown to segregate strongly to iron surfaces (Bishop and Rivière [1970]) and grain boundaries (Powell et al [1973]). Thus it is fairly certain that boron will not be the only impurity component present in excess at the interfaces. This assertion is confirmed for the surface by the Auger spectroscopy results in Chapter 6. However, the energy ratios measured on the two sets of alloys with different impurity contents at 1050°C lie on the same curve when plotted against boron concentration. Thus, even in the presence of these other impurities, boron appears to segregate strongly to interfaces in iron causing reductions in their energies. It is not known at present whether the boron segregates competitively, displacing the other impurity atoms from the

interfaces, or associatively by forming complexes with them, or whether any other interaction can occur between the various solute atoms.

The interfacial activity of a solute in a particular solvent is defined as the decrease in interfacial energy per atomic percent of bulk solute concentration. Hondros and McLean [1968] attempted to correlate the surface activity in a wide range of systems with other physical parameters. They found that the best correlation was obtained with maximum solubility, probably because this parameter reflects all types of atomic mismatching. Their plot of log (surface activity) vs log (maximum atomic solubility) is the basis of Fig 5.10.. Hondros [1969] considered grain boundary activity in the same way and produced a graph like the one shown in Fig 5.11.. The lines drawn on these figures are simply there to emphasise the general trend of the results and have no special significance. No account was taken in these figures of the temperature at which measurements were made, therefore they show only a general trend. However, they do give some indication of how interfacially active a solute may be in a particular solvent.

In order to compare the results of the present work with other investigations of interfacial energies affected by solutes, surface and grain boundary activities were calculated from the curves drawn in Figs 5.8 and 5.9. Because of the large uncertainties in the ratios obtained at 950°C the calculations were restricted to the results obtained from specimens annealed at 1050°C. Even at this temperature the exact shapes of the curves were not well defined but served to give an order of magnitude for the activities. The values

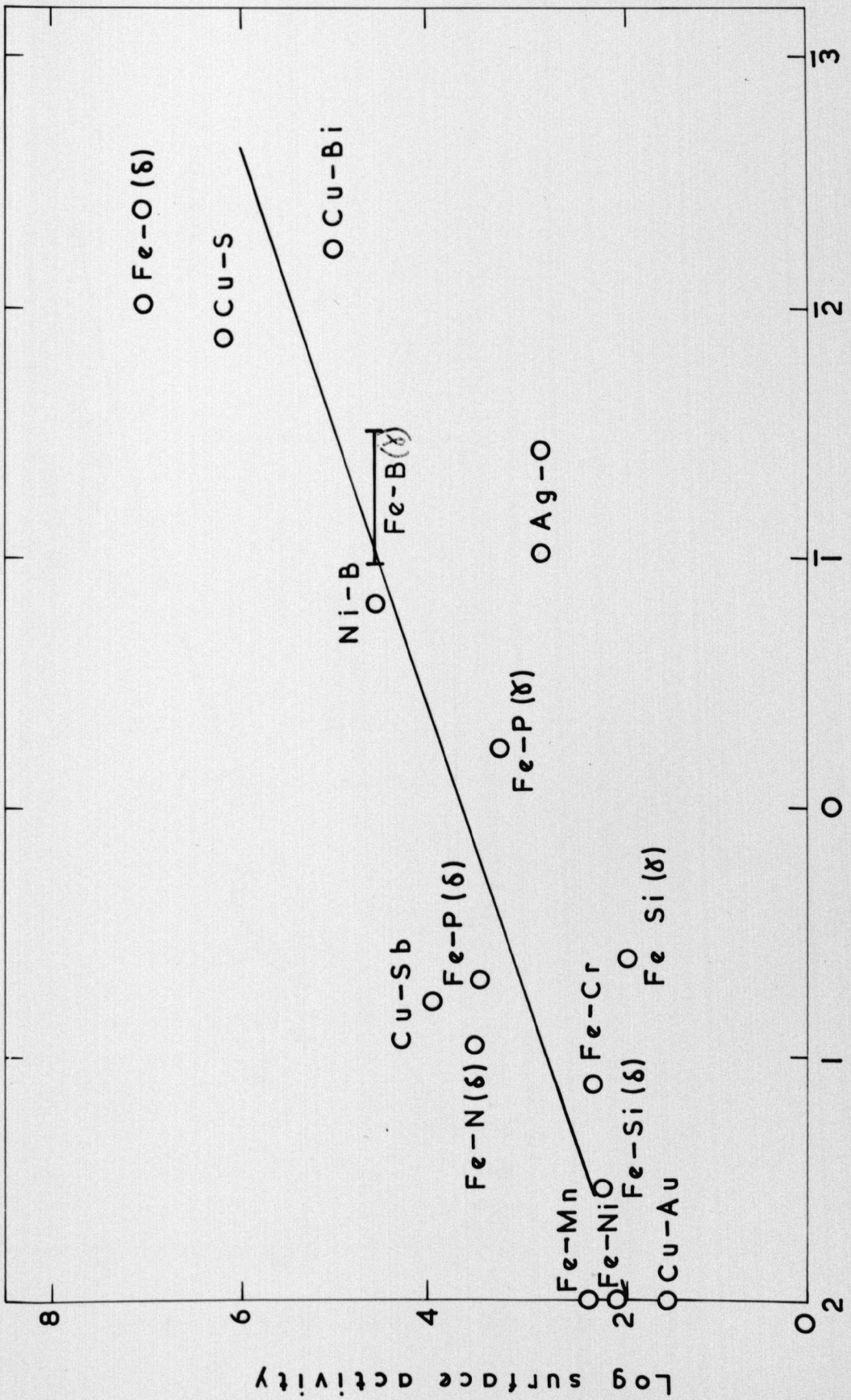

Figure 5.10. Correlation of surface activity with maximum atomic solid solubility.

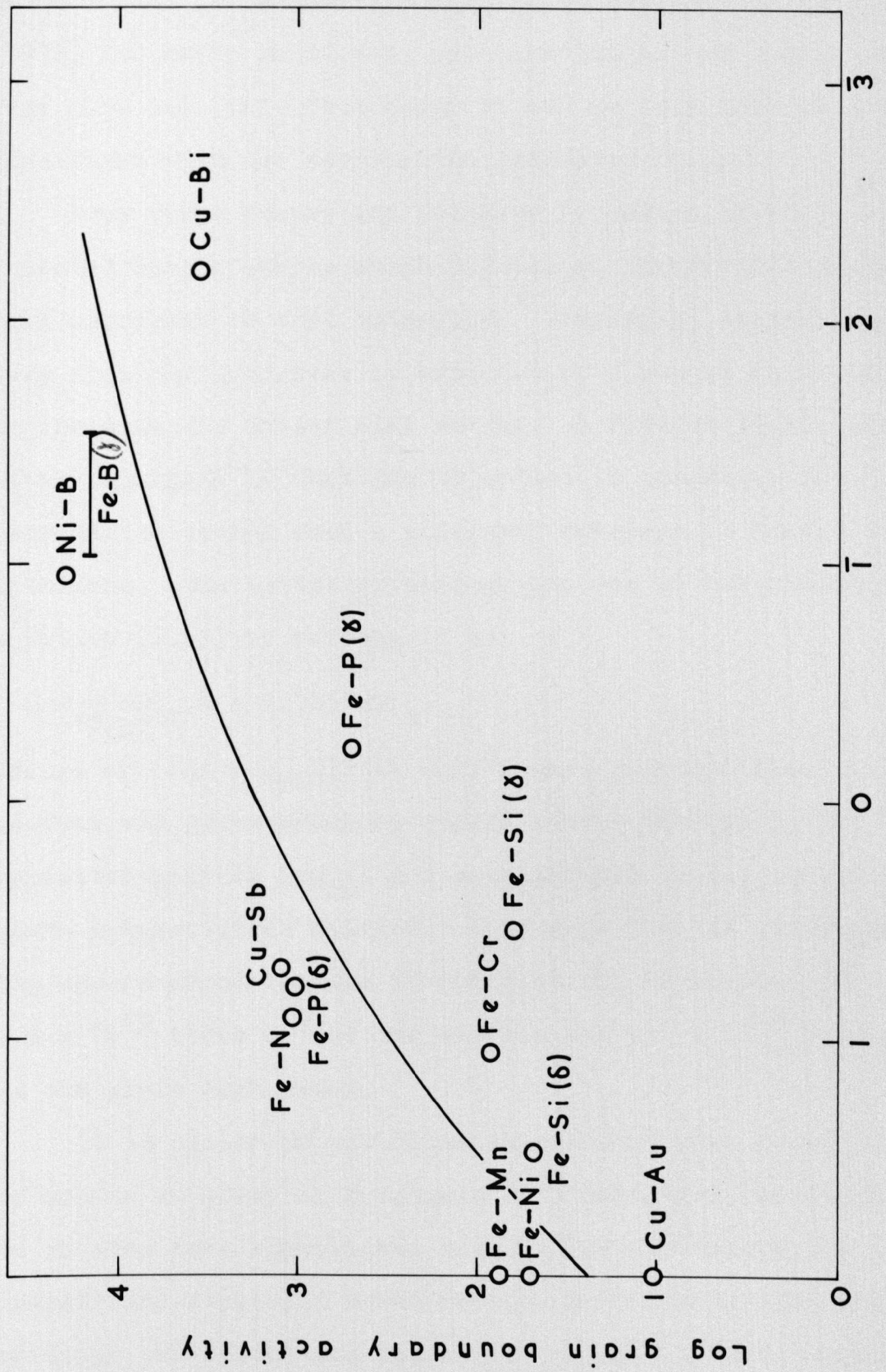

Figure 5.11. Correlation of grain boundary activity with maximum atomic solid solubility.

obtained were 3×10^4 mJ $m^{-2}(at\%)^{-1}$ for the surface activity and 1.5×10^4 mJ $m^{-2}(at\%)^{-1}$ for the grain boundary activity. These values are comparable with those obtained by Hodgson [1972] for boron in nickel, and were put on the graphs in Figs 5.10 and 5.11, from which it can be seen that they are consistent with the correlation indicated there.

From Gibbs adsorption isotherm (equation (2.17)), it is expected that a solute which reduces an interfacial energy will segregate to that interface. Similarly, segregation away from the interface is expected of a solute which tends to increase the interfacial energy. A further implication of Gibbs' analysis is that the interface is saturated and segregation ceases when a monolayer coverage is formed at the interface. The extent of segregation can be calculated from equation (2.17) by writing it as

$$\left(\frac{\partial \gamma}{\partial \log_{10} X}\right)_T = -2.303\, RT\Gamma_2. \qquad \ldots (5.2)$$

Values of $(\partial\gamma/\log_{10}X)T$ at 1050°C were obtained from the surface and grain boundary energy curves in Figs 5.8 and 5.9, replotted against $\log_{10}X$ and extrapolated to the concentration where saturation is reached. This gave rise to values of Γ_2, the excess concentration of boron at the interfaces, of 1.8×10^{19} atoms m^{-2} at the surface and 1.1×10^{19} atoms m^{-2} at the grain boundaries.

It is easier to visualise this interfacial concentration of solute in terms of fractions of a monolayer, although this is an even more approximate measure because values for the interfacial densities of atoms must be assumed. The surface coverage was calculated for a (100) plane to be 0.6 monolayer. The grain boundary coverage was calculated by assuming a

monolayer at the grain boundary to be a single close packed plane. This gave a coverage of 0.6 monolayer. These figures give only the order of magnitude of the coverages because of the uncertainties in the experimental results from which they are derived and the approximations involved in their calculation.. However, they do serve to show that the saturation coverage by boron of both surfaces and grain boundaries in austenitic iron is an appreciable fraction of a monolayer. In so doing, they are consistent with Gibbs' analysis of interfacial segregation and are substantially in agreement with work on other systems, some of which are mentioned in Chapter 2.

Seah and Hondros [1973] have defined a more precise parameter, the grain boundary enrichment factor, β, by which to compare segregation in different systems:

$$\beta = \frac{X_B/X_{B_o}}{X_c} = \left(\frac{\partial \gamma_{gb}/\partial X_c}{X_{B_o} RT}\right) = \frac{K}{X_{c_o}} \qquad \ldots (5.3)$$

where X_B = number of moles of adsorbate, X, per m^2 of grain boundary,

X_{B_o} = number of moles of X required per m^2 to form a close packed sheet 1 atom thick,

X_c = bulk atomic concentration of X,

X_{c_o} = limit of atomic solubility of X at the measurement temperature,

and K = $\exp(Q/RT)$ which for temperatures $\sim 1000^{\circ}K$ and Q 0-5 kcal $mole^{-1}$ is in the range 1 to 10.

For the iron-boron system the maximum solubility at $1050^{\circ}C$ from the phase diagrams in Fig 2.4is between 40 and 120 wt ppm ($2\text{-}6 \times 10^{-4}$ atom fraction). The value of β calculated from the present measurements for iron-boron alloys at $1050^{\circ}C$ is

4.3×10^3 and, as shown in Fig 5.12, this is in reasonable agreement with Seah and Hondros' correlation.

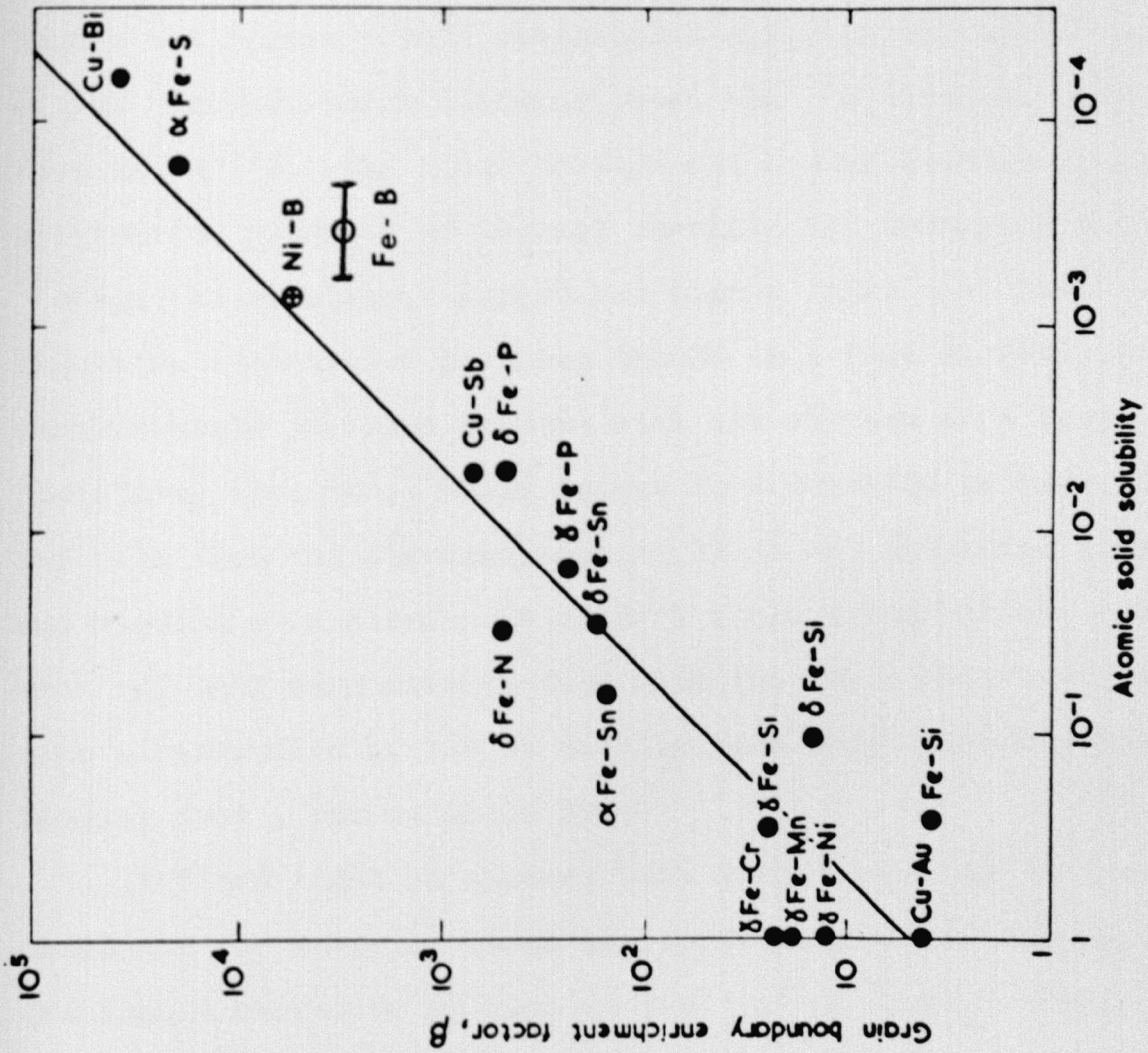

Figure 5.12. Correlation of grain boundary enrichment factor, β, with atomic solid solubility.

CHAPTER 6 ANCILLARY MEASUREMENTS

6.1 Boron Autoradiography

Autoradiography is a technique which enables the distribution of a particular element within the structure of a material to be determined. In some cases a radioactive isotope can be incorporated into the material and its distribution recorded on a photographic plate. For the case of boron, Hughes and Rogers [1967] developed a slightly different technique. Natural boron contains about 19% ^{10}B isotope, the rest being ^{11}B. The minor isotope has a high capture cross section for neutrons of thermal energies and undergoes the $^{10}B[n,\alpha]^{7}Li$ reaction. Hughes and Rogers found that the resulting α-particles produced tracks in a film of cellulose acetobutyrate in close contact with the surface of a boron-containing specimen. These tracks were revealed by removing the film from the specimen, etching it in hot potassium hydroxide and viewing on a microscope in dark field illumination. In this way they were able to determine the boron distribution with a resolution of 2μm in samples with boron concentrations ranging from 1 ppm to about 20%.

At first sight it appears that autoradiography is a good technique for studying boron segregation in metals and alloys and should therefore be used to back up the present work. However, Stein [1967] considered the application of autoradiography to the measurement of equilibrium segregation to grain boundaries and found that it was a rather insensitive technique for this purpose. He gave examples of several systems in which other measurements indicated the existence of equilibrium grain boundary segregation but where autoradiography

had failed to detect it. He thus set up a mathematical model of a grain boundary and considered the factors affecting the detection of segregation to this boundary. He found that in order to detect grain boundary segregation the range of energies of the emitted particles must be very low and the concentration of the segregation species must be 2-3 orders of magnitude greater in the grain boundary than in the grain interior. He thus concluded that detection of equilibrium grain boundary segregation by this technique was unlikely except in a few ideal cases.

This conclusion was backed up by the results of Williams' [1972] study of boron segregation in solution treated 316 steel in which he concluded that boron did not segregate to the grain boundaries at the solution treatment temperatures. This conclusion was based on measurements on specimens which had either been cooled in a stream of cold argon (~50°C/sec) or had been water quenched (~500°C/sec). In the former case some boron was seen to be segregated to the grain boundaries but no segregation could be detected in the latter case. He therefore deduced that the observed segregation was of a non-equilibrium type and occurred during cooling from the solution treatment temperature. The corollary of these observations, that equilibrium segregation of boron in 316 steel does not occur at solution treatment temperatures conflicts with the results of the grain boundary energy measurements described in Chapter 4, which were made on specimens from the same casts of steel as Williams used.

Another potential limitation of the technique which was highlighted by Williams' measurements is that when a specimen is subjected to a particular series of treatments the boron

analysis can only indicate where the boron is at the end of the experiment. Unless great care is taken to quench the specimens very quickly, the measured boron distribution may bear little resemblance to its distribution at the temperature of interest.

The materials used in the present work were examined by Applied Chemistry Division, Harwell, using autoradiography in the 'as received' condition and after the various grooving treatments. They were metallographically polished before application of the detecting film so that the internal boron distribution was examined. However, for the reasons given above the amount of information obtainable from these examinations was limited. The specimens were cooled in the furnace after the grooving treatments at initially $\gtrsim 50^{\circ}C$/min, a speed which was fast enough to prevent the groove shapes being significantly altered but which was quite slow enough for the boron to be redistributed. Thus the segregation of boron to the grain boundaries observed on some of the autoradiographs eg Fig 6.1a, was not the equilibrium segregation for the particular annealing temperatures. The distribution of boron-containing precipitates before and after the grooving anneals was seen clearly in the autoradiographs. In the case of the 316 steels annealed at $950^{\circ}C$ it was found (Fig 6.1) that after the heat treatment there was still evidence of the boron-containing precipitate stringers which were present in the 'as received' material. This indicated that the precipitates had not all been dissolved during this particular heat treatment.

Garnish and Hughes [1972 and 1973] have shown that autoradiography can also be used to give quantitative analysis

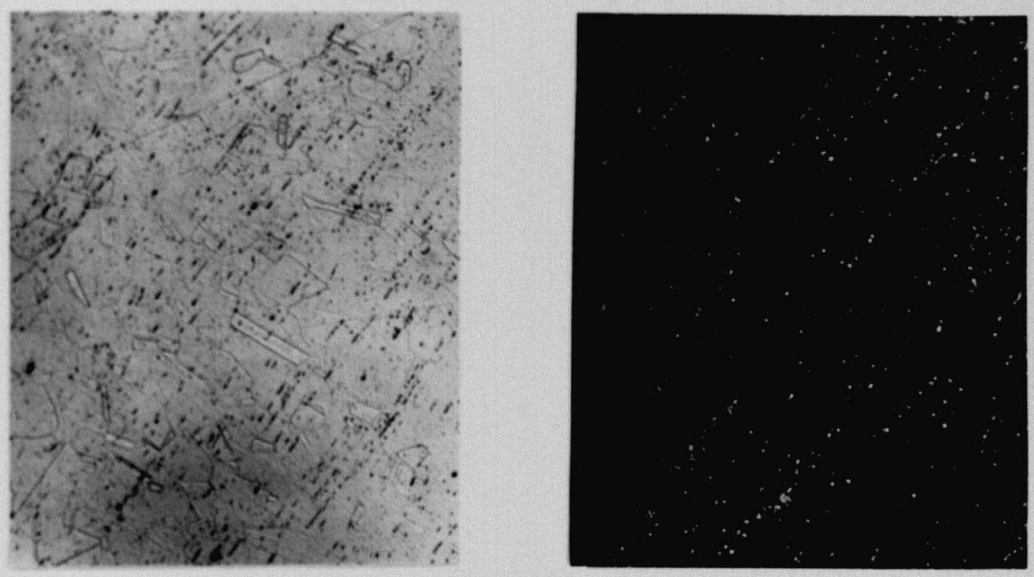

(a)

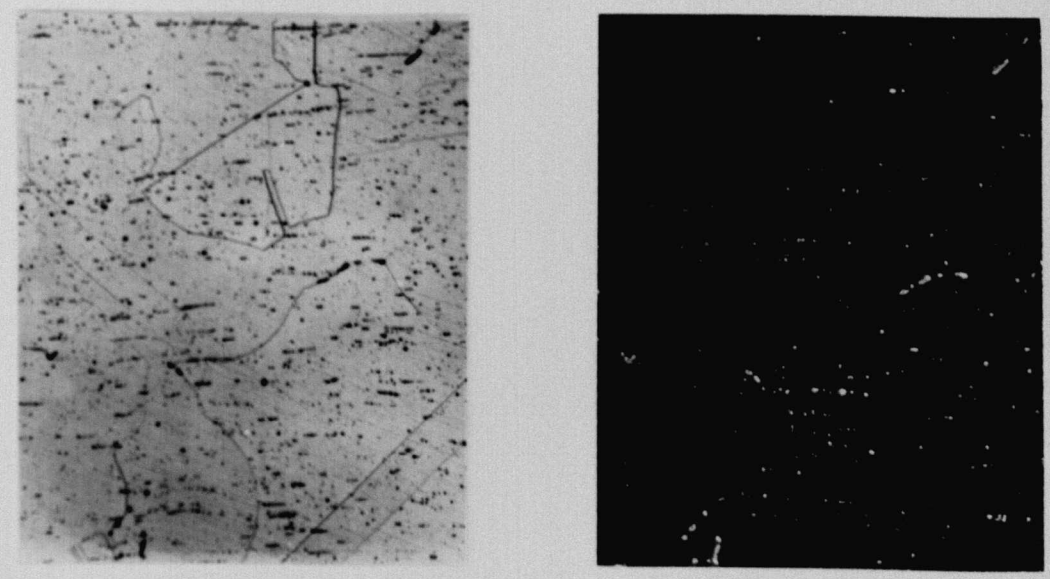

(b)

Figure 6.1. Micrographs and autoradiographs of steel II (a) as received and (b) after annealing 1 hour at 1050°C and 24 hours at 950°C. (X110)

of boron in a sample. For this the cellulose acetobutyrate film is spaced off from the specimen surface by ~0.5 mm so that the distribution of recorded tracks is more even. The individual tracks in a given area are counted and the boron concentration calculated from the known neutron dose rate. The process is repeated on several areas of the specimen to check for macroscopic inhomogeneities. The iron specimens were analysed for boron in this way after being grooved and measured and the results are given in Chapter 5. The main errors in such measurements arise from the limitations of optical track density determinations. Garnish and Hughes estimated that, when 1000 or more tracks were counted, the accuracy of the measurements were ±.10% for boron concentrations over 30 ppm, decreasing to ± 20% at 10 ppm and ± 70% at 1 ppm.

6.2 Auger Spectroscopy

Auger electron spectroscopy enables the top few atom layers of a specimen surface to be analysed. Auger electrons result from the transition of an excited atom (ionized in an inner shell) to a lower energy stage. In its simplest form the process is represented by the energy diagram in Fig 6.2. A primary electron (energy E_p) ionizes an atom in an inner level E_1. An electron from a higher level E_2 fills the gap in E_1. The energy $|E_1 - E_2|$ thus released can either be emitted as a photon (characteristic X-rays), or be transmitted to another electron in an energy level E_3, causing it to be emitted from the solid as an Auger electron. The Auger electron has the characteristic energy $E_a = |E_1| - |E_2| - |E_3|$. To be identified as an Auger electron, the emitted electron

Figure 6.2. Energy diagram for emission of Auger electrons.

must lose no energy before emerging from the surface. The probability of interaction by electrons with energies in the range 30-300 eV with atoms in the solid is very large, so effectively the two top atomic layers contribute the bulk of the Auger electron emission. At ionization energies E_p of less than 500 eV the probability of releasing a photon instead of an Auger electron is very low so that by bombarding the specimen with such electrons a spectrum of Auger electrons characteristic of the particular surface is obtained. The energy distribution is electronically differentiated to pick out the characteristic peaks.

Because some of the other elements present in the iron-boron alloys were potential surface and grain boundary segregants, two of the specimens were examined by Solid State Instruments Group using Auger electron spectroscopy. One specimen from each series of alloys was examined, alloys F5 and F9. The specimens were mechanically ground to a thickness of about 5μm and one side polished in the same way as the specimens which were subsequently grooved. The specimens were heated by passing a current through them so that measurements could be made at temperature. The specimen of alloy F5 was uneven in thickness and therefore heated unevenly along its length, the difference between the hot and cold ends being about 70°C. Thus, analyses were given for each end of the specimen whereas on the specimen of alloy F9, which heated evenly, average analyses were obtained. Each specimen surface was analysed 'as polished', after argon ion bombarding to remove adsorbed gases, at ~ 950°C, at room temperature after 30 mins at 950°C, at 1050°C and again at room temperature after 30 mins at 1050°C. The results obtained are summarised

in Table 6.1 where the numbers are approximate atomic percentages of the elements present on the surface.

The first thing which is evident from the results is that boron is by no means the only segregating element present in the alloys, indeed it is not even the major element present on the surface. However, it does segregate to the surface in appreciable quantities when the specimens are heated as shown by the presence of up to 3 at% B on the surface of alloy F5 whose bulk concentration is nominally 0.008 wt% (0.040 at%).

An interesting correlation is seen to exist between the boron and nitrogen segregation, Fig 6.3. A similar correlation has been observed previously on other iron and steel surfaces by Bishop and Rivière [1970]. The reason for this correlation is not known, whether B-N complexes are formed within the material and segregate as a unit, or whether the presence of one of these elements at the surface creates a structure which increases the segregation of the other. The fact that the concentration of B + N after cooling to room temperature is nearly twice that at the high temperatures suggests that a boron nitride may be precipitating on cooling. On the other hand, this may be just another example of non-equilibrium segregation acting to enhance the already existing high temperature segregation.

On the 'as polished' surfaces large amounts of oxygen and carbon were found. Under argon ion bombardment most of the oxygen was removed from the alloy F5 surface indicating that it was mostly adsorbed gas. However, the carbon remained on the surface, indicating that it was more strongly bound. For the alloy F9 the reverse was true, ie the carbon was

TABLE 6.1

Results of Auger Spectroscopic Analyses

Specimen F9 (50 ppm B)

Treatment	Fe	O	Ca	C	Cl	S	P	N	Ar	B
As polished	56.8	30.7	0.1	9.9	1.9	0.7	-	-	-	-
Ion bombarded	65.3	30.7	+	3.1	0.2	0.2	-	0.3	0.3	-
Repeat IB	65.2	30.7	+	3.1	0.2	+	-	-	0.9	-
At 950°C	84.3	10.0	0.3	-	-	5.0	-	-	-	0.5
At room temperature	91.6	4.9	1.3	0.1	-	0.6	+	1.0	-	0.6
At 1050°C	80.6	13.0	2.6	-	-	3.8	0.1	--	-	+
At room temperature	89.8	8.2	1.9	+	-	0.1	-	-	-	0.2
Specimen F5 (80 ppm B)										
As polished	44.8	40.6	4.1	8.5	0.5	0.5	0.5	0.5	-	-
Ion bombarded	75.8	15.3	0.1	7.5	-	-	-	1.0	0.4	-
Repeat IB	84.6	6.2	+	8.0	-	-	-	-	1.3	-
At 810°C	73.3	11.8	-	-	-	24.8	-	-	-	-
At 940°C	69.8	-	-	-	-	26.7	-	2.3	-	1.2
RT: cool end	82.3	-	-	0.6	-	16.5	-	0.5	-	+
RT: hot end	66.5	-	0.2	1.3	-	23.7	-	4.8	-	3.5
At 905°C	73.8	-	-	-	-	24.3	-	1.1	-	0.9
At 1030°C	70.5	-	-	-	-	25.9	-	2.0	-	1.6
RT: cool end	67.9	-	0.2	1.1	-	23.9	-	3.9	-	3.0
RT: hot end	74.0	-	-	1.1	-	17.8	-	3.9	-	3.0

+Detected but amount not measurable.

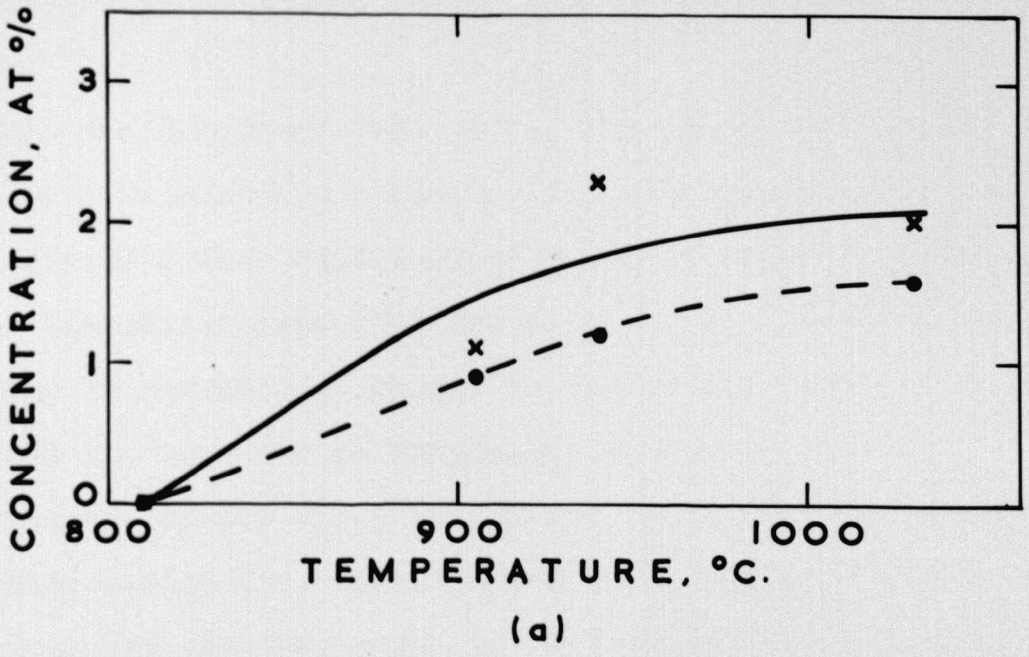

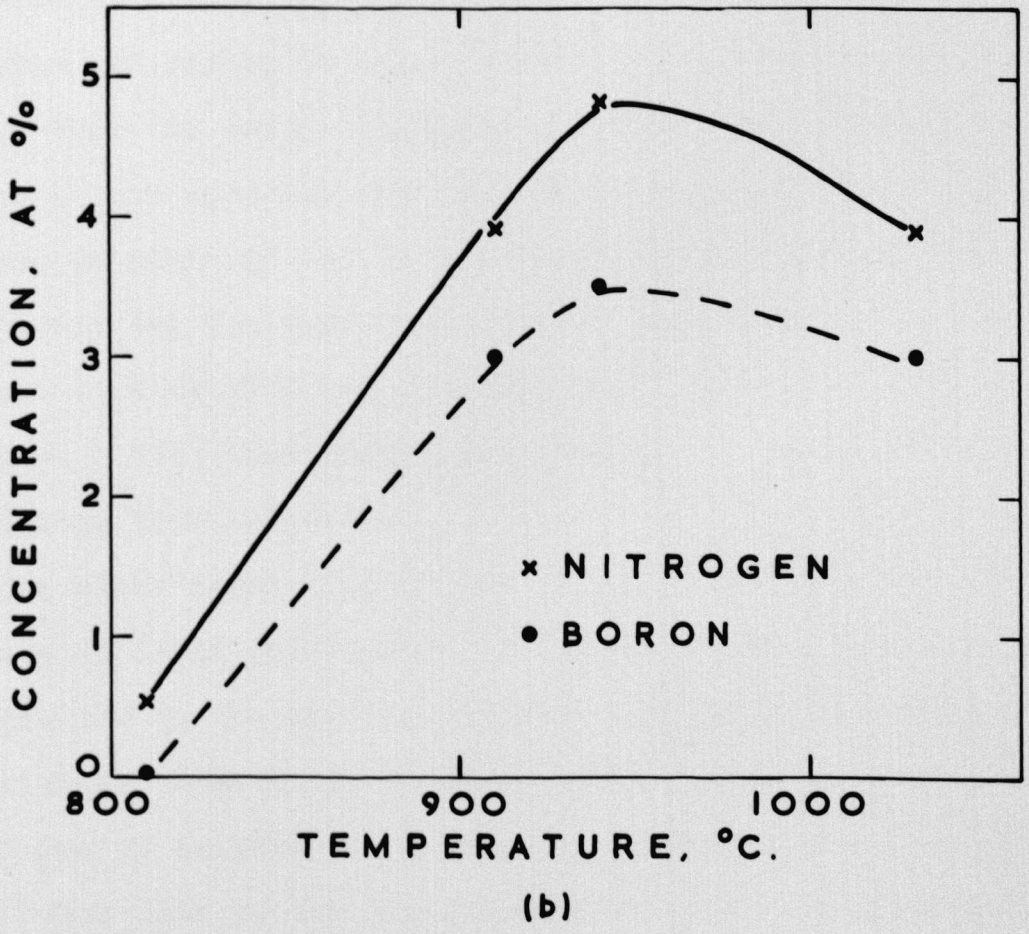

Figure 6.3. Surface concentration vs. temperature for boron and nitrogen on iron-boron alloy F5 (a) at temperature and (b) after cooling back to room temperature from plotted temperature.

removed by ion bombardment but the oxygen was unaffected suggesting that an actual oxide layer was present on the surface.

When the specimens were heated the carbon and oxygen concentrations on the surfaces of both alloys were reduced, presumably by either evolution of adsorbed gases or dissolution of the oxide layer into the bulk of the specimen. On the alloy F5 surface, no oxygen or carbon was detected at 950 or 1050°C but some carbon reappeared on cooling to room temperature. On the alloy F9 surface the carbon disappeared on heating but an appreciable quantity of oxygen remained throughout the measurements. The oxygen concentration was higher at 950 and 1050°C than on cooling back to room temperature. It is interesting, in view of the interactions of carbon and oxygen in iron discussed in Chapter 2 (2.3.3), to note that the oxygen completely disappeared from the surface of one specimen and the carbon remained (or rather returned on cooling) and in the other specimen the carbon disappeared but the oxygen remained. This very scanty evidence ties up with the suggestions of Tsukahara and Yoshikawa [1971] that oxygen at an interface tends to exclude carbon from that interface.

The other element which was observed to segregate to the surfaces in large quantities was sulphur. The quantities were smaller in the case of the purer alloy F9 but still appreciable. Bishop and Rivière [1970] observed large quantities of sulphur on other iron surfaces and showed that on removing some of the sulphur by reacting with oxygen or hydrogen the boron and nitrogen concentrations increased. Sulphur appears to be a very strongly segregating element in

iron and Powell et al [1973] have used Auger spectroscopy to show that low temperature intergranular embrittlement in iron is associated with segregation of sulphur to the grain boundaries.

From the known presence of interstitial solutes in the alloys used for the present work it was expected that interfacial segregation of several species would take place. The Auger analyses confirm that this is the case at least for the surface. The results obtained for the effects of boron segregation on grain boundary and surface energies described in Chapter 5 therefore apply to iron alloys of the particular compositions used and not to a pure binary iron-boron system. However, the similarity of the effects of boron in the two series of alloys of different purities suggests that boron has a strong enough driving force for segregation, that it will segregate and lower the interfacial energies in iron alloys even in the presence of other segregating elements such as sulphur.

CHAPTER 7 DISCUSSION

Measurements have been made in this work of the effects of boron on the surface and grain boundary energies of AISI 316 austenitic stainless steel and pure fcc iron. Hodgson [1972] measured the effects of boron on the same energies in pure nickel which is also fcc. Her results were very similar to those obtained for iron and so will be considered in this discussion alongside the present iron and steel results. Boron has a very low solubility in iron, nickel and austenitic steel. It therefore follows that its atoms have a high degree of misfit in these lattices and thus should experience a large driving force for segregation to any available distorted regions such as surfaces and grain boundaries.

Bishop and Rivière [1970] showed using Auger spectroscopy that boron does segregate to iron surfaces, though not to the exclusion of other elements such as sulphur, oxygen, carbon and nitrogen. Hodgson [1972] found similar results in nickel boron alloys. This technique has not yet been applied to the segregation of boron in austenitic steels but Williams [1972] used autoradiography to look for boron segregation to grain boundaries in AISI 316 steel. By using suitable cooling conditions he produced observable non-equilibrium segregation but was unable to detect any equilibrium segregation of boron.

In the measurement of interfacial energies from the shapes of the intersections of several interfaces after long annealing times any effects of solutes on these energies must be due to equilibrium segregation at the annealing temperature. Hodgson made such measurements at 900 and 1000°C on nickel alloys containing up to 0.005 wt% boron, the highest

concentration being outside the solubility limit for boron in nickel. The present measurements were made on iron containing up to 0.020 wt% boron, close to the maximum solid solubility, at 950 and 1050°C, and on 316 steel containing 0.001 and 0.0060-0.0065 wt% boron, probably within the solubility limit, at 950 to 1250°C. The accuracy of the energy values obtained for the steels and iron alloys were discussed in Chapters 4 and 5 respectively and are typical of the type of measurement used.

The effects of boron on the surface energies, which were measured using the assumption of constant twin boundary energy, are summarised in Table 7.1. In the nickel alloys at 900 and 1000°C and in the iron alloys at 1050°C adding boron was found to decrease the surface energy, indicating that segregation of boron to the surface had taken place at the high temperatures, up to a certain concentration where saturation apparently occurred. Further additions of boron had no effect on the surface energy. Saturation appeared to occur in the nickel alloys at between 0.006 and 0.010 wt% and the saturation value of surface energy was 35% below the value for pure nickel at 1000°C and 20% below at 900°C. Boron reduced the iron surface energy by up to 20% at 0.005 wt% and 1050°C. In the case of the iron alloys at 950°C and the 316 steels the effect of boron on the surface energy was not entirely clear, though a reduction of about 10% was apparent with 0.0035 wt% boron in iron at 950°C. Five out of the eight pairs of measurements on the steels showed a reduction of between 10 and 30%. The other three showed no change or a slight increase in the surface energy on increasing the boron content. This uncertainty was probably due to interference from other impurities in

TABLE 7.1

Reductions in surface energies on increasing boron concentration

	Temp °C	Change in B concn, ppm	Reduction in γ_{sv} %	mJ m^{-2}
Fe alloys	950	0 → 40†	12	280
	1050	0 → 60†	22	380
Steels I & II	950	10 → 60	-6	-35
	1050	10 → 60	29	255
	1150	10 → 60	18	180
	1250	10 → 60	9	70
Steels III & IV	950	10 → 65	12	70
	1050	10 → 65	0	0
	1150	10 → 65	20	220
	1250	10 → 65	-8	-53
Ni alloys*	900	0 → 100†	20	400
	1000	0 → 100†	35	700

†Approximate concentration at which saturation of the surface occurred.

*Data from Hodgson [1972].

the materials which could also segregate to the surface. However, in the cases where an effect of boron on the surface energy was defined it was similar in the iron, nickel and 316 steels, both in the size of the effect produced and the bulk concentration of boron at which the minimum value of the surface energy was reached.

A fuller comparison between the measurements on iron, nickel and 316 steel can be made for the grain boundary energies, Table 7.2, which were also reduced by boron additions, indicating equilibrium segregation of boron to the grain boundaries at the annealing temperatures used. In all these materials the effect of boron on the grain boundary energy was greater than its effect on the surface energy when expressed as a percentage of the energy for boron 'free' (or in the case of 316 steel, 10 ppm boron) material. However, because the grain boundary energy is always smaller than the surface energy the drop in absolute energy was usually greater for the surface than for the grain boundaries, cf Tables 7.1 and 7.2. This qualitative statement is applicable to the measurements on iron and nickel alloys but its applicability to the steel measurements is less clear, largely because of the uncertainties in the surface energy values.

The effects of boron on the grain boundary energies were similar in all three materials. In iron at 1050°C a minimum surface energy ~30% below the value for pure iron was reached at a boron concentration of 0.005 wt%. In 316 steel at 1050°C increasing the boron concentration from 0.001 to ~0.006 wt% decreased the grain boundary energy by ~30% and in nickel at 1000°C the minimum grain boundary energy ~50% below the value for pure nickel was obtained for a boron concentration of

TABLE 7.2

Reductions in grain boundary energies on increasing boron concentration

	Temp °C	Change in B concn, ppm	Reduction in γ_{sv} %	mJ m^{-2}
Fe alloys	950	0 → 40†	19	240
	1050	0 → 80†	40	350
Steels I & II	950	10 → 60	12	45
	1050	10 → 60	34	210
	1150	10 → 60	39	310
	1250	10 → 60	20	130
Steels III & IV	950	10 → 65	16	55
	1050	10 → 65	29	160
	1150	10 → 65	29	200
	1250	10 → 65	25	150
Ni alloys*	900	0 → 100†	35	360
	1000	0 → 100†	50	420

†Approximate concentration at which grain boundary saturation occurred.

*Data from Hodgson [1972].

$\sim$0.01 wt%. The similarity between these results is marked, despite a wide variation in interstitial impurity content of the base materials. The nickel alloys had the lowest interstitial contents, up to 0.004 wt% C and 0.004 wt% S (O not quoted), and the effects of boron seem to be most easily seen in them. However, even in the 316 steels the boron has large effects on at least the grain boundary energies.

The large reductions in surface and grain boundary energies caused by additions of boron to iron, nickel and 316 steel indicate that the boron segregates to these interfaces at the annealing temperatures used. For the iron and nickel alloys, by treating them as simple binary systems of boron in dilute solution in a metal base, it was possible to calculate values of the interfacial activities and excess concentrations of boron in each base material. The interfacial activities, the rates of change of interfacial energies with bulk boron concentration at concentrations approaching zero, were compared with those for other systems using Hondros' and McLean's correlations, Fig 5.10. As can be seen from this figure the activity values calculated for boron in both iron and nickel were fairly high ($\sim 10^4$ mJ m^{-2} per at%) and fitted well with the general trend of increasing activity as bulk solubility decreases.

The excess concentrations of boron at the interfaces calculated from Gibbs' adsorption isotherm were similar for iron and nickel: 1.8×10^{19} and 1.1×10^{19} atoms m^{-2} at the surface and grain boundaries respectively of iron at 1050°C, and 5.2×10^{18} atoms m^{-2} at both types of interface in nickel at 1000°C. Another way of expressing the excess concentration of a solute at an interface is as a fraction of a monolayer,

but this is rather more approximate because of a lack of knowledge of the exact atomic spacing in interfacial regions. Hondros and McLean [1968] and Hondros [1969] have given collections of interfacial concentrations expressed in this way and shown that for most strongly segregating solutes a value of ~1/3 to 1 1/3 monolayer is obtained. Thus the values of 0.6 monolayer of boron at iron surfaces and grain boundaries calculated in the present work seems reasonable. Seah and Hondros [1973] found a good correlation between a 'grain boundary enrichment factor', β (see equation (5.3)) and the limit of atomic solubility at the temperature of the measurements. A value of β of 4.3×10^3 was calculated for boron in iron at 1050°C which is in reasonable agreement with Seah and Hondros' correlation (see Fig 5.12). It is also very similar to the value of 5.6×10^3 for nickel-boron at 1000°C, thus further emphasising the similarity of the action of boron in nickel and in γ-iron noted from the original energy measurements. The similarity of the effect of boron on the grain boundary energies in 316 steel also leads to the supposition that boron is acting in much the same way in this more complex material at the temperatures used for the energy measurements, where the steel has a single phase structure.

Segregation of solutes to grain boundaries is often associated with changes in the mechanical properties of materials. Some examples of grain boundary embrittlement at low temperatures and reduction of creep ductility at high temperatures associated with grain boundary segregation were given in Chapter 2 (Section 2.3.3). Boron has been found to increase the creep ductility and creep rupture life of 316 steel in the temperature range 600-700°C (Williams, Harries

Furnival [1972]). They also found that the improvement in creep properties was associated with a reduction in the incidence of grain boundary cracks. The present work has shown that boron segregates to the grain boundaries in this steel at higher temperatures, 950-1250°C. The question thus raised is whether boron at the grain boundaries reduces the tendency for them to fracture by its effect on their energies, in contrast to the effect of most other segregating solutes so far investigated which tend to embrittle boundaries.

When a material fractures in a brittle or a semibrittle manner, either at very low temperatures or during creep at high temperatures, it does so by the growth and coalescence of one or more cracks. These may form either within grains or along grain boundaries. When the cracks are formed or extended, in order to produce the new surfaces an amount of energy must be supplied by the release of stored elastic energy which is equal to $2\gamma_{FS} - \gamma_{GB}$ per unit area of grain boundary fractured or $2\gamma_{FS}$ per unit area of transgranular crack formed. (At high temperatures energy is also absorbed in plastic deformation.) Here γ_{FS} is the surface free energy of the newly formed fracture surface and γ_{GB} is the free energy of the grain boundary immediately prior to fracture. These quantities are not the same as γ_{sv} and γ_{gb}, the equilibrium surface and grain boundary free energies, though in high temperature creep the conditions may be such that $\gamma_{GB} = \gamma_{gb}$. If the values of γ_{FS} and/or γ_{GB} are altered, for instance by segregation to the grain boundaries prior to fracture, then the surface energy requirement will also be altered. If $2\gamma_{FS}$ is reduced due to the segregation by an amount larger than the reduction in γ_{GB}, then the surface free

energy necessary to produce fracture along the grain boundary is lowered. If $2\gamma_{FS} - \gamma_{GB}$ is increased then fracture along the grain boundaries is inhibited.

Referring to Tables 7.1 and 7.2 it can be seen that for the iron and nickel alloys the equilibrium interfacial energies are changed on saturation with boron in such a way that $2\gamma_{sv} - \gamma_{gb}$ is always reduced. This is also true in 5 out of the 8 pairs of results for the steels, the exceptions being those which showed an apparent slight rise or no change in surface energy on increasing the boron concentration. The first implication of these results is that the grain boundaries in iron and nickel and probably 316 steel should be embrittled by segregated boron. It has already been mentioned that $\gamma_{FS} \neq \gamma_{sv}$, though at high temperatures γ_{GB} is probably equal to γ_{gb}. In the iron and nickel alloys it was shown that the saturation surface and grain boundary concentrations expressed in atoms per m^2 were approximately equal (ie $\Gamma^{sv} \simeq \Gamma^{gb}$). Thus when a grain boundary fractures the newly formed surface will have only half its equilibrium concentration of boron and thus $\gamma_{FS} > \gamma_{sv}$. However, even if we assume that the reduction in γ_{FS} between pure iron (or nickel) and iron + 0.006 wt% boron (or Ni + 0.010 wt% B) is equal to only half the reduction in γ_{sv}, then $2\gamma_{FS} - \gamma_{GB}$ ($= 2\gamma_{FS} - \gamma_{gb}$) will still be reduced according to the figures in Tables 7.1 and 7.2. (In fact the reduction in γ_{FS} will probably be rather more than this as the rate of change in surface energy tends to decrease with increasing boron concentration.) If we apply the same argument to the five pairs of steel results for which $2\gamma_{sv} - \gamma_{gb}$ is reduced by increasing the boron concentration then for three out of the five, $2\gamma_{FS} - \gamma_{gb}$ would definitely be reduced

and for the other two it might increase. However, because of the relative lack of data for the steels this argument is less certain.

From the above consideration of interfacial energies it appears that boron segregated at the grain boundaries of iron, nickel and possibly 316 steel should cause embrittlement of the boundaries and thus, for example reduce creep rupture lives and ductilities at temperatures of 950°C and above. However, this is manifestly not the case in 316 steel at 600-700°C as has been shown by Williams et al [1972]. By analogy it might be expected that boron would cause low temperature embrittlement in iron and nickel. However, Taga and Yoshikawa [1971] showed strengthening of iron grain boundaries at low temperatures in the presence of boron.

The comparison of interfacial energy data with mechanical property data for alloys containing boron thus stresses the importance of taking into account the many other factors involved in deformation and fracture processes. In systems where impurities are associated with embrittlement it is easy to see correlations between interfacial energy changes and reduction in a parameter indicating grain boundary strength or cohesion. However, by studying systems in which an interfacially active solute is associated with strengthening of the boundaries it has been possible to show that such changes in interfacial energy are not necessarily sufficient to produce grain boundary embrittlement. Instead the embrittling tendency can be overcome by other effects of the solute, in the case of the 316 steel interaction with carbide precipitates and for iron at low temperatures probably interaction with other impurities.

REFERENCES

Adair A M, Spretnak J W, and Speiser R [1955], Trans Met Soc AIME, 203, 353.

Astrom H U [1956], Acta Met, 4, 562.

Bishop H E and Rivière J C [1970], Acta Met, 18, 813.

Blakely J M [1961], PhD Thesis, University of Glasgow.

Blakely J M and Mykura H [1962], Acta Met, 10, 565.

Blakely J M and Mykura H [1963], Acta Met, 11, 399.

Brenner S S and McKinney J T [1968], App Phys Lett, 13, 29.

Busby P E, Warga M E and Wells C [1953], Trans Met Soc AIME, 197, 1463.

Dulieu D and Nutting J [1964], ISI Spec Rep, 86, 140.

Elliot R P [1965], 'Constitution of Binary Alloys, First Supplement', McGraw-Hill.

Garnish J D and Brown A [1972], AERE Report R 7179.

Garnish J D and Hughes J D H [1972], J Mat Sci, 7, 7.

Garnish J D and Hughes J D H [1973], J Inst Met, 101, 108.

Gibbs J W [1928], 'Collected Works', Longmans.

Gjostein N A [1961], Trans Met Soc AIME, 221, 1039.

Gjostein N A [1967], 'Surfaces and Interfaces' I, 271, Syracuse University Press.

Gjostein N A [1970], Met Trans, 1, 315.

Gleiter H and Chalmers B [1972], Progr in Materials Sci, 16.

Goldschmidt H J [1971], JISI, 209, 900.

Guggenheim E A [1940], Faraday Soc Trans, 36, 397.

Guggenheim E A [1967], 'Thermodynamics', 5th Edition, North Holland Publishing Co, Amsterdam.

Hansen M [1958], 'Constitution of Binary Alloys', McGraw-Hill.

Hasegawa M and Okamoto M [1965], J Jap Inst Metals, 29, 328.

Herring C [1951], 'The Physics of Powder Metallurgy', p 176, McGraw-Hill.

Hilliard J E, Cohen M and Averbach B L [1960], Acta Met, 8, 26.

Hodgson B K [1972], PhD Thesis, University of Warwick.

Hodgson B K and Mykura H [1973], J Mat Sci, 8, 565.

Honda R and Taga H [1968], Met Sci J, 2, 172.

Hondros E D [1965], Proc Roy Soc, A286, 479.

Hondros E D [1969], Interfaces Conf, Melbourne.

Hondros E D [1970], Techniques of Met Res, 4, 293 (Intersci Publishers, J Wiley).

Hondros E D [1972], Met Sci J, 6, 110.

Hondros E D and McLean D [1968], SCI Monograph, 28, 39.

Hughes J D H and Rogers G T [1967], J Inst Met, 95, 299.

Inman M C, McLean D and Tipler H R [1963], Proc Roy Soc, A273, 538.

Inman M C and Tipler H R [1963], Met Rev, 8, 105.

Jandeska W F and Morral J E [1972], Met Trans, 3, 2933.

Jones H and Leak G M [1967], Met Sci J, 1, 211.

Jones H [1971], Met Sci J, 5, 15.

Joshi A and Stein D F [1970], Met Trans, 1, 2543.

Joshi A and Stein D F [1971], JIM, 99, 178.

King R J, Downs M J, Clapham P B, Raine K W and Talim S P [1972], J Phys E, 5, 445.

Kudrman J and Čadek J [1969a], Czech J Phys B, 19, 1337.

Kudrman J and Čadek J [1969b], Phil Mag, 20, 413.

Low J R [1969], Trans Met Soc AIME, 245, 2481.

McAllister P V and Cutler I B [1969], J Am Cer Soc, 52, 348.

McAllister P V and Cutler I B [1970], Met Trans, 1, 313.

McAllister P V, Spretnak J W and Speiser R [1954], Trans ASM, 46, 499.

McLean D [1957], 'Grain Boundaries in Metals', OUP.

McLean M and Mykura H [1964], Acta Met, 12, 326.

Marcus P W and Palmberg H L [1969], Trans Met Soc AIME, 245, 1664.

Mistler R E and Coble R L [1968], J Am Cer Soc, 51, 472.

Mullins W W [1956], Acta Met, 4, 421.

Mullins W W [1957], JAP, 28, 333.

Mullins W W [1960], Trans Met Soc AIME, 218, 354.

Mullins W W [1962], 'Metal Surfaces', P 17, ASM.

Mullins W W and Shewmon P G [1959], Acta Met, 7, 163.

Murr L E [1968], Acta Met, 16, 1127.

Murr L E [1970], Phys Stat Sol A, 3, 447.

Murr L E, Wong G I and Horylev R J [1973], Acta Met, 21, 595.

Mykura H [1957], Acta Met, 5, 346.

Mykura H [1961], Acta Met, 9, 570.

Neumann G and G M [1972], 'Surface Self-Diffusion of Metals', Diffusion Information Centre.

Nicholson M E [1954], Trans Met Soc AIME, 200, 185.

Palmberg P W and Marcus H L [1969], Trans ASM, 62, 1016.

Powell B D, Westwood H J, Taplin D M R and Mykura H [1973], Metallurgical Trans (in press).

Price A T, Holl H A and Greenough A P [1964], Acta Met, 12,49.

Rivière J C [1968], private communication.

Robertson W M [1970], Techniq Met Res, 4, 349 (Intersci Publishers, J Wiley).

Seah M P and Hondros E D [1973], Scripta Met, 7, 735.

Smith C S [1948], Trans Met Soc AIME, 175, 15.

Stein D F [1967], Trans Met Soc AIME, 239, 1721.

Stein D F, Joshi A and Laforce R P [1969], Trans ASM, 62, 776.

Stone P G [1967], ISI Publication 97, 505.

Taga H and Yoshikawa A [1971], Proc ICSTIS, Suppl Trans ISI Jap, 11, 1256.

Tipler H R and McLean D [1970], Met Sci J, 4, 103.

Tolman F R and Wood J G [1956], J Sci Instr, 33, 236.

Tsukahara Y and Yoshikawa A [1971], Proc ICSTIS, Suppl Trans ISI Jap, 11, 1259.

Udin H [1952], 'Metal Interfaces', p 114, ASM.

Voce E and Hallowes H P C [1947], J Inst Metals, 73, 323.

Westbrook J H [1964], Met Rev 9, 415.

White S S, Adams C M and Wulff J [1960] quoted in Hilliard, Cohen and Averbach [1960].

Williams T M [1972], Met Sci J, 6, 68.

Williams T M and Barrand P [1965], JIM, 93, 447.

Williams T M, Harries D R and Furnival J [1972], JISI, 210, 351.

Williams T M and Talks M G [1972], JISI, 210, 870.

APPENDIX

JOURNAL OF NUCLEAR MATERIALS 39 (1971) 59–68. © NORTH-HOLLAND PUBLISHING CO., AMSTERDAM

THE SURFACE AND INTERFACIAL ENERGIES OF THE URANIUM-URANIUM CARBIDE SYSTEM

E. N. HODKIN, D. A. MORTIMER, M. G. NICHOLAS and D. M. POOLE

UKAEA, Solid State Division, Atomic Energy Research Establishment, Harwell, Didcot, Berks., UK

Received 12 October 1970

The surface and interfacial energies of the U-UC system have been determined within the temperature range 850–1720 °C from sessile drop experimental data together with other data published previously by the authors. The values obtained, in units of J/m², can be described as a function of temperature, t °C, by the following equations.

Surface energy of UC,
$\gamma_{UC-A} = (0.728 \pm 0.041) - 10^{-5}\ (t - 1325)$,
$1325 < t < 1720$.

Grain boundary energy of UC,
$\gamma_{UC-UC} = (0.274 \pm 0.015) - 4 \times 10^{-6}\ (t - 1325)$,
$1325 < t < 1720$.

Interfacial energy between U and UC,
$\gamma_{U-UC} = (0.141 \pm 0.008) - 7 \times 10^{-6}\ (t - 1100)$,
$1100 < t < 1550$;
$\gamma_{U-UC} = (0.141 \pm 0.008) - 6 \times 10^{-5}\ (t - 1100)$,
$850 < t < 1100$.

Surface energy of liquid U,
$\gamma_{LU} = 1.45 \pm 0.012$,
$1190 < t < 1600$.

Surface energy of liquid U saturated with C,
$\gamma_{LU(C)} = 1.44 - 2.35 \times 10^{-3}\ (t - 1325)$,
$1325 < t < 1600$.

Les énergies de surface et interfaciale du système U-UC ont été déterminées dans le domaine de température 850–1720 °C à partir des données expérimentales concernant l'équilibre d'une goutte sessile et aussi à partir des données publiées antérieurement par les auteurs. Les valeurs obtenues, exprimées en J/m² peuvent être décrites en fonction de la température t °C, par les équations suivantes:

Energie superficielle de UC,
$\gamma_{UC-A} = (0.728 \pm 0.041) - 10^{-5}\ (t - 1325)$,
$1325 < t < 1720$.

Energie des joints de grain de UC,
$\gamma_{UC-UC} = (0.274 \pm 0.015) - 4 \times 10^{-6}\ (t - 1325)$,
$1325 < t < 1720$.

Energie interfaciale entre U et UC,
$\gamma_{U-UC} = (0.141 \pm 0.008) - 7 \times 10^{-6}\ (t - 1100)$,
$1100 < t < 1550$;
$\gamma_{U-UC} = (0.141 \pm 0.008) - 6 \times 10^{-5}\ (t - 1100)$,
$850 < t < 1100$.

Energie superficielle de l'uranium liquide,
$\gamma_{LU} = 1.45 \pm 0.012$,
$1190 < t < 1600$.

Energie superficielle de l'uranium liquide saturé en carbone,
$\gamma_{LU(C)} = 1.44 - 2.35 \times 10^{-3}\ (t - 1325)$,
$1325 < t < 1600$.

Die Oberflächen- und Grenzflächenenergien γ im System U-UC wurden zwischen 850 und 1720 °C durch Messung des Benetzungswinkels und aus früher veröffentlichten Arbeiten anderer Autoren bestimmt. Die erhaltenen Werte [J/m²] können als Funktion der Temperatur t (°C) durch folgende Gleichungen dargestellt werden:

Oberflächenenergie von UC:
$\gamma_{UC-Ar} = (0{,}728 \pm 0{,}041) - 10^{-5}\ (t - 1325)$,
$1325 < t < 1720$.

Korngrenzenenergie von UC:
$\gamma_{UC-UC} = (0{,}274 \pm 0{,}015) - 4 \times 10^{-6}\ (t - 1325)$,
$1325 < t < 1720$.

Grenzflächenenergie zwischen U und UC:
$\gamma_{U-UC} = (0{,}141 \pm 0{,}008) - 7 \times 10^{-6}\ (t - 1100)$,
$1100 < t < 1550$;
$\gamma_{U-UC} = (0{,}141 \pm 0{,}008) - 6 \times 10^{-5}\ (t - 1100)$,
$850 < t < 1100$.

Oberflächenenergie von flüssigem U:
$\gamma_{LU} = 1{,}45 \pm 0{,}012$,
$1190 < t < 1600$.

Oberflächenenergie von flüssigem U mit C gesättigt:
$\gamma_{LU(C)} = 1{,}44 - 2{,}35 \times 10^{-3}\ (t - 1325)$,
$1325 < t < 1600$.

1. Introduction

Values for the surface and grain boundary energies of nuclear fuels such as UC are needed for theoretical descriptions and predictions of fission product bubble growth. At present the only published value for the surface energy of UC is the 1 ± 0.3 J/m² at 1100 °C estimated by Livey and Murray [1]) from indirect experimentation and no published value for the grain boundary energy of UC is available, although Livey and Murray assumed that it was approximately half the surface energy. Because of the sparsity of the data it was considered to be worthwhile attempting to determine values for these two energies over a wide range of temperatures by applying the multiphase equilibration technique to the U-UC system. In this technique, the geometric changes produced by vectorial interaction of interphase boundaries at intersecting interfaces are measured [2]). The intersections involved are shown in fig. 1 and if torque terms are ignored, the equilibrium configurations are defined by the relationships:

$$2\,\gamma_{UC-A}\cos(\psi/2)=\gamma_{UC-UC} \qquad (1)$$

$$2\,\gamma^{*}_{UC-A}\cos(\psi^{*}/2)=\gamma_{UC-UC} \qquad (2)$$

$$2\,\gamma_{U-UC}\cos(\phi/2)=\gamma_{UC-UC} \qquad (3)$$

$$\gamma_{U-UC}\cos\eta+\gamma_{LU(C)}\cos\theta=\gamma^{*}_{UC-A}, \qquad (4)$$

where γ_{UC-A} and γ^{*}_{UC-A} are the surface energies of UC in argon and in argon contaminated with uranium vapour respectively, γ_{UC-UC} is the grain boundary energy of UC, γ_{U-UC} is the energy of the U-UC interface and $\gamma_{LU(C)}$ is the surface energy of a sessile drop of liquid uranium that is in equilibrium with UC.

Values for the angles ψ, ψ^{*} and ϕ obtained in this laboratory have been reported previously [3, 4]) and this paper presents data for the angles η and θ, and for the surface energy of liquid uranium in contact with UC. These new data were derived from "sessile drop" experiments in which drops of liquid uranium rest on UC substrates in an argon atmosphere and adopt configurations similar to that of fig. 1(d). The geometries of the drops were measured to obtain values for η and θ and precise measurements of the contour of the drop surface were used to derive values of the liquid surface energy.

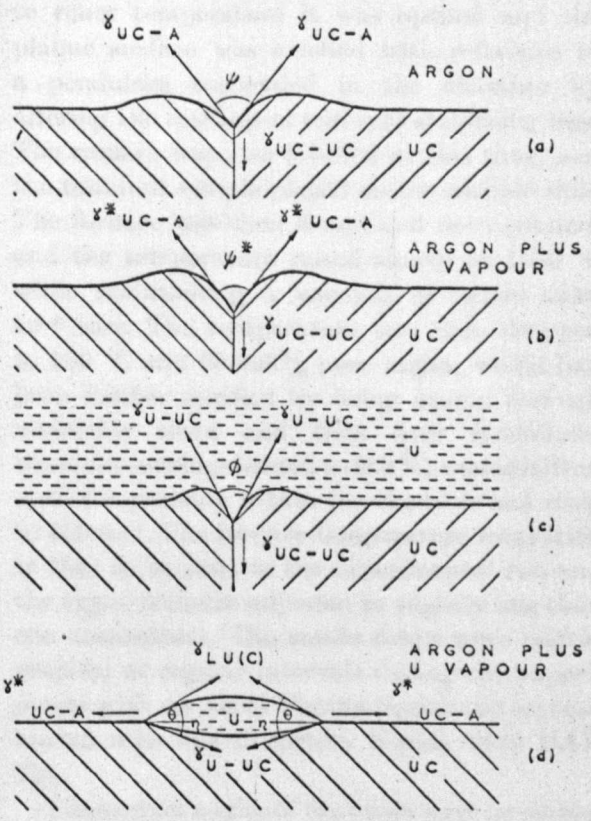

Fig. 1. The geometries generated by several types of energetic interactions at phase interfaces.

The equilibrium values for the five angles and for $\gamma_{LU(C)}$ were substituted into eqs. (5), (6) and (7) – rearrangements of eqs. (1) to (4) – to derive values for the surface and grain boundary energies of UC and the U-UC interfacial energy.

$$\gamma_{UC-A}=\frac{\gamma_{LU(C)}\cos\theta\cos\frac{1}{2}\phi\cos\frac{1}{2}\psi^{*}}{\cos\frac{1}{2}\psi\,(\cos\frac{1}{2}\phi-\cos\eta\cos\frac{1}{2}\psi^{*})} \qquad (5)$$

$$\gamma_{UC-UC}=\frac{2\gamma_{LU(C)}\cos\theta\cos\frac{1}{2}\phi\cos\frac{1}{2}\psi^{*}}{\cos\frac{1}{2}\phi-\cos\eta\cos\frac{1}{2}\psi^{*}} \qquad (6)$$

$$\gamma_{U-UC}=\frac{\gamma_{LU(C)}\cos\theta\cos\frac{1}{2}\psi^{*}}{\cos\frac{1}{2}\phi-\cos\eta\cos\frac{1}{2}\psi^{*}}. \qquad (7)$$

2. Experimental techniques

The uranium carbide was in the form of slabs approximately 1 cm × 1 cm × 0.4 cm, cut from arc-cast ingots obtained from AERE and IRD Ltd., which metallographic examination showed to be single-phase. The uranium samples were 0.4 cm cubes cut from a Springfields Refined Consolidated Uranium billet.

Chemical analyses of both the carbide and the metal are presented in table 1.

TABLE 1
Chemical analyses

I. Uranium Carbide

Carbon (wt%)	Nitrogen (wt%)	Oxygen (wt%)	Other details
4.59	0.02	0.03	Uranium rich structure, used in determination of ϕ values
4.67	0.024	0.028	Stoichiometric structure – as defined by metallography – used in determination of η, ψ, ψ^* and θ

II. Uranium (Springfields Refined Consolidated Billet EU 129)

Carbon (ppm)	Oxygen (ppm)	Silicon (ppm)	Nitrogen (ppm)	Iron (ppm)	Aluminium (ppm)
17	30	< 5	< 5	< 5	< 5

The surfaces of the carbide slabs and metal cubes were ground on silicon carbide papers down to 600 grade using Hyprez fluid as a lubricant. The carbide surfaces were further polished on pads impregnated with diamond dust down to 0.1 μm particle size, again using Hyprez fluid as a lubricant.

Both carbide and metal samples were cleaned after this surface preparation by being washed and ultrasonically agitated in methyl alcohol and dried in a blast of hot air.

The carbide slabs were outgassed in a vacuum furnace at 1700 °C for half an hour, after which the furnace pressure had fallen to less than 1×10^{-6} torr. When the furnace had cooled to room temperature it was opened and the plaque surface was levelled with reference to a pendulum suspended in the chamber by altering the settings of external stabilising legs. The camera was also levelled at this time, and the uranium sample placed on the carbide slab. The furnace was then closed and re-evacuated, and the temperature raised slowly to 1050 °C while maintaining a vacuum of better than 10^{-6} torr. The temperature was then dropped to 900 °C and 99.999% pure argon, which had been further purified by being passed through molecular sieve and then over zirconium-titanium turnings heated to 800 °C, was admitted until the pressure within the chamber had risen to 500 torr. The furnace temperature was raised to that to be used in the experimental run and the argon pressure adjusted to slightly less than one atmosphere. The sessile drops were photographed at regular intervals during the experiments with an Asahi Pentax Spotmatic camera loaded with low distortion Kodak 2496 RAR film.

The contact angles of the drops were measured from enlargements with an estimated accuracy of ± 2°. Because the geometries of the sessile drops varied widely over the range of experimental conditions employed, as indicated by the variation of contact angle values from 110 to 37°, three different methods were used to derive liquid surface energy values from accurate measurements of certain dimensions of the photographs of the drop profiles. In planning this work it was intended to derive the surface energy values using the procedure described by Bashforth and Adams [5]) which involves measurement of the three dimensions of the sessile drop shown in fig. 2 and use of a set of tables which they calculated. [White [6]) has recently published an amplified version of these tables]. Unfortunately this method can be applied only to drops with contact angles greater than 90° and thus, as will be seen, it could not be used for most of the uranium drops.

Two other techniques were used to derive surface energy values for sessile drops with contact angles of less than 90°. Ivashchenko

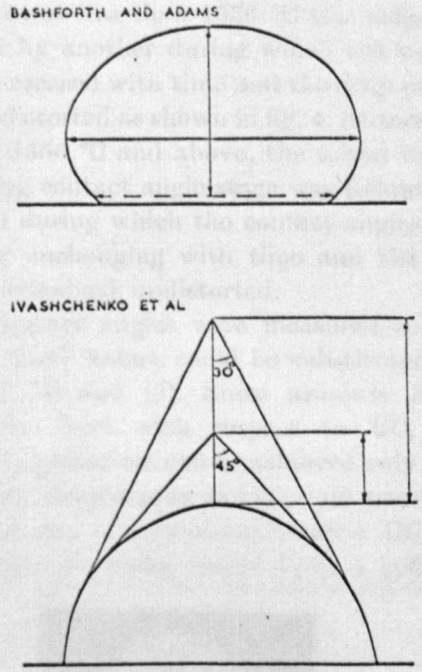

Fig. 2. The dimensions that need to be measured to calculate the surface energy of a sessile drop using the techniques developed by Bashforth and Adams and Ivashchenko et al.

et al.[7,8]) have developed a method for deriving the surface energies of drops with contact angles greater than 60° from measurements of two dimensions, defined by certain tangents to the drop profile as shown in fig. 2. This technique was used for the uranium drops that had contact angles of less than 90° but more than 60°. Most of the drops, however, had contact angles of less than 60°, and for these a computer programme was used which was originally published by Maze and Burnet[9]), and subsequently adapted for use in this laboratory. In order to use the programme it was necessary to measure the x–y co-ordinates of a large number of points on the drop profile with considerable accuracy. In practice, eighty pairs of co-ordinates were measured with an accuracy of $\pm$ 2 μm ($\sim$ 0.01%). This was a tedious and exacting task which was not undertaken when the other techniques could be used.

The microstructures of the solidified samples were revealed by sectioning perpendicular to the drop-plaque interfaces and grinding with pads impregnated with diamond dust down to 0,25 μm using "Hyprez" fluid as a lubricant. The samples were etched in a 1 : 1 : 1 HNO_3 : CH_3COOH : H_2O mixture and photographed using a Vickers M 55 metallograph. Quantitative metallographic evaluation was carried out using a Metals Research Ltd. Quantimet Image Analysing Computer.

3. Results and calculation of surface and interfacial energies

3.1. *0*

The contact angle measurements are plotted as a function of time and temperature in fig. 3. In all cases the contact angles decreased with time in the first stage of the runs, but at

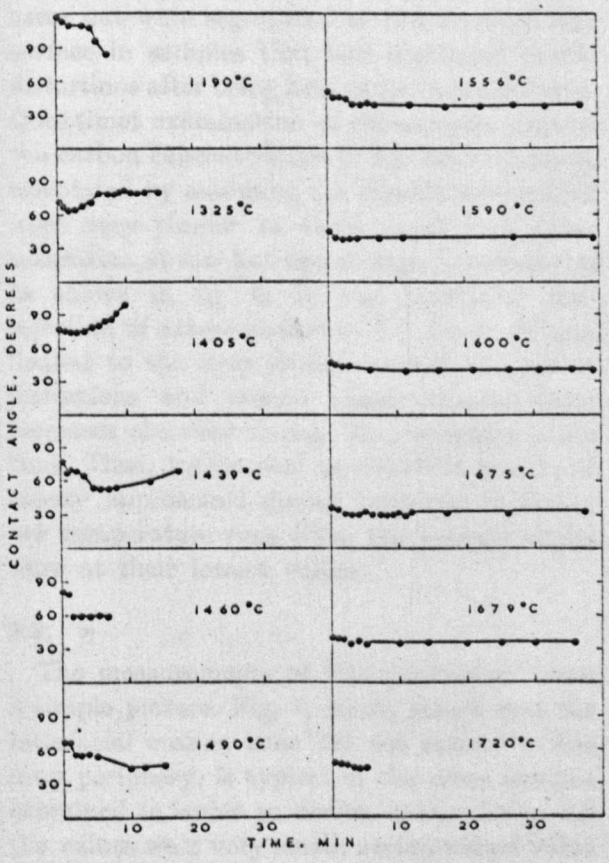

Fig. 3. The contact angles between uranium sessile drops and uranium carbide plaques at various temperatures.

temperatures less than 1556 °C this stage was followed by another during which the contact angles increased with time and the drop profiles became distorted as shown in fig. 4. At temperatures of 1556 °C and above, the initial rapidly decreasing contact angle stage was followed by a second during which the contact angles were virtually unchanging with time and the drop profiles remained undistorted.

The contact angles were measured so that "equilibrium" values could be substituted into eqs. (5), (6) and (7). Since uranium is not chemically inert with respect to UC, true chemical equilibrium can be achieved only when the sessile drop/plaque samples are converted into a plaque of hypostoichiometric UC. For the present purposes, however, it is sufficient to achieve mechanical equilibrium, that is, a sessile drop configuration which does not change with time. This equilibrium condition was attained in the high temperature experiments, with the possible exception of the 1720 °C run which was of very short duration, but not in the low temperature experiments.

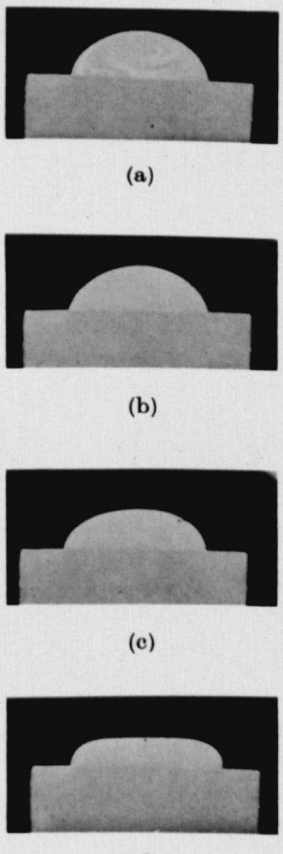

Fig. 4. Photographs showing change in contact angle and flattening of the uranium sessile drop profile at 1325 °C. (a) at temp.; (b) after 3 min.; (c) after 5 min.; (d) after 15 min.

Further insight into the anomalous wetting behaviour displayed during the low temperature runs was sought by qualitative and quantitative examination of metallographically prepared cross-sections of solidified samples that had been used in both high and low temperature runs. As fig. 5 shows, intergranular penetration and erosion of the UC occurred to an extent which increased with temperature. In addition, dendrites of what were thought to be UC were uniformly distributed throughout the uranium in samples that had been held at high temperatures but were segregated to the uranium free surface in samples that had displayed profile distortions after being held at low temperatures. Quantimet examination of the samples showed the carbon concentrations of the drop interiors, calculated by assuming the dendrites were UC, were very similar to those needed to cause saturation at low but not at high temperatures as shown in fig. 6. It was concluded that rejection of excess carbon as UC dendrites that floated to the drop surface caused the profile distortions and second stage contact angle increases observed during the low temperature runs. Thus, mechanical equilibrium was most closely approached during both the high and low temperature runs when the contact angles were at their lowest values.

3.2. η

The measurements of this parameter reveal a simple picture. Fig. 7, which shows that the interfacial erosion zone did not extend to the drop periphery, is typical of the cross sections examined in order to derive values for η. All the values were very small, no individual value being greater than 2°. As 2° is the estimated accuracy of such measurements the true values of η may well have been 0°. In practice, these

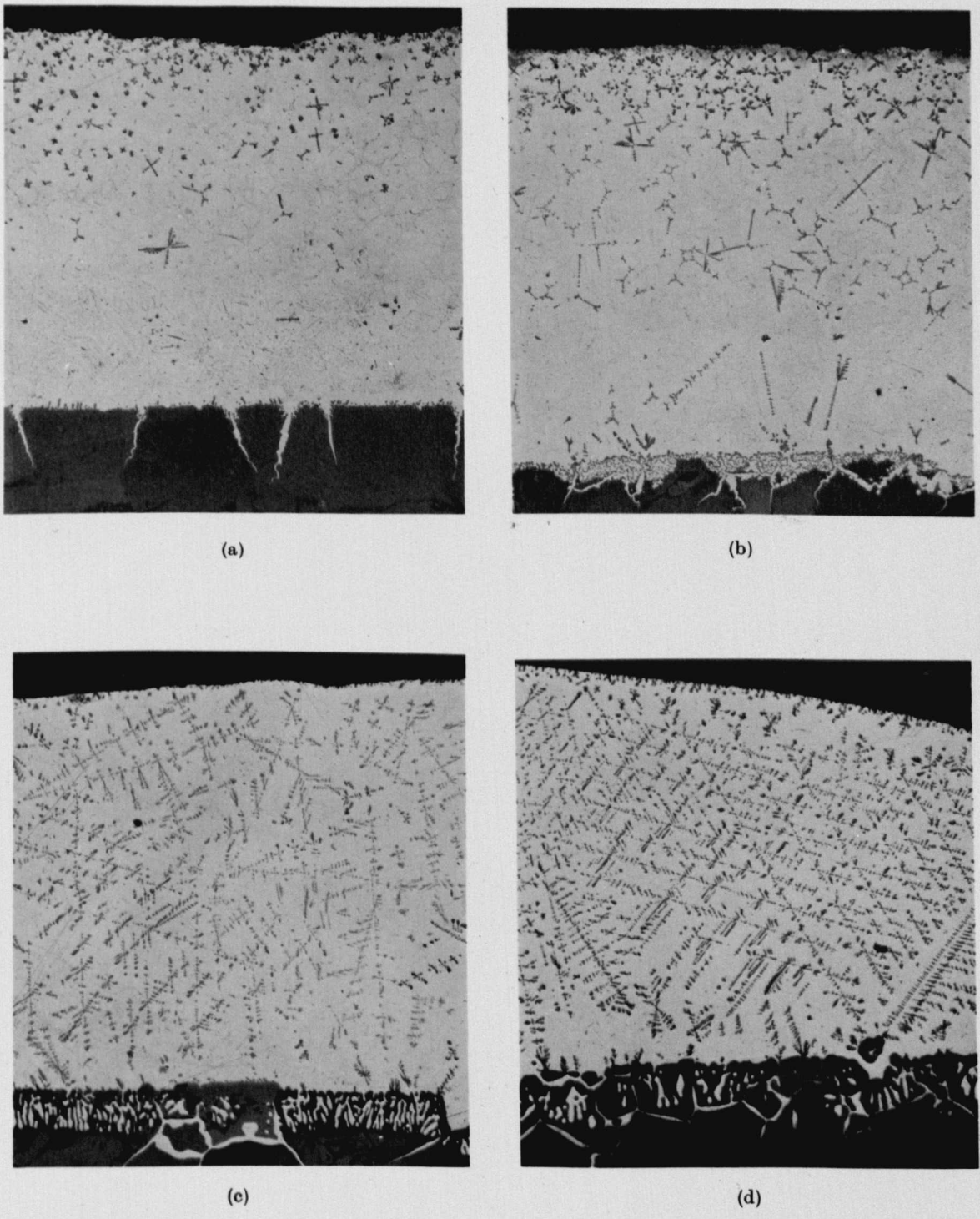

(a) (b)

(c) (d)

Fig. 5. Micrographs of uranium sessile drops on uranium carbide plaques showing segregation in the solidified drop and reaction at the carbide interface. (a) 1325 °C; (b) 1405 °C; (c) 1556 °C; (d) 1675 °C. ×40

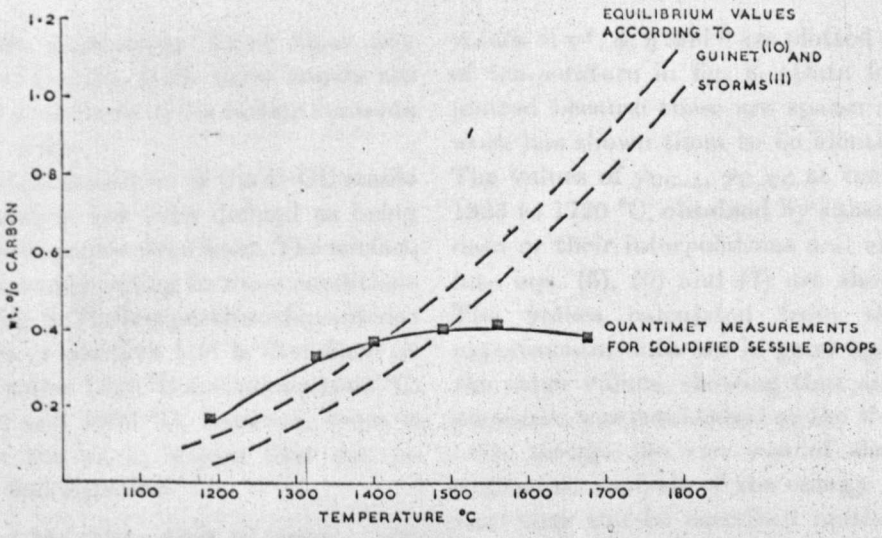

Fig. 6. The concentration of carbon in liquid uranium plotted as a function of temperature.

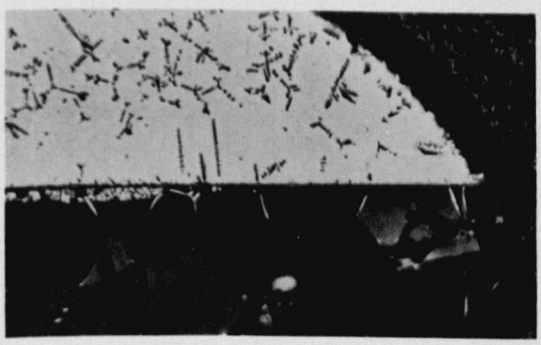

Fig. 7. Micrograph showing the edge of a uranium sessile drop on a uranium carbide plaque (15 min, 1490 °C). ×28

values are so small that cos η in eqs. (5), (6) and (7) can be approximately equated to one.

3.3. $\gamma_{LU(C)}$

Surface energy values* derived for seven sessile drops from nineteen photographs taken while the drops were undistorted are presented in table 2. The data as a whole display a trend indicating that the surface energy decreases with time at temperature. Similarly the energy values derived from the highest temperature

* In calculating the values it was assumed that the density of the sessile drops was that of pure uranium [12]). This assumption was not strictly accurate because of the uptake of carbon into the liquid.

TABLE 2

Variation of the surface energy of liquid uranium with time at various temperatures

Temp. (°C)	Time (min)	θ (°)	Liquid surface energy (J/m²)	Technique
1190	2	112	1.440	Adams and Bashforth
1325	0	68	1.461	Ivashchenko
	1	64	1.475	Ivashchenko
	2	63	1.440	Ivashchenko
1405	3	61	1.200	Computer
1460	6½	59	1.093	Computer
1556	2	47	1.437	Computer
	8	39	1.552	Computer
	11	39	1.113	Computer
	32	38	0.882	Computer
1600	0	46	1.462	Computer
	1	45	1.508	Computer
	2	44	1.428	Computer
	3	43	1.365	Computer
	11	42	1.169	Computer
	39	40	0.781	Computer
1720	0	49	0.931	Computer
	1	48	0.959	Computer
	3	46	0.931	Computer

experiment are appreciably lower than any other comparable data. Both these trends are probably due to increases in the carbon contents of the sessile drops.

The equilibrium condition of the U-UC sessile drop/plaque system has been defined as being when the contact angles were least. The surface energy values corresponding to these conditions are plotted in fig. 8. The temperature dependence of these values is complex and is ill-defined at temperatures below 1325 °C and above 1600 °C. Between 1325 and 1600 °C, however, there is a decrease in the $\gamma_{LU(c)}$ values that can be described by the equation

$$\gamma_{LU(c)} = 1.44 - 2.35 \times 10^{-3} \ (t - 1325), \quad (8)$$

where t is the temperature in °C.

3.4. Calculation of γ_{UC-A}, γ_{UC-UC} and γ_{U-UC}

With the measurement of equilibrium values of θ, η and $\gamma_{LU(c)}$ it is now possible to calculate the surface and interfacial energies of the U-UC system at several temperatures. The equilibrium values of ψ^*, ϕ, η and θ are plotted as a function of temperature in fig. 8. [Data for ψ are not plotted because these are sparse and previous work has shown them to be identical to ψ^* [3]]. The values of γ_{UC-A}, γ_{U-UC} at temperatures of 1325 to 1720 °C, obtained by substituting these data or their interpolations and extrapolations into eqs. (5), (6) and (7) are shown in fig. 8. The values calculated from the 1720 °C experimental data are in good agreement with the other values, showing that an equilibrium condition was established at the U-UC interface even though the run was of short duration. Statistical analysis of the energy values shows that they can be described mathematically as a function of the equilibration temperature, t °C, by the equations,

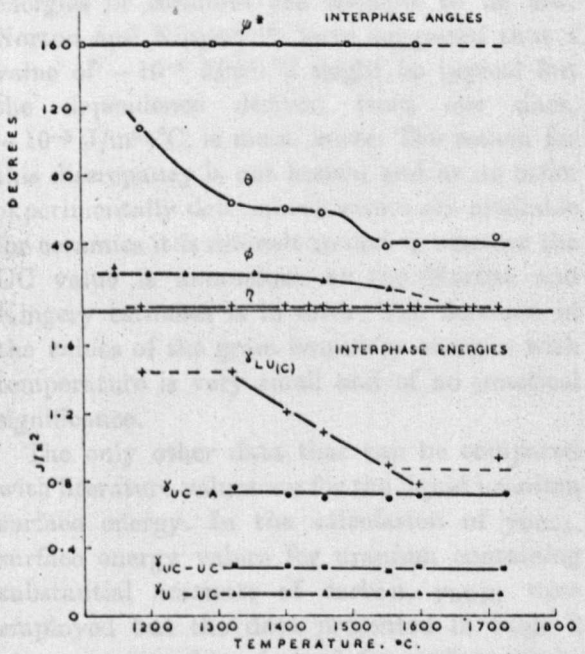

Fig. 8. Data characterising the equilibrium interface interactions of the uranium-uranium carbide system at various temperatures.

$$\gamma_{UC-A} = (0.728 \pm 0.041) - 10^{-5} \ (t - 1325), \quad 1325 < t < 1720 \quad (9)$$

$$\gamma_{UC-UC} = (0.274 \pm 0.015) - 4 \times 10^{-6} \ (t - 1325), \quad 1325 < t < 1720 \quad (10)$$

$$\gamma_{U-UC} = (0.141 \pm 0.008) - 7 \times 10^{-6} \ (t - 1100), \quad 1100 < t < 1550. \quad (11)$$

Values for the ($\gamma_{U-UC}/\gamma_{UC-UC}$) ratio have been reported previously [4]) for equilibration temperatures below the melting point of uranium. If eq. (10) can be extrapolated, it can be used in conjunction with these ratios to calculate the interfacial energy between UC and solid uranium at temperatures of 850 to 1100 °C. The results of these calculations can be summarised as

$$\gamma_{U-UC} = (0.141 \pm 0.008) - 6 \times 10^{-5} \ (t - 1100), \quad 850 < t < 1100.$$

4. Discussion

The work described in this paper represents the final phase in a programme to determine the surface and interfacial energies of the U-UC system over a wide range of temperatures as a contribution to nuclear fuel development. However, the data should also be a contribution to ceramic science in general because few values for the surface and grain boundary energies of

ceramics are available and as far as we are aware, no other data are available for any single ceramic over a range of temperatures.

The few available data for carbide surface energies lie within the range 0.3–3.0 J/m² [13, 14]) and the new values obtained for UC lie well within this range. They are about 25% lower than the only published value for UC, Livey and Murray's [1]) estimate of 1 J/m², but as Livey and Murray claimed an accuracy of only ± 30%, the new values can be regarded as a substantial confirmation of their estimate.

In contrast, the new values obtained for the grain boundary energy of UC differ markedly from the approximate value of 0.5 J/m² suggested by Livey and Murray. This suggestion was based on an assumed grain boundary to surface energy ratio of 0.50 as compared to the 0.377 actually found for UC [3]). The high ratio used by Livey and Murray is characteristic of ionic solids such as Al_2O_3 [15]) whereas the actual ratio of 0.377 is similar to that for fcc metals (UC has a fcc lattice structure) and is consistent with the generally metallic nature of UC.

The temperature dependences of the surface energies of ceramics are thought to be low. Norton and Kingery [16]) have suggested that a value of -10^{-4} J/m²·°C might be typical but the dependence derived from our data, -10^{-5} J/m²·°C, is much lower. The reason for this discrepancy is not known and as no other experimentally determined values are available for ceramics it is difficult to decide whether the UC value is anomalous or the Norton and Kingery estimate is in error. The decrease in the values of the grain boundary energies with temperature is very small and of no practical significance.

The only other data that can be compared with literature values are for the liquid uranium surface energy. In the calculation of γ_{UC-A}, surface energy values for uranium containing substantial amounts of carbon, $\gamma_{LU(C)}$ were employed but the data presented in table 2 also contain values derived from photographs taken in the very early stages of the sessile drop experiments and these should be approxi-

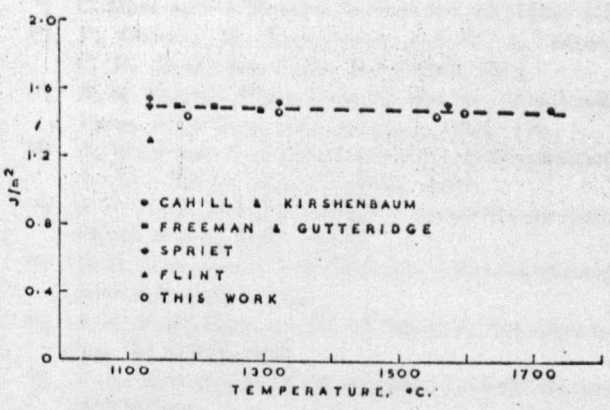

Fig. 9. The liquid surface energy of nearly pure uranium compared with published values.

mately equal to that of pure uranium. These early stage values, which lie in the range 1.45 ± 0.012 J/m², are plotted in fig. 9 along with other values for uranium known to the authors. It can be seen that the early stage values are in reasonable agreement with those of Cahill and Kirshenbaum [17]) and Freeman and Gutteridge [18]) obtained from maximum bubble pressure experiments and the single value of Spriet [19]) obtained from a drop weight experiment. The value derived by Flint [20]) from pendant drop experiments is much lower, possibly due to oxygen contamination.

There is no literature data for the surface energy of liquid uranium-carbon alloys and therefore no direct comparison with the results of the programme can be made. However, the 25–40% decrease in the liquid surface energy of uranium due to carbon pick-up was not unexpected since carbon is known to decrease the surface energies of other liquid metals and decreases of 30–50% due to surface segregation of other active species have been reported [21]). The negligible temperature dependence of the surface energy of nearly pure liquid uranium suggests that the marked temperature dependence of the $\gamma_{LU(C)}$ values (fig. 8) may have been primarily a reflection of the changing carbon content.

Acknowledgements

The authors wish to acknowledge the useful-

ness of several interesting discussions held with Dr. J. E. Antill.

References

1) D. T. Livey and P. Murray, Plansee Proc. (1955) 375
2) C. Herring, Physics of powder metallurgy, W. E. Kingston, ed. (McGraw-Hill, New York, 1951) p. 3
3) E. N. Hodkin, M. G. Nicholas and D. M. Poole, J. Nucl. Mater. 25 (1968) 284
4) E. N. Hodkin, M. G. Nicholas and D. M. Poole, J. Nucl. Mater. 27 (1968) 8
5) F. Bashforth and J. C. Adams, An attempt to test theories of capillary action (University Press, Cambridge, 1883)
6) D. W. G. White, Internal Report PM-I-67-4, Queen's Printers, Ottawa, Canada (1967)
7) Yu. N. Ivashchenko, V. N. Eremenko, Russian J. Phys. Chem. 39 (2) 1965 278
8) Yu. N. Ivashchenko, B. B. Bogatyrenko and V. N. Eremenko, Surface phenomena in melts and powder metallurgy processes, Izd. Akad. Auk. Ukraino SSR. Kiev (1963) 391
9) C. Maze and G. Burnet, Surface Sci. 13 (1969) 451
10) P. Guinet, H. Vaugoyeau and P. L. Blum, C. R. Acad. Sci. Paris 261 (1965) 1312
11) E. K. Storms, The refractory carbides (Academic Press, New York and London, 1967) 176
12) A. V. Grosse, J. A. Cahill and A. D. Kirshenbaum, J. Am. Chem. Soc. 83 (1961) 4665
13) J. J. Duga, Surface energy of ceramic materials, DCIC Report 69-2 (1969)
14) D. A. Mortimer and M. Nicholas, UKAEA Report AERE-M 2247 (1969)
15) J. F. Shackeford and W. D. Scott, J. Am. Ceram. Soc. 51 (1968) 686
16) F. K. Norton and W. D. Kingery, USAEC Report NYO-3144
17) J. A. Cahill and A. D. Kirshenbaum, J. Inorg. Nucl. Chem. 27 (1965) 73
18) R. F. A. Freeman and W. A. Gutteridge, Fulmer Research Institute, private communication (1970)
19) B. Spriet, Mém. Sci. Rev. Métall. 50 (7) (1961) 531
20) O. Flint, J. Nucl. Mater. 16 (1965) 260
21) P. Kozakovitch, Surface phenomena of metals, Soc. Chem. Ind. Monograph 28 (1968) 223